Received: 1 May 2024 | Revised: 30 June 2024 | Accepted: 6 July 2024

DOI: 10.1002/jmor.21751

RESEARCH ARTICLE

JOURNAL OF morphology WILEY

Bee morphology: A skeletomuscular anatomy of *Thyreus* (Hymenoptera: Apidae)

Odair M. Meira[1,2] | Rolf G. Beutel[1] | Hans Pohl[1] | Thomas van de Kamp[3,4] | Eduardo A. B. Almeida[2] | Brendon E. Boudinot[1,5,6]

[1]Institut für Zoologie und Evolutionsforschung, Friedrich-Schiller-Universität Jena, Jena, Germany

[2]Laboratório de Biologia Comparada e Abelhas, Departamento de Biologia, Faculdade de Filosofia, Ciências e Letras de Ribeirão Preto (FFCLRP), Universidade de São Paulo, Ribeirão Preto, São Paulo, Brazil

[3]Institute for Photon Science and Synchrotron Radiation (IPS), Institute for Photon Science and Synchrotron Radiation (IPS), Karlsruhe Institute of Technology (KIT), Eggenstein-Leopoldshafen, Baden-Württemberg, Germany

[4]Laboratory for Applications of Synchrotron Radiation (LAS), Karlsruhe Institute of Technology (KIT), Karlsruhe, Baden-Württemberg, Germany

[5]National Museum of Natural History, Smithsonian Institution, Washington, District of Columbia, USA

[6]Naturmuseum Frankfurt, Senckenberg Research Institute, Frankfurt am Main, Hessen, Germany

Correspondence

Eduardo A. B. Almeida, Laboratório de Biologia Comparada e Abelhas, Departamento de Biologia, Faculdade de Filosofia, Ciências e Letras de Ribeirão Preto (FFCLRP), Universidade de São Paulo, Av. Bandeirantes, 3900, Ribeirão Preto, 14040-901 SP, Brazil.
Email: eduardoalmeida@usp.br

Funding information

São Paulo Research Foundation, Grant/Award Numbers: 2018/09666-5, 2019/09215-6, 2021/07258-0, 2022/11349-3; Coordenação de Aperfeiçoamento de Pessoal de Nível Superior—Brasil (CAPES); Alexander von Humboldt Stiftung (2020–2022); Smithsonian Institution (2022–2023)

Abstract

Although the knowledge of the skeletal morphology of bees has progressed enormously, a corresponding advance has not happened for the muscular system. Most of the knowledge about bee musculature was generated over 50 years ago, well before the digital revolution for anatomical imaging, including the application of microcomputed tomography. This technique, in particular, has made it possible to dissect small insects digitally, document anatomy efficiently and in detail, and visualize these data three dimensionally. In this study, we document the skeletomuscular system of a cuckoo bee, *Thyreus albomaculatus* and, with that, we provide a 3D atlas of bee skeletomuscular anatomy. The results obtained for *Thyreus* are compared with representatives of two other bee families (Andrenidae and Halictidae), to evaluate the generality of our morphological conclusions. Besides documenting 199 specific muscles in terms of origin, insertion, and structure, we update the interpretation of complex homologies in the maxillolabial complex of bee mouthparts. We also clarify the complicated 3D structure of the cephalic endoskeleton, identifying the tentorial, hypostomal, and postgenal structures and their connecting regions. We describe the anatomy of the medial elevator muscles of the head, precisely identifying their origins and insertions as well as their homologs in other groups of Hymenoptera. We reject the hypothesis that the synapomorphic propodeal triangle of Apoidea is homologous with the metapostnotum, and instead recognize that this is a modification of the third phragma. We recognize two previously undocumented metasomal muscle groups in bees, clarifying the serial skeletomusculature of the metasoma and revealing shortcomings of Snodgrass' "internal–external" terminological system for the abdomen. Finally, we elucidate the muscular structure of the sting apparatus, resolving previously unclear interpretations. The work conducted herein not only provides new insights into bee morphology but also represents a source for future phenomic research on Hymenoptera.

KEYWORDS

Apidae, Apoidea, exoskeleton, Hymenoptera, morphology

1 | INTRODUCTION

There are over 20,000 species of bees (Hymenoptera: Apoidea: Apiformes), forming a widely distributed group of insects found in all terrestrial ecosystems outside the polar regions (Danforth et al., 2019; Michener, 2007). Like all other organisms, bees interact with their environment using morphological structures. Consequently, detailed knowledge of the structure and function of body parts of extant and extinct species is essential to appreciating their success and evolution. As our understanding of bee phylogeny has become increasingly more stable in recent decades (Almeida et al., 2023; Danforth et al., 2013; Michener, 2007), we have gained a consistent foundation that allows us to direct our questions, for example, about how the groundplan of bees emerged, remodeled, and diversified through their evolutionary history.

Interest in bee morphological investigations, with an emphasis on comparative anatomy, has grown in recent years and has generated important insights into the structure and variation of skeletal morphology as a source of data for phylogenetic reconstructions (Alexander & Michener, 1995; Gonçalves et al., 2022; Meira & Gonçalves, 2018, 2021; Melo, 1999; Porto & Almeida, 2019, 2021; Porto et al., 2016, 2017; Roig-Alsina & Michener, 1993). There is an intricate system formed by the chitinous exoskeleton of an insect and the muscles attached to skeletal structures, referred to as the skeletomusculature. The works of Snodgrass on the skeletomusculature of the adult honey bee (*Apis mellifera*) form a central corpus of anatomical knowledge for the whole body (Snodgrass, 1925, 1942, 1956). Other important skeletomuscular treatments have focused on specific tagmata, such as Wille (1956) for the mesosoma, and Urban (1963), Graf (1965), and Youssef (1971) for the head. These studies predated the development of digital imaging techniques, which have been shown to substantially improve morphological documentation by allowing for nondestructive virtual dissections, extensive data exploration, and figure production (Friedrich & Beutel, 2008b; Friedrich et al., 2014).

Microcomputed tomography (μ-CT) is a particularly powerful technique for the morphological study of insects (Herman, 2009). Because μ-CT scanning and reconstruction can reveal three-dimensional (3D) details to the submicron level of resolution, this technique has become widespread in entomological research (e.g., Blanke et al., 2015; Brock et al., 2022; Hillen et al., 2023; Hörnschemeyer et al., 2002; van de Kamp et al., 2011, 2014, 2018, 2022; Püffel et al., 2021; Rühr et al., 2021). For the morphological study of extant Aculeata, μ-CT has been applied to Formicidae (e.g., Aibekova et al., 2022; Booher et al., 2021; Boudinot et al., 2021, 2022; Griebenow et al., 2023; Klunk et al., 2023; Liu et al., 2019; Richter et al., 2020, 2021, 2022, 2023), spheciform Apoidea (Willsch et al., 2020, Sphecidae and Ampulicidae), and some anatomical systems of the honey bee (e.g., Alba-Tercedor & Alba-Alejandre, 2019; Berry & Ibbotson, 2010; de Paula et al., 2022; Ramirez-Esquivel & Ravi, 2023; Ribi et al., 2008).

In the present study, we applied synchrotron μ-CT to compare females of *Thyreus* (Apidae: Nomadinae: Melectini) and *Lasioglossum* (Halictidae: Halictinae: Halictini). Whereas *Lasioglossum* represents the usual biology of bees that build a nest and provision for their offspring, *Thyreus* is an example of a cuckoo bee. This biology is referred to as "brood parasitic" (Danforth et al., 2019; Litman, 2019), "cleptoparasitic" (e.g., Michener, 2007), or "kleptoparasitic," denoting the specialized biology of an adult female locating and then entering the nest of another bee species to lay her eggs in the host brood cell. This life-history is associated with the lack of behaviors and morphological traits associated with the collecting of pollen provisions in flowers as found in most bee species; the parasite offspring will rely on the host provisions for nourishment of her own. Brood parasitic bees are also characterized by adaptations (morphological, behavioral, and physiological traits) that enable them to operate stealthily, evading detection by their hosts and enhancing the likelihood of their offspring's survival. *Thyreus* is part of the diverse nomadine clade of Apidae, with over 1300 brood parasitic species (Sless et al., 2022).

The main objectives of the present work were to document and illustrate the skeletomuscular system of a medium-sized hymenopteran species using synchrotron μ-CT data, and to revisit the anatomical work of Snodgrass (1925, 1942, 1956) on the honey bee, Michener (1944) on all bees, and Prentice (1998) on Apoidea. The morphological variation within bees is vast, and the species selected as targets for this study would provide the chance to compare representatives of bee clades that diverged in the Early Cretaceous (Almeida et al., 2023). These species constitute a phylogenetic (different families) and morphological (long-tongued bees and short-tongued bees) counterpoint that can provide insights into the evolution of bees. The skeletomusculature of bees has been virtually unexplored with these modern techniques and allow the evaluation of homology hypotheses proposed by previous authors (e.g., Michener, 1944; Snodgrass, 1942) while establishing the first whole-body 3D anatomical atlas of the bee skeletomuscular system.

2 | MATERIALS AND METHODS

2.1 | Taxon sampling

We examined one female of *Thyreus* cf. *albomaculatus* (De Geer) (Apidae: Nomadinae: Melectini; specimen code: USNMENT01900218; scan code: BB311). Anatomical features of *Thyreus* were compared with characters found in one female *Lasioglossum* (Halictidae: Halictinae: Halictini, unpublished data) and one male of *Andrena* (Andrenidae: Andreninae: Andrenini; specimen code: USNMENT01900300; scan code: BB113). The bees were preserved in 95% ethanol and subsequently analyzed using synchrotron microcomputed tomography (SR-μ-CT). The voucher specimens are deposited in the Senckenberg Naturmuseum Frankfurt Hymenoptera Collection (SMFH).

2.2 | Synchrotron X-ray microtomography

Synchrotron X-ray microtomography (SR-μ-CT) was performed at the Imaging Cluster of the KIT Light Source (Karlsruhe Institute of Technology) using a filtered polychromatic X-ray beam produced by a

1.5 T bending magnet with a spectrum peak of about 15 keV. The beam was filtered with 0.5 mm aluminum. We employed a fast indirect detector system consisting of an LSO:Tb scintillator (Cecilia et al., 2011) and a diffraction-limited optical microscope (Optique Peter; Douissard et al., 2012) coupled to a 12-bit pco.dimax high-speed camera with 2016 × 2016 pixels (dos Santos Rolo et al., 2014). The specimens were scanned within 95% ethanol. For each scan, we acquired 3000 projections at 70 fps at ×2 (BB311) or ×5 (BB113 and *Lasioglossum*) optical magnification, resulting in an effective pixel size of 6.1 or 2.44 µm, respectively. Since the specimens were too large vertically for the field of view, they were scanned in several height steps. The control system concert (Vogelgesang et al., 2016) was used for automated data acquisition and online reconstruction of tomographic slices for data quality assurance. Final 3D tomographic reconstructions were performed by tofu (Faragó et al., 2022) and additionally included phase recovery (Paganin et al., 2002), ring removal, 8-bit conversion, and mixing of phase and absorption 3D reconstructions to increase the contrast between the background and homogeneous regions while highlighting the edges.

2.3 | 3D image data processing

Regions of interest were segmented using Amira 6.5 (Visage Imaging GmbH). They were subsequently exported with the "multiExport" plug-in script (Engelkes et al., 2018) in Amira 6.2 as tiff image stacks. 3D rendering was performed with the VG Studio 3.2.5 program. Subsequently, the figures were arranged in Adobe Photoshop® CS6 (Adobe System Incorporated).

2.4 | Anatomical terminology

We evaluated homology hypotheses for all described structures in this work; consequently, we synthesize terminology across numerous studies. In cases where new interpretations are proposed, the terms are highlighted in bold the first time they appear in the text. At the broadest level, we derived our concepts and terminology primarily from the following sources. Meira and Gonçalves (2021), Wipfler et al. (2011), and Richter et al. (2020) for cephalic musculature, Friedrich and Beutel (2008a) and Beutel et al. (2014) for the mesosoma, and Lieberman et al. (2022) for the propodeum and metasoma, all with reference to Snodgrass (1925, 1942, 1956). For the sclerites of the head, mesosoma, and metasoma, terminological preferences primarily follow Michener (1944, 2007), and for the sting apparatus Vilhelmsen (2000) and Packer (2003), with further reference to Lieberman et al. (2022). For the cephalic endoskeleton we follow Porto et al. (2016), for the prosternum, propleuron, mesofurca/metafurca, and mesophragma, we follow Porto et al. (2017) complemented with (personal observations by Brendon E. Boudinot). For terminology related to the skeletomusculature, we are using direct spelling, as a result, there may be some variations in hyphenation when describing the names of muscle groups.

Some term choices need clarification, especially where they have been recently proposed or their usages modified. **Sitophore** is here understood as "a sclerotization in the proximal hypopharyngeal wall connection to the pharyngeal rods" of the pharyngeal plate (Porto & Almeida, 2019). We use **oral arm** (Zimmermann & Vilhelmsen, 2016) and **oral arm process** (Richter et al., 2023) for the apical structure of the pharyngeal plate. For the articulatory structure of the pronotum and mesepisternal region, we use the term **mesepisternal clip** (Rosa & Melo, 2023). As the identity of the lateral areas of the mesothorax are still debatable and it is hard to precisely identify their homology, here we will refer to this region as the mesopectus. In our interpretation, the mesopectus is composed of the mesepisternum, mesepimeron, and mesothoracic endosternum. In a similar way to the mesothorax, the lateral areas of the metathorax will be referred to as the metapectus. To clarify the segmental identity of the axillary sclerites at the bases of both pairs of wings, we refer to those of the anterior wing as **mesoaxillary sclerites** and those of the posterior wing as **metaaxillary sclerites**; without this distinction, the axillary sclerites receive identical names, hence cannot be meaningfully referred to out of descriptive context. We restrict the term **apodeme** to skeletal structures, such as the "cervical apodeme," which is a sclerotic structure of the propleuron, and not to the connective tissues of some muscular insertions, for which we use the term **tendon**. In our usage of "tendon," we are not referring to the mesodermal endoskeleton of wingless insects that is replaced with cuticle in the Pterygota, but rather to the extracellular matrix (i.e., the material) that joins any striated muscle fiber to any tendon cell of the epidermis (e.g., the reviews of Sink [2006] and Schulman et al. [2015]). Therefore, we distinguish between the developmental state of endoskeletal elements and the material that joins muscle to the epidermis. Tendons are understood here as the connective tissue that bridges the muscle to the cuticular structure (Bitsch & Bitsch, 2002), and apodemes as invaginations of the cuticle (Girón et al., 2023). The insertion of muscle IvIm7 on the sternum has a very short apodeme, which we refer to as the **scar**, as it is scar-like in appearance during volume rendering. In the metasomal/abdominal region, we will refer to the abdominal segments using roman numerals (e.g., tergum I) and to the metasomal segments using arabic numerals (e.g., tergum 1).

3 | RESULTS

The skeletomusculature of *Thyreus albomaculatus* was rendered as 3D reconstructions of internal and external anatomy (Figure 1), which will be detailed in the sections below following the anteroposterior sequence of tagmata.

3.1 | Head of *T. albomaculatus*

3.1.1 | External head capsule (Figures 2 and 3)

The cuticular surface of the head and other body regions is covered by a layer of long whitish setae, which are adpressed in some areas.

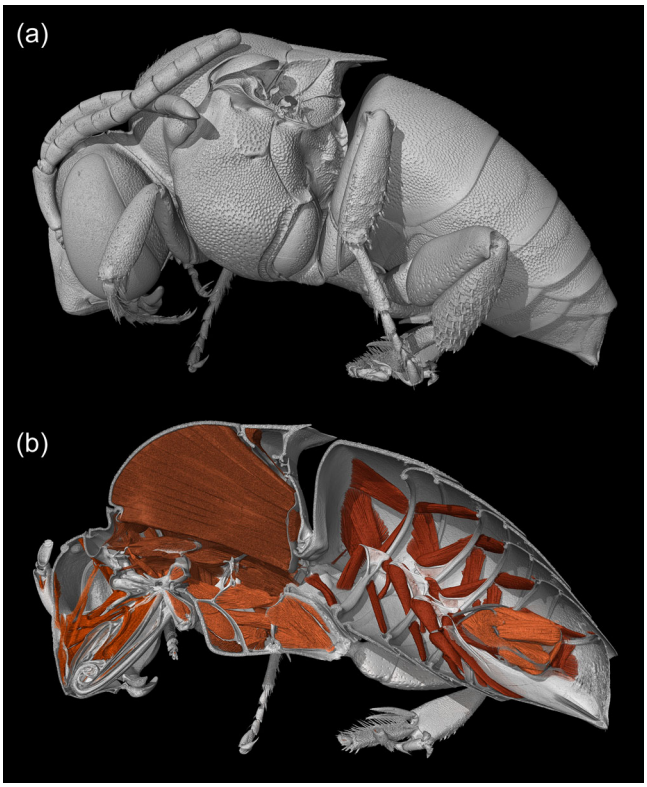

FIGURE 1 Reconstruction of the morphology of *Thyreus albomaculatus*. (a) External habitus and (b) internal sagittal bisection.

The color of the cuticle is black, and the surface displays a very dense pattern of distinct grooves (diameter ca. 20 µm), which are more or less adjacent to each other. The cuticle of the external elements of the head capsule is ca. 0.10–0.08 mm thick.

The head of the female *T. albomaculatus* (Figures 2 and 3) appears compact, not compressed anteroposteriorly, and only moderately declined in its resting position. It is ca. 3.00 mm high between the distal labral margin and the ocellar region and about 2.45 mm long from the labral apex and the occipital foramen. In frontal view (Figure 2a), it appears transversely oval. Large and evenly convex compound eyes occupy a large proportion of the lateral cephalic surface (Figure 2a,b), extending from the uppermost head region almost to the primary mandibular articulation; they are approximately oval but more than twice as wide ventrally than dorsally; the surface is largely smooth, with numerous minute cornea lenses. Three strongly convex, well-developed ocelli are present in the vertexal region (Figure 2a,c), with the median ocellus slightly larger (ca. 0.32 mm) than the lateral ones (ca. 0.25 mm) and inserted slightly below them. The roundish antennal foramen (Figure 2a,b) is located in the middle region of the frontal surface of the head capsule, about halfway between the anterior clypeal margin and the ocelli; their diameter is ca. 0.35 mm, and they are enclosed by a distinctly raised antennal rim; an antennifer is not visible. Below the antennal foramen, a subantennal groove (Figure 2a) is present, extending from the inner margin of the foramen to the epistomal sulcus; the distance between the mesal margins is ca. 0.5 mm, and the distance between the lateral margin and the compound eye is ca. 0.3 mm; internally, this groove corresponds to the dorsal sheet of the anterior tentorial arm (Figures 5c,d, 6c–f, and 8). Remnants of dorsal ecdysial sutures are not present. The hexagonal clypeus (Figure 2a,b) has a nearly straight distal (ventral) margin and is delimited from the genal and frontal regions by the faintly recognizable epistomal sulcus, which obliquely converges dorsad before becoming transverse and nearly straight slightly below the subantennal groove. The frontal region (Figure 2a,b) between the antennal area is distinctly raised, with a distinctly developed frontal line (or "median crest"), which is about half as long as the distance between the dorsal clypeal margin and the median ocellus; this structure corresponds with a short internal **frontal ridge** (Figure 8b). The anterior tentorial pits (Figures 2a and 5a,b) are oval and distinctly visible, externally adjacent with the upper portion of the oblique part of the epistomal sulcus, and their diameter is ca. 0.05 mm. The genal area (Figures 2b–d, 3, 4a, and 5c,d), posterad the compound eyes, is short.

The posterior head region (Figures 2c,d and 3) is fully exposed. The small occipital foramen (Figures 2c,d and 3) ("foramen occipitale") is roughly quadrangular to triangular, ca. 0.7 mm high and 0.5 mm wide, and connected by the cervical membrane with the prothorax; it is divided into a smaller dorsal notoforamen and a larger ventral neuroforamen by the **tentorio-tentorial bridge** (Figures 2c,d and 3). The occipital carina (*sensu*, e.g., Sharkey & Wharton, 1997) (Figures 2c,d and 3) separates the occiput from the remainder of the head; this carina is drawn out ventrad and then curves inwards and obliterates towards the hypostomal carina (Figures 2c,d and 3). The occiput is largely smooth and glabrous and surrounds the occipital foramen (Figures 2c,d and 3). The postocciput is the region mediad the arched sulcus of the occiput (Porto et al., 2016) (Figures 2c,d and 3); together with this sulcus, the **supratentorial carina** (Figure 3) forms a curved element, which reaches the **supratentorial invagination** (Figure 3) dorsally and obliterates before it reaches the postgenal bridge ventrally. The postoccipital sulcus (Figure 3) is located laterally to the occipital foramen as a depression that connects the posterior tentorial pit (Figure 3) and the tentorio-tentorial bridge pit (Figure 3). The **dorsal**, **lateral**, and **ventral postoccipital lips** enclose the occipital foramen (Figure 3). A concave sclerotized postgenal bridge (Figures 2c,d and 3) (= subforaminal bridge) is present between the occipital foramen and the hypostoma; it is laterally divided along its lateral margin by a longitudinal bulge located at the dorsal end of the postgena. The hypostoma (Figures 5, 6a–d,f, and 7a) is firmly fused with the tentorium (see cephalic endoskeleton). The postoccipital bridge is a sclerotized, deeply concave area above the **subforaminal groove** (Figures 2c,d and 3). The large hypostoma ("fossa of the proboscis") is enclosed by strongly pronounced longitudinal hypostomal carinae (Figures 2c,d and 5c,d), which diverge proximally over a short distance, then run parallel until they reach the mandibular articulating area, and then abruptly bend laterad towards the primary mandibular articulation.

Occipital and postoccipital muscle (Figure 4): **Idlm1**, M. prophragma-occipitalis (Sn: 40), **O** (= origin): dorsolaterally on the prophragma, **I** (= insertion): dorsolaterally on the postocciput, close to the insertion of Idlm1b; **Idlm2**, M. pronoto-occipitalis (Sn: 41), **O**:

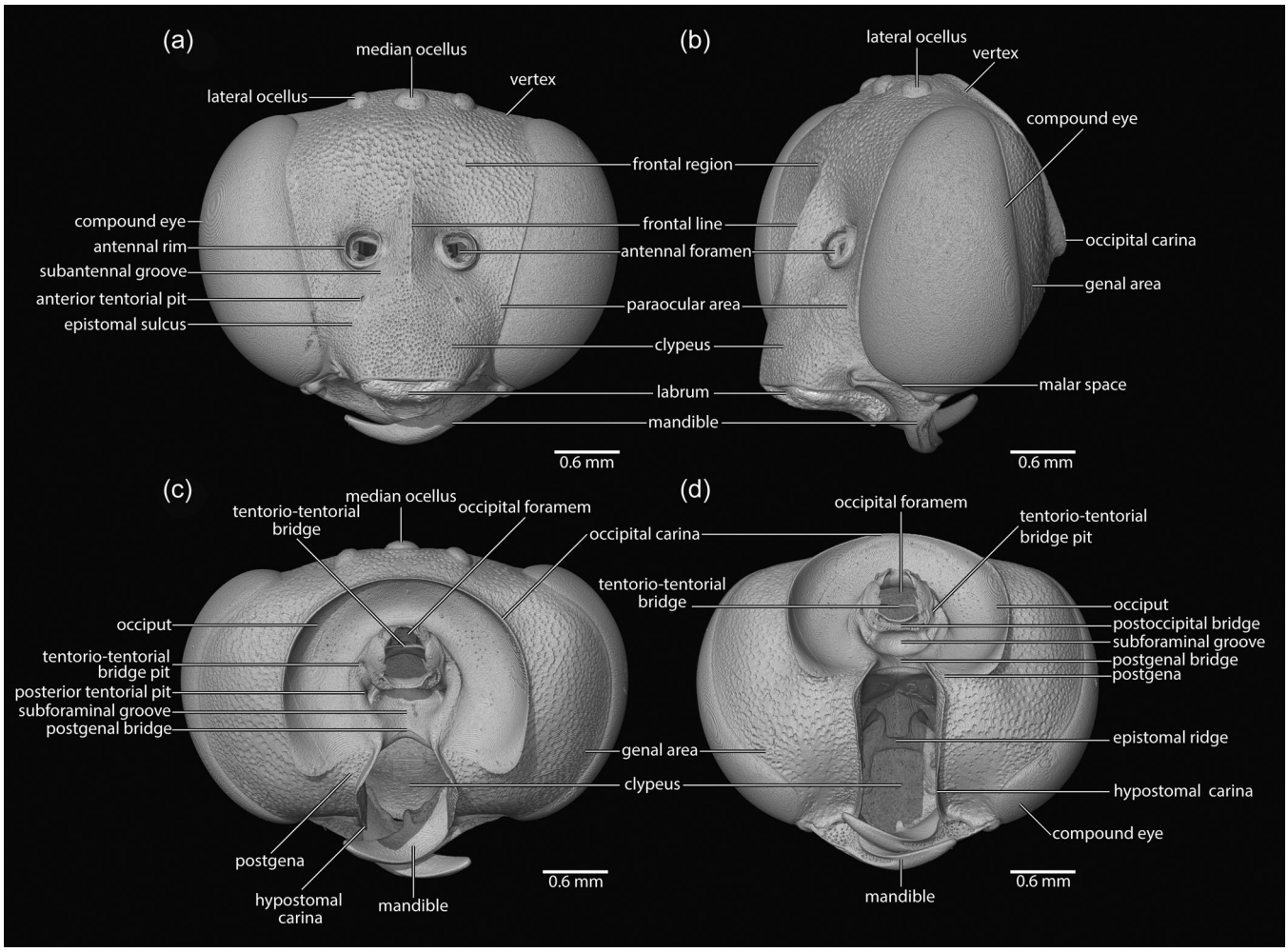

FIGURE 2 External head capsule of *Thyreus albomaculatus*. (a) Anterior view. (b) Anterolateral. (c) Posterior view. (d) Posteroventral view.

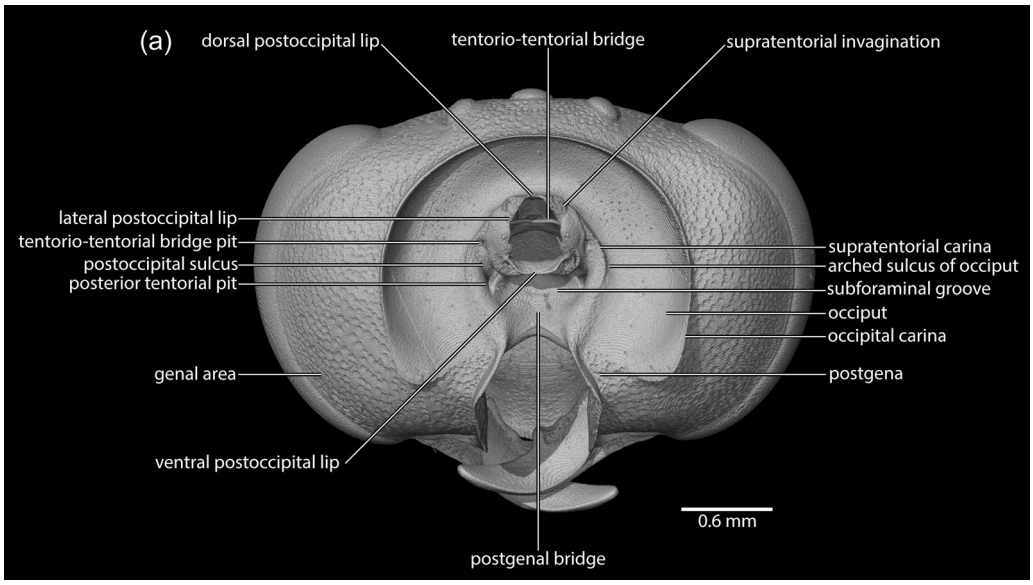

FIGURE 3 Occipital structures of *Thyreus albomaculatus*. (a) Posterior view of the head.

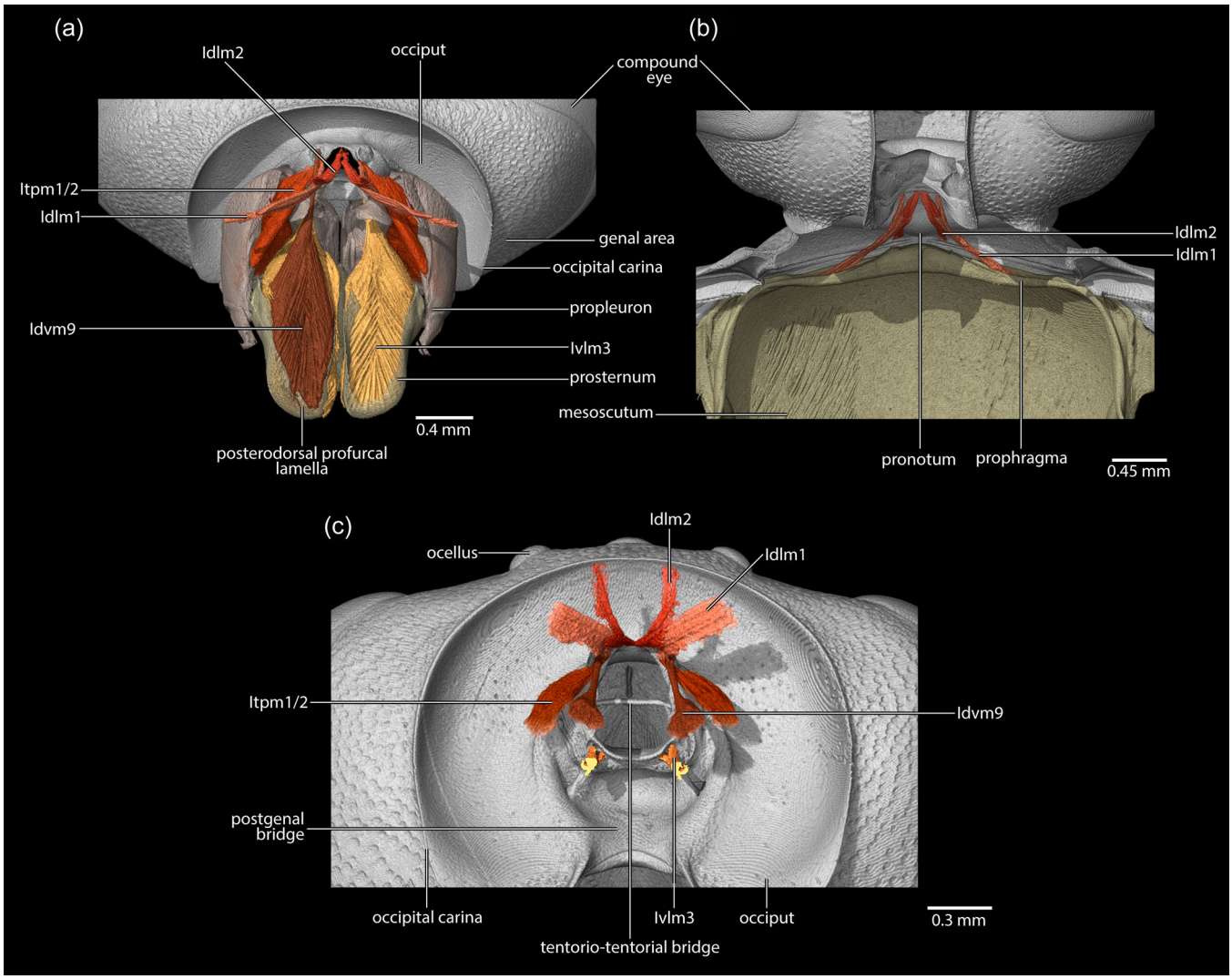

FIGURE 4 Muscles attached to the head of *Thyreus albomaculatus*. (a) Dorsal view of prosternum. (b) Muscles attached to pronotum and prophragma, ventral view of the mesoscutum. (c) Insertion points of prothoracic muscles, posterior view of the head.

dorsomedially on the pronotum, close to the origin of Idlm5b, **I**: dorsomedially on the postocciput, close to the insertion of Idvm9; **Itpm1**, M. pleurocrista-occipitalis (Sn: 42a), a thin muscle, **O**: dorsal propleural margin, posteromediad Itpm3, **I**: laterodorsally on the postocciput, close to Idvm9, on a tendon shared with Itpm2a and Itpm2b; **Itpm2a**, M. propleuro-occipitalis dorsal (Sn: 42b), **O**: on the ventral propleural area, dorsad Itpm2b, **I**: laterodorsally on the postocciput, close to Idvm9, on a tendon shared with Itpm1; **Itpm2b**, M. propleuro-occipitalis ventral (Sn: 42c), **O**: on the ventral propleural area, ventrad Itpm2b, **I**: laterodorsally on the postocciput, close to Idvm9, on a tendon shared with Itpm2; **Idvm9**, M. profurca-occipitalis (Sn: 43), a broad profurcal muscle, **O**: dorsally on the anterodorsal and posterodorsal profurcal lamellae on the posterior profurcal branch, above the origin of Ivlm3, **I**: dorsolaterally on the postocciput, close to the insertion of Itpm1/2; **Ivlm3**, M. profurca-tentorialis (Sn: 44), a broad profurcal muscle, **O**: dorsally on the anterior and posterior profurcal branch, below the origin of muscle Idvm9, **I**: ventrolaterally on the postocciput close to the posterior tentorial pit.

3.1.2 | Cephalic endoskeleton (Figures 5–8)

The cephalic endoskeleton (Figures 5–7a and 8) is strongly developed. The tentorium is complete and forms a complicated 3D structure that fuses with the hypostoma and postgena (Figures 5a,b, 6a–d, and 7a). Separate and externally visible invagination pits are present for the short and broad posterior tentorial arms, that is, the posterior tentorial pits (Figures 2c and 3), which are separated just ventrad the **tentorio-tentorial bridge pits** (Figure 3c,d), with both pairs of external openings located ventrolaterad and laterad the occipital foramen, respectively. The tentorio-tentorial bridge (Figures 2c,d, 3, 5b, 6a–e, and 7a) is slightly arched and hollow. The anterior tentorial arms laterally connect with the composite lamella (Figures 5c,d, 6a,b,e,f, and 7a) that is formed by the **tentorio-postgenal bridge** and the hypostoma. Medially on the **composite lamella**, there is a weakly developed ridge that appears to be a remnant of the postgenal ridge (Figures 6a,b,e and 7a) in *T. albomaculatus*, and extends to the

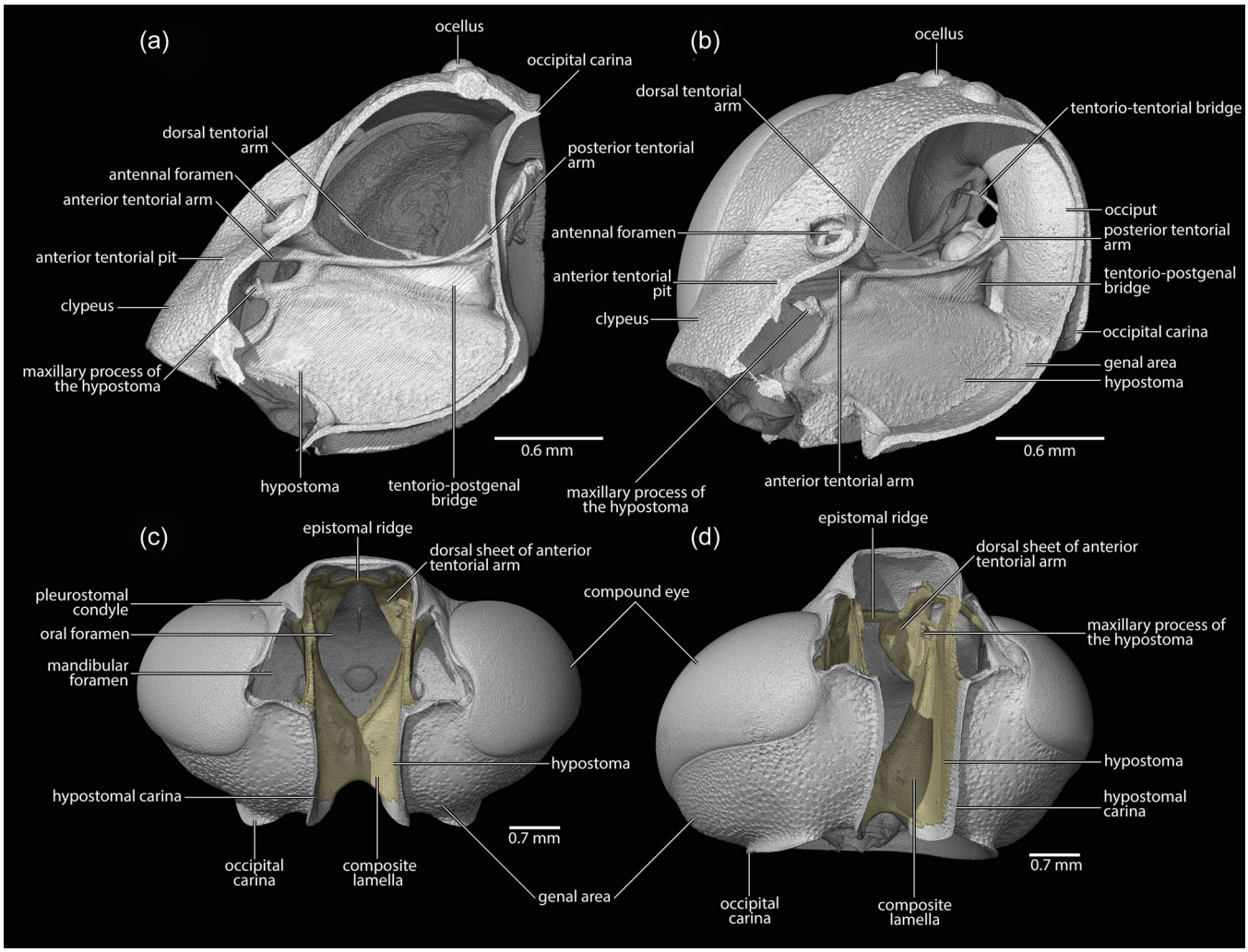

FIGURE 5 Head and cephalic endoskeleton of *Thyreus albomaculatus*. (a) Head, hypostoma, and tentorium, lateral view of the head. (b) Head, hypostoma, and tentorium, anterolateral view of the head. (c) Head, hypostoma, and tentorium, oral view of the head. (d) Head, hypostoma, and tentorium ventrolateral view of the head.

tentorio-postgenal ridge (Figures 6b,e and 7a). Anteriorly, another connection is present between the hypostoma and the anterior tentorial arm, the **tentorio-hypostomal bridge** (Figures 5a,b, 6a–d, and 7a), which is recognizable as a lateral triangle between the tentorio-postgenal ridge and the **hypostomal ridge** (Figures 6b and 7a). The anterior tentorial arms originate from the small anterior tentorial pits (Figures 2a, 5a,b, 6a–e, and 7a); internally, their proximal portions are massive and extend broadly along the posterior clypeal margin, forming the dorsal sheet of the anterior tentorial arm (Figures 5c,d, 6c–f, and 8a,b), which connects the anterior tentorial arm to the antennal foramen; the broad expansions are mesally directed projections and fused with the epistomal ridge (Figures 2d, 5c,d, 6e,f, and 8a,b). The dorsal tentorial arm (Figures 5a,b, 6b–e, and 7a) originates medially on the anterior tentorial arm and is medially directed but does not connect to the antennal foramen. An anterior hypostomal extension forms the maxillary process of the hypostoma (Figures 5a,b,d, 6c,d,f, and 7a) for reception of the proximal part of the cardo.

3.1.3 | Labrum (Figure 9)

The well-developed, flap-like labrum (Figure 9a–d) is movably attached to the anterior clypeal margin (Figure 9a); it is posteriorly directed at rest, almost horizontally oriented, and covers the proximal portion of the maxillolabial complex (= labiomaxillary complex, e.g., Michener, 1944); its lateral margin is slightly curved (Figure 9b,d) and its anterior margin slightly convex (Figure 9b,d), completely lacking a median notch or concavity; the upper surface is slightly convex proximally and slightly concave distally. A sharp edge with a short median tip is followed by a transverse concavity (Figure 9c). Short setae are inserted at the distal edge (Figure 9b,d). The dorsal and ventral labral walls lie closely together, with the latter forming the anteriormost part of the epipharynx. No typical tormae are present, but approximately cone-shaped posterolateral convexities close to the rounded posterolateral corners of the labrum.

Labral muscles (Figures 9d and 15a): **0lb1**, M. frontolabralis (Sn: 1), **O**: medially on the frontal region, distinctly anterior to the ocelli and

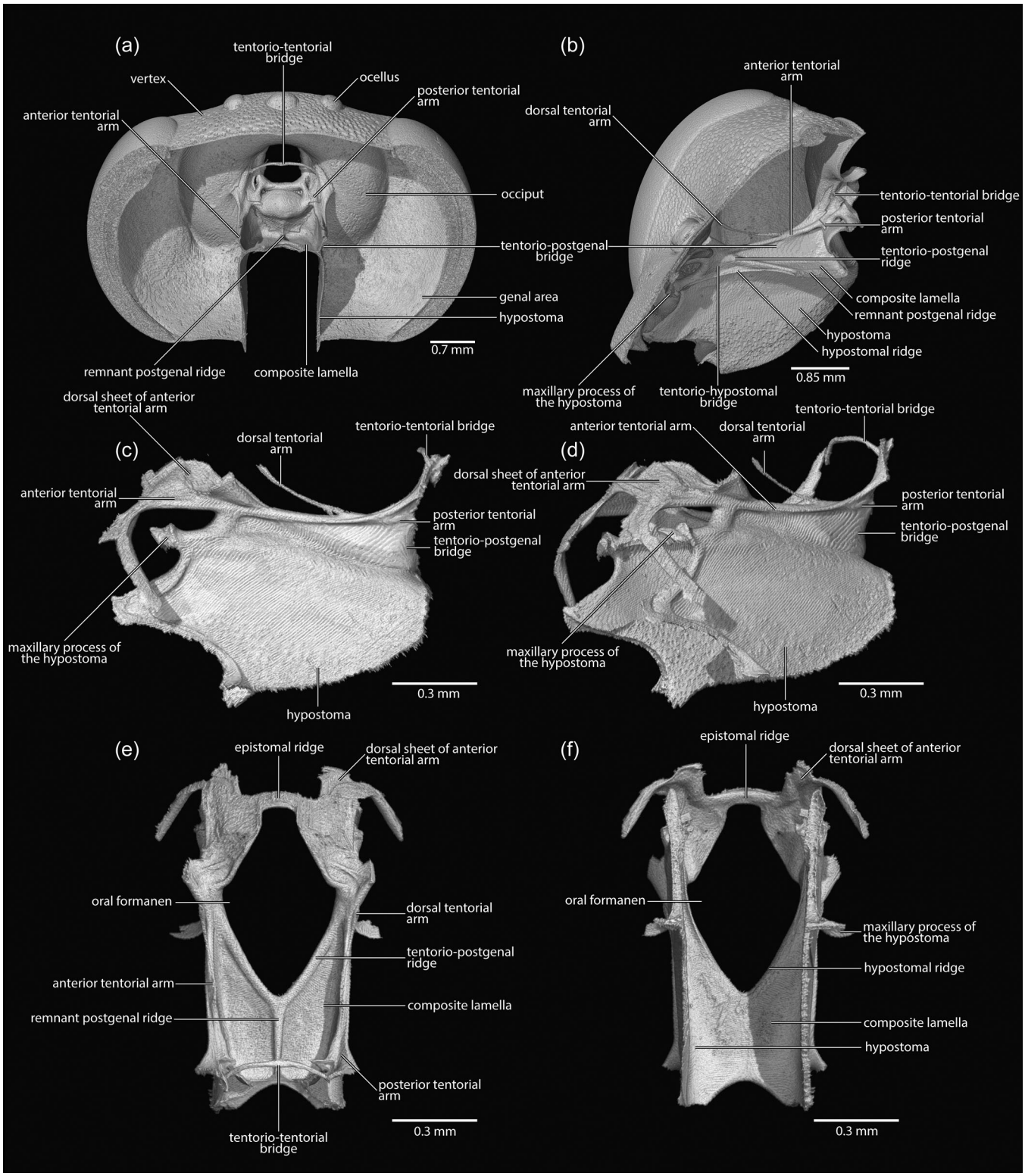

FIGURE 6 Cephalic endoskeleton of *Thyreus albomaculatus*. (a) Head, hypostoma, and tentorium, anterodorsal view of the head. (b) Head, hypostoma, and tentorium, anteromesal view of the head. (c) Hypostoma and tentorium, lateral view of the hypostoma. (d) Hypostoma and tentorium, anterolateral view of the hypostoma. (e) Hypostoma, epistomal sulcus, and tentorium, dorsal view of the hypostoma. (f) Hypostoma, epistomal sulcus, and tentorium, ventral view of the hypostoma.

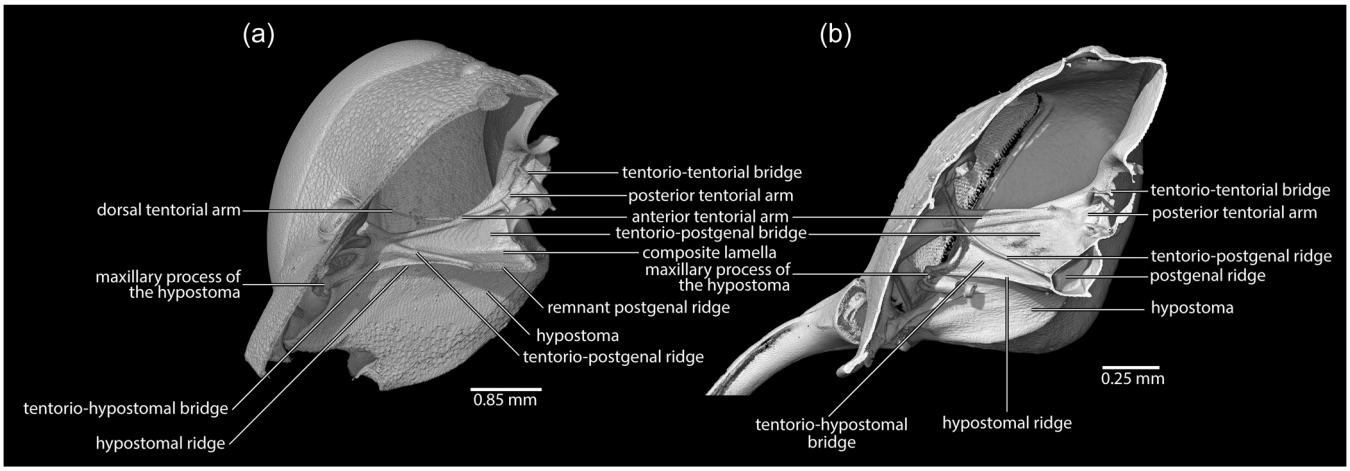

FIGURE 7 Comparison of the cephalic endoskeleton of bees. (a) Head of *Thyreus albomaculatus*, anterolateral view. (b) Head of a male of *Andrena* sp., anterolateral view.

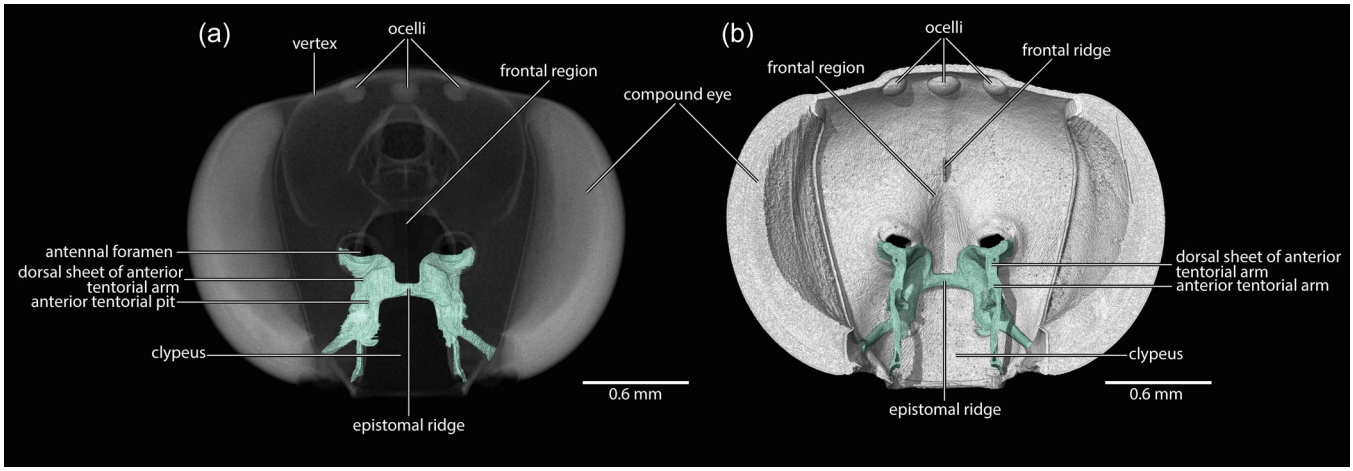

FIGURE 8 Epistomal sulcus of *Thyreus albomaculatus*. (a) Head and epistomal sulcus through transparency, head capsule semitransparent, anterior view of the head. (b) Head and epistomal sulcus, posterior view of the head.

mesad the anterior subunit of 0hy1, with only a small part attached to the median frontal ridge, **I**: mesally on the cone-shaped lateral convexities of the labrum on the oral surface.

3.1.4 | Antennae (Figure 10)

The antenna is compact and short, not reaching the posterior margin of the mesosoma. The scape (Figure 10a,b) is elongate, curved, very slightly widening distally; a basal semi-spherical bulb is separated from the cylindrical main part of the segment by a very deep constriction. The pedicel (Figure 10b) is small, with a maximum length of 1/5 of the scape, and narrower, subcylindrical, widening slightly distally. The flagellum 1 is ca. 2.5 times as long as the pedicel; it is slightly widening distally and has an oblique distal edge; flagellomeres 2–9 are almost as long as 1 and the general structure is cylindrical; they are very tightly connected without exposed articulatory membranes and forming a very compact structural unit; their distal edges are oblique; the apical flagellomere (F10) is of similar length but cone-shaped and apically acuminate.

Antennal muscles (Figure 10a,b): **0an1**, M. tentorioscapalis anterior (Sn: 5), a well-developed bundle converging on a thin tendon, **O**: composite lamella of the cephalic endoskeleton, **I**: anteromesally on the base of the scapus; **0an2-4**, Mm tentorioscapalis posterior (Sn: 2), lateralis (Sn: 3), and medialis (Sn: 4), all of similar shape as 0an1, also converging on a thin tendon, **O**: composite lamella of the cephalic endoskeleton, **I**: each with a thin tendon on the scapal base, dorsomesally, dorsolaterally and ventrolaterally; the exact homology is ambiguous. Both intrinsic antennal muscles are well-developed; **0an6**, M. scapopedicellaris lateralis (Sn: 6), **O**: middle region of the anterior wall of the cylindrical main part of the scapus, **I**: laterally on the pedicellar base; **Oan7**, M. scapopedicellaris medialis (Sn: 7), larger than 0an6, **O**: basal and middle regions of the lateral wall of the scapus, **I**: mesally on the base of the pedicel.

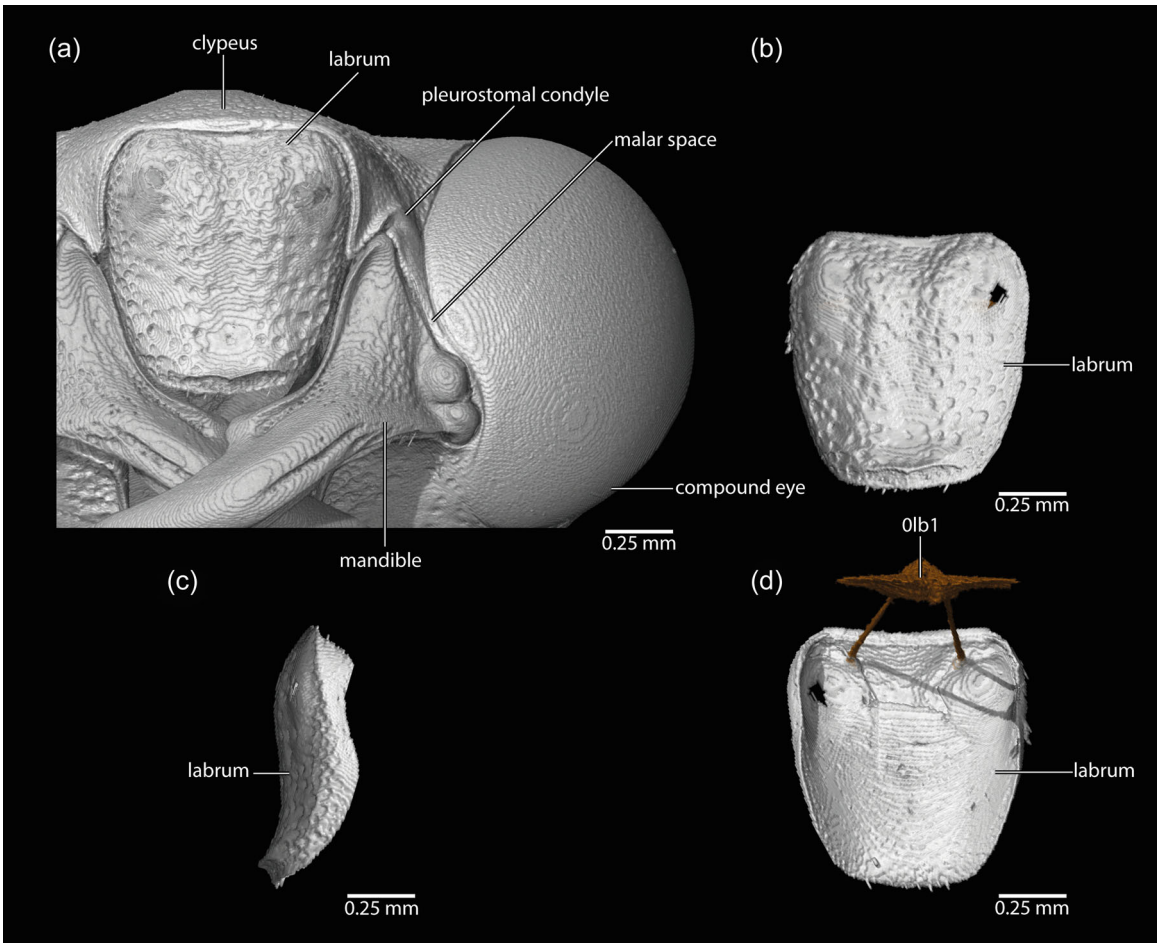

FIGURE 9 Labrum of *Thyreus albomaculatus*. (a) Labrum and head, anteroventral view of the head. (b) Labrum, posterior view. (c) Labrum, lateral view. (d) Labrum and labral musculature, ventral view of the labrum.

3.1.5 | Mandibles (Figure 10)

The well-developed mandibles (Figure 10c,d) are largely symmetrical, relatively slender, almost falcate, and distinctly intercrossing medially in their resting position; their articulations are dicondylic (Figure 10c). The basal part is triangular in cross-section (Figure 10c) and forms the mandibular acetabulum (Figure 10c) that inserts into the pleurostomal condyle (Figures 5c and 9a). From the acetabulum a straight line reaches the abductor swelling and the mandibular condyle that lie close together (Figure 10c). The curved adductor angle (Figure 10c) is located internally in this triangular basal part. The mesal mandibular base is slightly convex but a mola is not developed. A relatively slender, curved, and apically acuminate apical tooth (Figure 10c,d) is more than 1/3 as long as the entire mandible. The carina mandibularis (Figure 10d) extends over the proximal 2/3 of the mandible; it separates the mesal area from the dorsal surface. A distinct mesal concavity is present in the middle region of the mandible, dorsally delimited by the carina mandibularis, and ventrally by a curved blunt edge enclosed by two asymmetrical and apically blunt teeth (Figure 10d). On the outer surface of the mandible, three distinct grooves can be observed. The condylar groove (Figure 10c) extends from the mandibular condyle to nearly the apical tooth. Parallel to this, the outer groove (Figure 10c) runs alongside. Additionally, the acetabular groove (Figure 10c) runs from the mandibular acetabulum to the median area of the outer surface.

Mandibular muscles (Figure 10c,d): **0md1**, M. craniomandibularis internus (vK: M. 11; Sn: 9), the largest muscle of the head, composed of several subcomponents and numerous fibers, **O**: very large surface area of the upper 2/3 of the head capsule, **I**: with the strongly developed, broad adductor tendon on the mesal mandibular base; **0md2**, M. craniomandibularis externus (vK: M. 12; Sn: 8), about 1/3 of the volume of M. 11, **O**: posteroventrally on the head capsule, laterad the oral foramen, **I**: with the comparatively narrow abductor tendon on the lateral edge of the mandible; **0md6**, M. tentorio-mandibularis (vK: M. 13; not observed by Snodgrass [1942]), a single thin bundle, **O**: ventrally from the anterior end of the anterior tentorial arm, **I**: dorsomesally on the inner surface of the mandible.

3.1.6 | Maxillolabial complex (Figures 11–13)

The maxillae and the labium form the maxillolabial complex (Figure 11a–d), which functions as the main element of the food

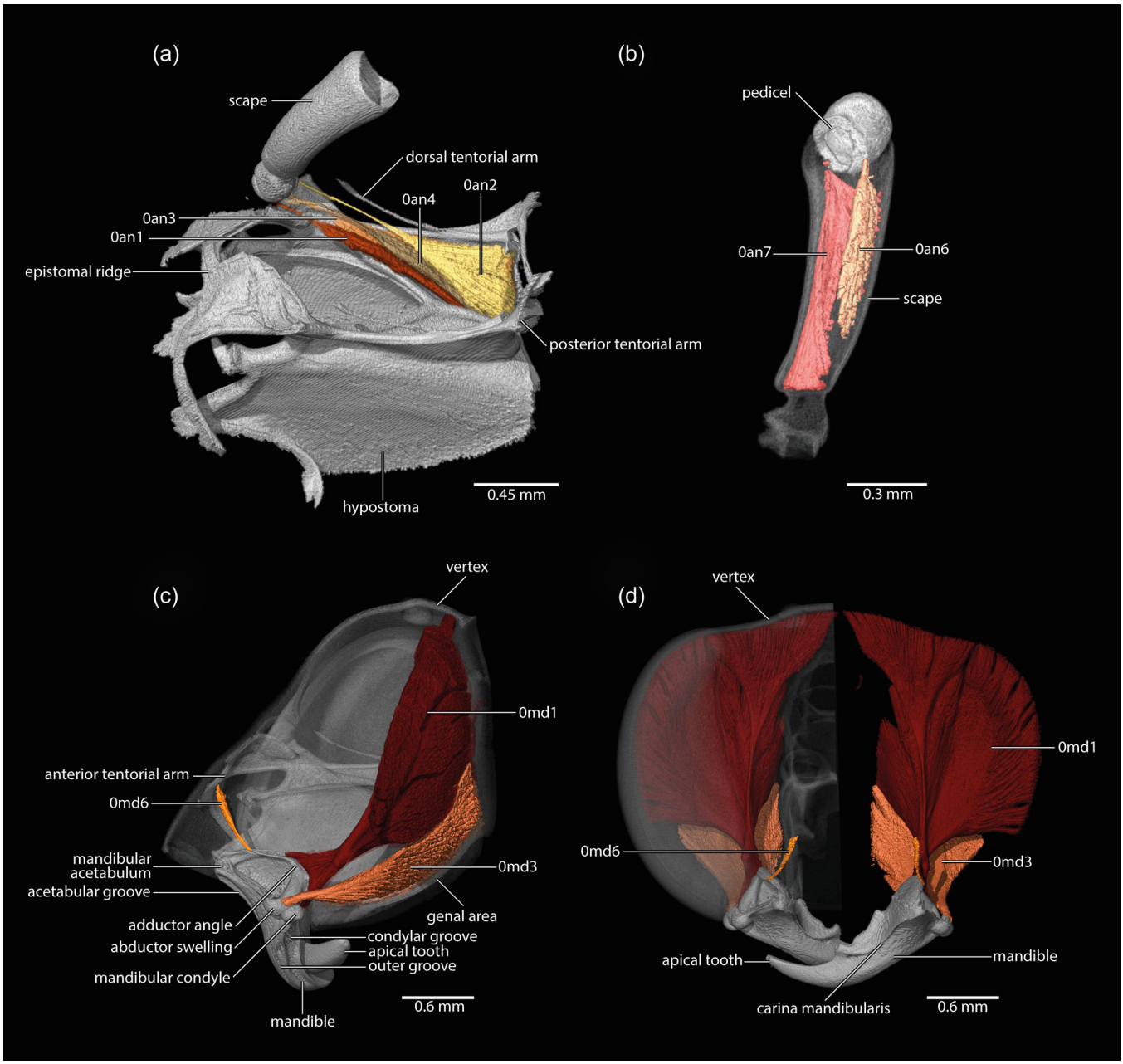

FIGURE 10 Antennal and mandibular musculature of *Thyreus albomaculatus*. (a) Hypostoma, tentorium, scape, and extrinsic antennal musculature, dorsolateral view of the hypostoma. (b) Scape, pedicel, and intrinsic antennal musculature, scape semitransparent, anterior view. (c) Head, hypostoma, tentorium, mandible, and mandibular musculature, head semitransparent, lateral view of the head. (d) Mandible and mandibular musculature, head semitransparent, anterior view of the head.

uptake apparatus, that is, the "tongue"; it is inserted in the membranous area covering the hypostoma; in its folded condition the entire structure is ca. 2.45 mm long. The elongated, rod-like, and seemingly bipartite cardo (Figures 11b–d and 12f) forms the proximal articulatory element of the maxillary part; the bifid apex of its thin proximal element articulates with the anterior maxillary process of the hypostoma. The stipes (Figures 11b,d and 12a,b,e,g) articulates with the cardinal apex; it forms the lateral element of the maxillolabial complex; it is as long as the entire folded structure, narrowed proximally but approximately parallel-sided over most of its length, and apically truncated with rounded edges; a hook-shaped structure (Figure 12b) is present on its dorsal edge at about 1/3 of the length; apically it articulates with the galea (Figures 11b,d and 12e,g); the maxillary palp (Figure 12b) is small and 2-merous. The large galea (Figures 11a,b,d and 12c,d,e,g) is slightly longer than the stipes; its lower edge is evenly rounded, and it narrows towards its rounded apex. The lacinia is indistinct, present as a vestigial lobe-like structure not visible in the scan data, hence not illustrated here.

The main portion of the postmentum is subdivided into a small, narrow median lobe (Figure 11b,c) and an intermediate subcomponent;

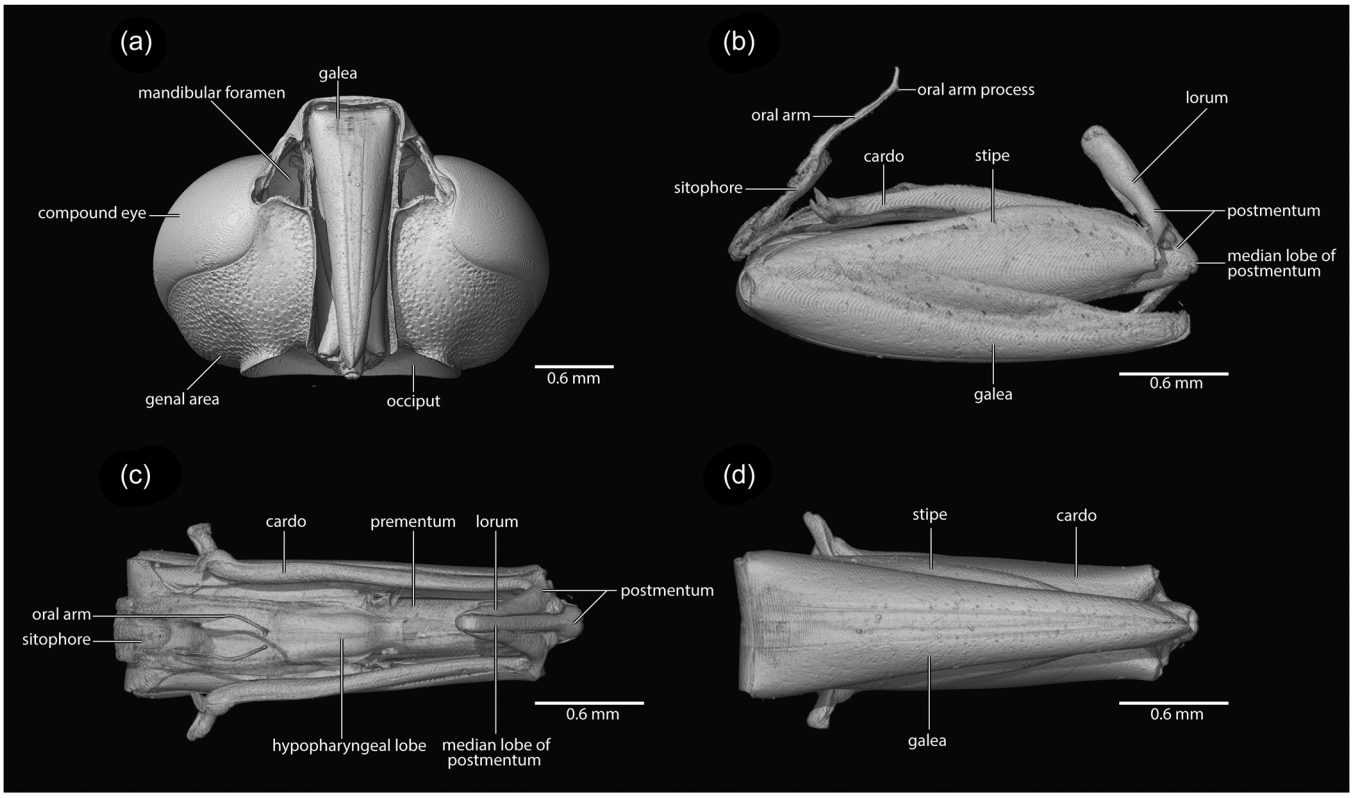

FIGURE 11 Maxillolabial complex of *Thyreus albomaculatus*. (a) Head and maxillolabial complex, ventral view of the head. (b) Maxillolabial complex, lateral view of the stipe. (c) Maxillolabial complex, dorsal view of the prementum. (d) Maxillolabial complex, ventral view of the prementum.

it is implanted in the hypostomal membrane and parallel-sided over most of its length but distinctly widened and almost knob-like distally; the V-shaped lorum (Figure 11b,c), a specialized postmental element, articulates with the median lobe base of the postmentum and connects it with the cardinal bases (Figure 11b,c). The large prementum (Figures 11c, 13b–d, and 14a,b), the main ventral element of the maxillolabial complex, articulates with the widened distal part of the postmentum (Figure 11c); it is slightly longer than the stipites, of triangular to parabolic shape, narrow proximally, and evenly widening distally; the cuticle in the median region appears thinner and forms a very faintly impressed longitudinal furrow. The apical margin of the prementum (Figure 14a) is almost straight, only very slightly concave, with acute apicolateral edges. The unsclerotized hypopharynx forms the upper wall of the prementum; it is flanked by the rod-like premental ligular arms (Figures 13c,d and 14b). The salivary opening lies at the distal hypopharyngeal margin. The long glossae (Figure 13b,d) form the tube-like tongue; this elongate structure is basally coiled within the prementum. The paraglossae (Figure 13b,d) are present at its base as short, lobe-like structures. The labial palps (Figure 13b,c) are slender and rod-like and almost as long as the prementum; the proximal segment comprises ca. 80% of the total length; the distal portion of the palp is bent outwards.

Maxillary muscles (Figure 12e–g): **0mx1**, M. craniocardinalis externus (vK: M. 15; Sn: 10), a large, flattened, fan-shaped muscle, **O**: large area of the inner surface of the hypostoma and genal area, **I**: on the base of the cardo by means of a strongly developed tendon; **0mx3**, M. tentoriocardinalis (vK: M. 17; Sn: 11), a thin bundle, **O**: from the clypeus, close to the origin of the anterior tentorial arm, **I**: distally on the cardo, at the articulation with the stipes; **0mx4**, M. tentoriostipitalis anterior (Sn: 12), **O**: on the clypeus, anterior to 0mx3, **I**: inner surface of the posteriormost stipes, sharing a tendon with 0mx5; **0mx5**, M. tentoriostipitalis posterior (Sn: 13), **O**: on the anterior tentorial arm insertion, posterior to 0mx3, **I**: inner surface of the posteriormost stipes, sharing a tendon with 0mx4; **0mx6**, M. stipitolacinialis (vK: M. 20; Sn: 16), a well-developed muscle, **O**: basal region of stipes, **I**: base of vestigial lacinia; **0mx7**, M. stipitogalealis (vK: M. 21; Sn: 15), a well-developed muscle, **O**: middle region of stipes, **I**: base of galea. The intrinsic muscle of the maxillary palp described by Snodgrass (14, muscle of the maxillary palpus, 1942) is absent; **0mx2.** M. craniolacinialis (vK: M. 19) is also missing.

Labial muscles (Figure 13a–d): **0la5**, M. tentoriopraementalis (vK: M. 29; Sn: 18), a long muscle, slender over most of its length and connected with a thin tendon, but distinctly widening towards its area of origin (of somewhat irregular shape in the µ-CT scan), **O**: area of origin of the anterior tentorial arm, close to the origin of 0mx3, **I**: base of the prementum with a thin tendon; **0la6**, M. tentorioparaglossalis (vK: M. 31; Sn: 17), an extremely elongated, zigzag-shaped muscle, **O**: laterally on the postoccipital ridge, **I**: on the base of the paraglossae; **0la11**, M. praementoparaglossalis (vK: M. 31; Sn: 19), a well-developed slender muscle with a thin tendon, **O**: posterior prementum, **I**: basal region of ligular arm; **0la12**, M. praementoglossalis (vK: M. 32; Sn: 20), similar to 0la11 in shape, **O**: posterior

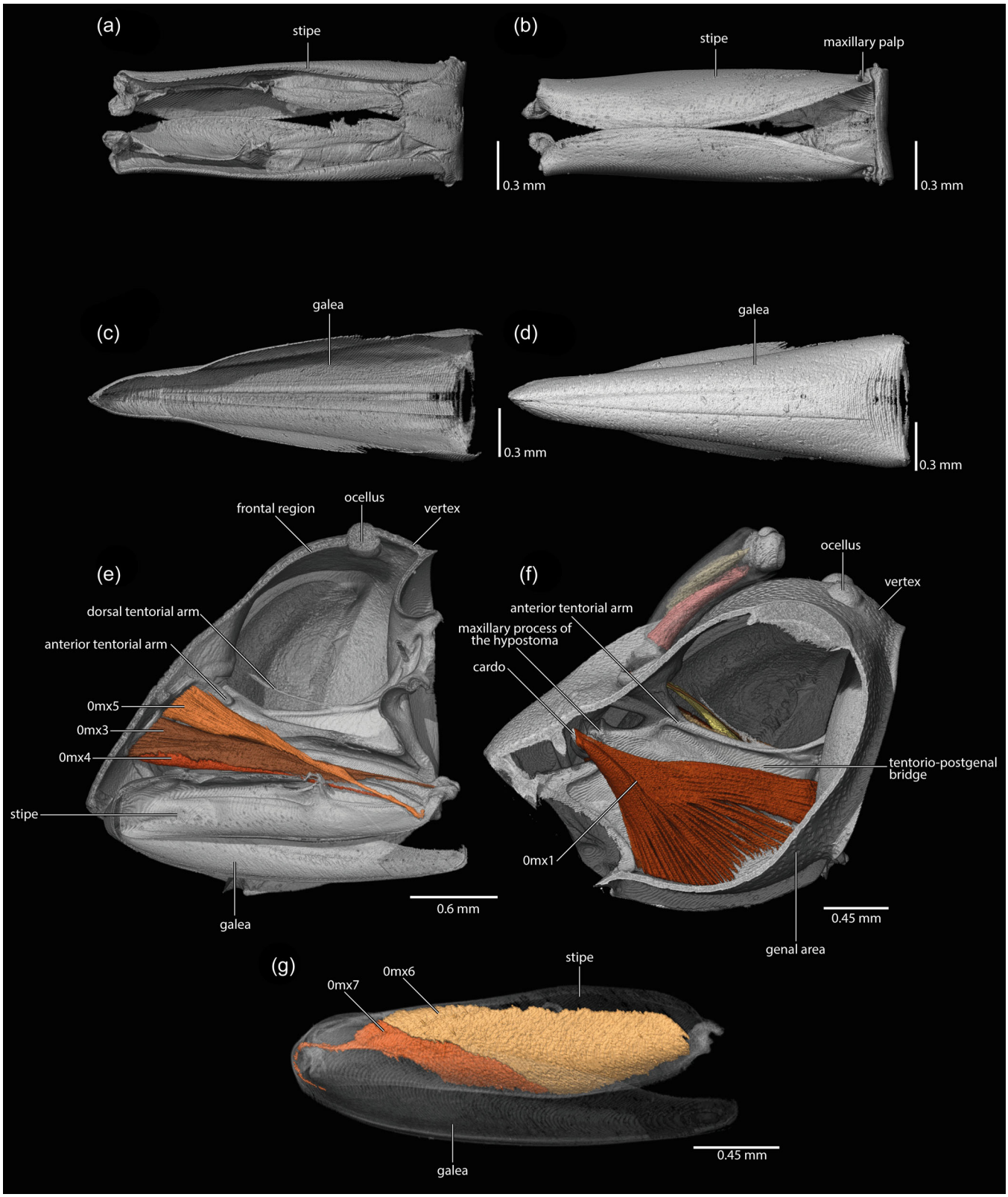

FIGURE 12 Maxillary musculature of *Thyreus albomaculatus*. (a) Stipe, dorsal view. (b) Stipe, ventral view. (c) Galea, dorsal view. (d) Galea ventral view. (e) Head, maxilla, and extrinsic maxillary musculature, lateral view of the head. (f) Head, hypostoma, tentorium, maxillary process of the hypostoma and cardo, lateral view of the head. (g) Maxilla and intrinsic maxillary musculature, sclerotized parts semitransparent, lateral view of the stipe.

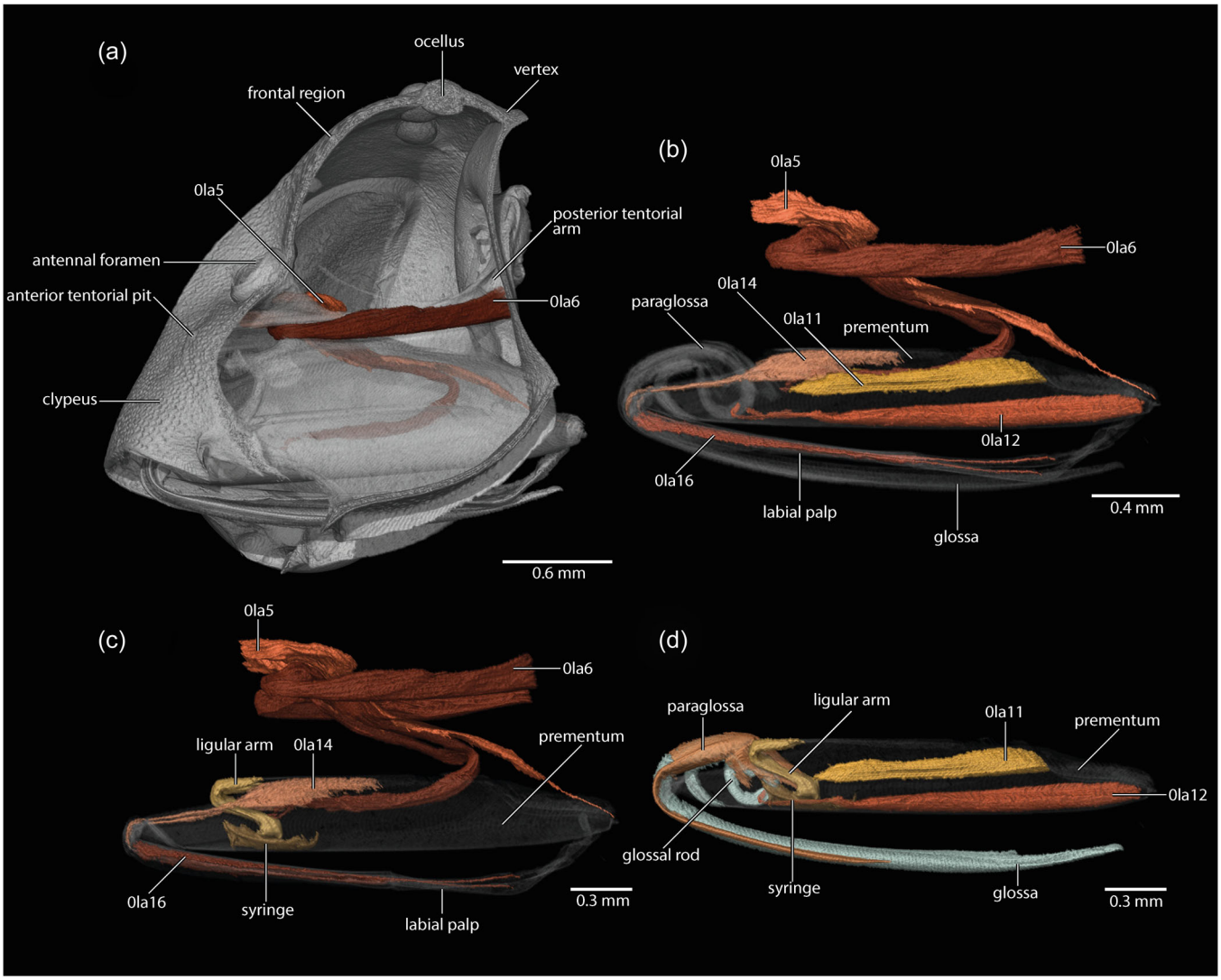

FIGURE 13 Labial musculature of *Thyreus albomaculatus*. (a) Head and extrinsic labial musculature, hypostoma semitransparent, lateral view of the head. (b) Labium, extrinsic and intrinsic labial musculature, sclerotized parts semitransparent, lateral view of prementum. (c) Extrinsic labial muscles and labial palpi musculature, sclerotized parts semitransparent, lateral view of prementum. (d) Intrinsic labial musculature, prementum semitransparent, lateral view of prementum.

prementum, very close to 0la11, **I**: glossal rods; **0la14**, M. praementopalpalis externus (vK: M. 34; Sn: 21), **O**: from the lateral wall of anterior half of the prementum, **I**: on the base of palpomere 1; **0la16**, M. palpopalpalis labii primus (vK: M. 35; Sn: 22), a very long and thin muscle, **O**: basal region of palpomere 1, **I**: base of palpomere 2; **0la17**, M. palpopalpalis labii secundus, (vK: M. 36), absent; **0la8**, M. submentopraementalis (Vk: M. 28), absent; **0la5**, M. tentoriopraementalis superior (vK: M. 30), absent; **0la13**, M. praementopalpalis internus (vK: M. 33), absent.

3.1.7 | Preoral cavity (Figure 14)

µ-CT scans are not optimal for describing and visualizing membranous structures, which impedes the documentation of some parts of the preoral cavity. Therefore, the epipharynx and hypopharynx and also elements of the salivarium will not be resolved in detail here. A deeper treatment of these structures can be found in Snodgrass (1942).

Together with the labium, bees have what is known as the sucking pump, a structure with walls equipped with a complex system of various muscles and extending from the functional mouth opening to the constriction of the esophagus. This cephalic digestive tract is subdivided into an anterior part, traditionally termed the cibarium, and a posterior part termed the pharynx. The former is composed of epipharyngeal and hypopharyngeal elements including sclerotized oral arms and is partly open laterally but posteriorly closed as a prepharyngeal tube. The latter is a closed tube enclosed by a ring muscle layer and starting with the anatomical mouth opening below the frontal ganglion. As the muscles of the preoral cavity in bees

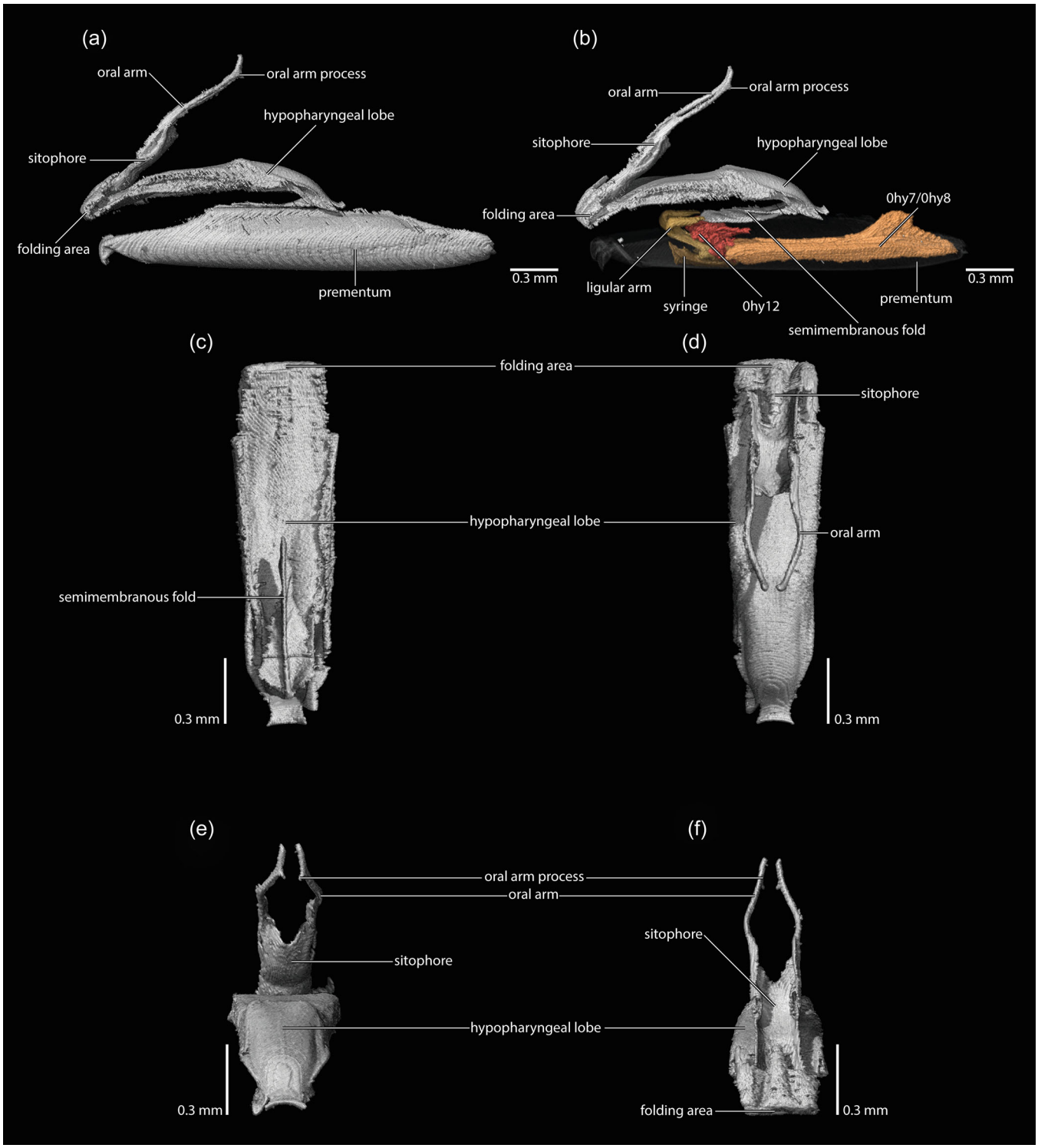

FIGURE 14 Pharyngeal plate of *Thyreus albomaculatus*. (a) Pharyngeal plate and prementum, lateral view of prementum. (b) Pharyngeal plate, prementum, and intrinsic hypopharyngeal musculature, prementum semitransparent, lateral view of prementum. (c) Pharyngeal plate, ventral view of hypopharyngeal lobe. (d) Pharyngeal plate, dorsal view of hypopharyngeal lobe. (e) Pharyngeal plate, posterior view of hypopharyngeal lobe. (f) Pharyngeal plate, anterior view of hypopharyngeal lobe.

generally attach to the specialized sclerite termed pharyngeal plate, we will describe this structure and the cibarial musculature together and subsequently the pharyngeal musculature, composed of ring muscles, longitudinal muscles, and dorsal dilators.

3.1.8 | Pharyngeal plate (Figures 14 and 15)

The pharyngeal plate (Figure 14a–f), often termed "oral plate" or "sitophore" by previous authors (Michener, 1944; Snodgrass, 1942;

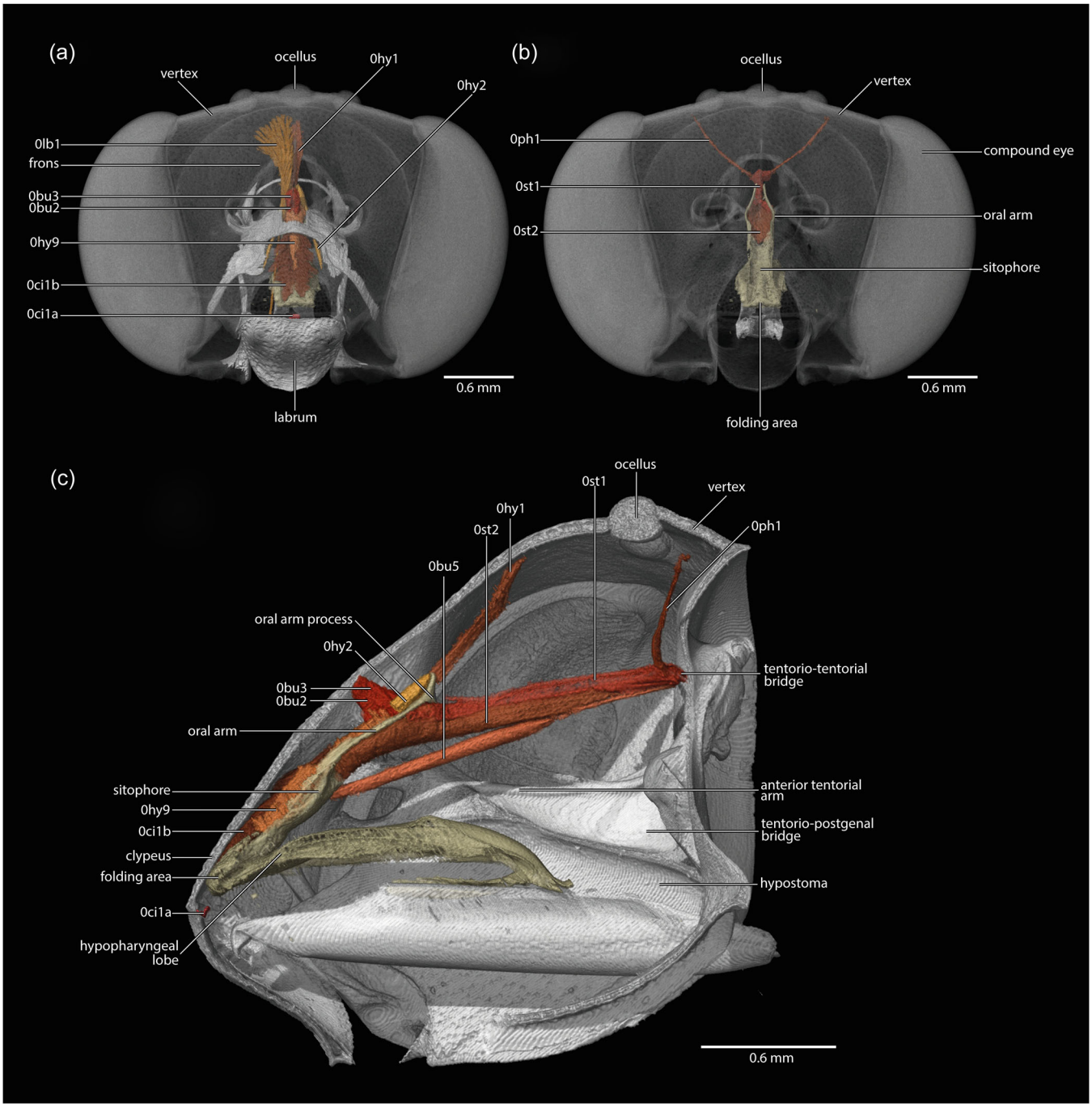

FIGURE 15 The sucking pump of *Thyreus albomaculatus*. (a) Labral, cibarial, and hypopharyngeal musculature, head semitransparent, anterior view of the head. (b) Pharyngeal musculature, head semitransparent, anterior view of the head. (c) Labral, cibarial, hypopharyngeal, and pharyngeal musculature, lateral view of the head.

Vilhelmsen, 1996), is a sclerite located on the anteriormost portion of the sucking pump, anterior to the pharynx and adjacent to the functional mouth anteriorly, that is, the external opening of the cibarium. This plate-like structure is composed of three, sometimes not well-delimited regions, being the sitophore, oral arms, and hypopharyngeal lobe. The sitophore (Figures 14a,b,d–f and 15b,c) is a sclerotized rectangular plate, proximal to the functional mouth opening that bears the opening of the salivary glands (not visible in the renders). From the sitophore, paired rod-like supporting structures posterodorsally extend into the pharynx, the oral arms (*sensu* Zimmermann & Vilhelmsen, 2016) (Figures 14a,b,d–f and 15b,c); close to the apex of these rods the oral arm process (Richter et al., 2023) is present as a spine-like structure (Figure 14a,b,e,f). Ventrad the sitophore, a folding area (Figures 14a–d,f and 15b,c) demarks the separation between the sitophore and hypopharyngeal lobe. The latter (Figures 14a–f

and 15b,c) extends anteroventrally and is connected with the prementum by a feebly sclerotized semimembranous fold (Figure 14b).

Hypopharyngeal lobe muscles (Figure 14b): **Ohy12**, M. hypopharyngosalivarialis (vK. M. 37; Sn: 23), **O**: dorsolaterally from the anterior part of the hypopharynx, **I**: dorsolaterally on the salivary duct; **Ohy7/8**, M. praementosalivarialis anterior and posterior (vK. M. 38, 39; Sn: 24), one strongly developed bundle, **O**: laterally on the posterior prementum, **I**: ventrolaterally on the sclerotized part of the salivary duct.

Sitophore muscles (Figure 15a–c): **0c1a**, M. clypeopalatalis anterior (Sn: 25), a single stout and short bundle, **O**: medially on the clypeolabral border region, **I**: anteriormost epipharynx; **Oci1b**, M. clypeopalatalis posterior (Sn: 26–30), a series of relatively short posteriorly slanting muscles, **O**: clypeus, **I**: sitophore and oral arm; **0hy9**, M. oralis transversalis (Sn: 31), a transverse muscle over the sitophore, **O**: left side of the sitophore and oral arm, **I**: right side of the sitophore and oral arm; **0bu5**, M. tentoriobuccalis anterior (vK: M. 48; Sn: 37), a well-developed long unpaired muscle, **O**: medially on the tentorial bridge, **I**: ventromedially on the posterior edge of the sitophore (erroneously identified as M. tentoriohypopharyngalis [M. 42] in *Macroxyela* (Beutel & Vilhelmsen, 2007).

Oral arm muscles (Figure 15a,c): **0hy1**, M. frontooralis (Sn: 33), a flattened, triangular muscle attached on a long and thin tendon, **O**: frons, laterad of 0lb1, distinctly anterior to the ocelli, **I**: at the oral arm process proximad on the oral arm at the pharyngeal plate; **Ohy2**, M. tentoriooralis (Sn: 32), **O**: ventrally on the insertion of the anterior tentorial arm, **I**: oral arm process of the oral arm at the pharyngeal plate.

3.1.9 | Pharynx (Figure 15)

The moderately wide pharynx (Figure 15a–c) lies in the upper third of the cephalic lumen; as part of the sucking pump, it extends from the frontal ganglion and oral arm to the esophagus constriction; it is straight over most of its distance but bends abruptly downwards shortly before it reaches the occipital foramen.

Pharyngeal muscles (Figure 15a–c): **0bu2**, **3**, M. frontobuccalis anterior and posterior (vK: M. 45, 46; Sn: 34, 35), a compact unit formed by two well-developed bundles, **O**: mesal region of the anterior frons, **I**: dorsally on the anteriormost pharynx; **0ph1**, M. verticopharyngalis (vK: M. 51; Sn: 36), an extremely thin paired muscle, **O**: dorsal vertexal region, posterior to the lateral ocelli, **I**: dorsally on the postcerebral pharynx, close to the anterior end of the esophagus and the occipital foramen; **0st1**, M. annularis stomodaei (vK; M. 68; Sn: 39), a well-developed ring muscle layer is present over the whole length of the pharynx; **0st2**, M. longitudinalis stomodaei (vK; M. 69; Sn: 38), a well-developed longitudinal muscle is present on the dorsal side of the pharynx; **0bu4**, M. tentoriobuccalis lateralis (vK: M. 49), absent; **0bu6**, M. tentoriobuccalis posterior (vK: M. 50), absent; **0ph2**, M. tentoriopharyngalis (vK: M. 52), absent; **0la5**, M. transversalis buccae (vK: M. 67), absent.

3.2 | Mesosoma of *T. albomaculatus*

The mesosoma (Figure 16) comprises the three thoracic segments (prothorax, mesothorax, metathorax), their appendages, and the first true abdominal segment (propodeum = abdominal segment I). It is approximately spherical, with a pattern of fine punctuation dorsally on the cuticular surface, and less densely spaced ventrally. The maximum diameter of the mesosoma is ca. 3 mm.

3.2.1 | Prothorax (Figures 16a–e and 17–19)

The prothorax bears the head anteriorly and the procoxae posteroventrally; posteriorly, it is connected with the mesothorax. As in other groups of Hymenoptera, it is a highly modified structure. It is divided into the pronotum and a compact subunit comprising the propleurae and the prosternum, which together form the propectus or pleurosternal complex (Snodgrass, 1942).

Pronotum (Figure 16a–e)

The pronotum is a collar-shaped structure but does not fuse ventrally. The dorsomedial area (Figure 16a–c) is narrow, but it widens laterally, where it forms the pronotal lobes posteriorly (Figure 16a,c–e) that are located above the first pair of spiracles. The pronotum encloses a wide opening that surrounds the propectus (Figure 16b,c).

Propleurae *(Figures 16b,c, 17, and 19a,b)*

Each propleuron is a plate of irregular shape, with approximately five sides (Figures 17a,b,f, and 18b); it is subdivided by the lateral propleural margin and propleural carina (Figure 17c) into an exposed ventral region and a concealed lateral area (Figure 17a). On the side of the propleural carina, the distinct lateral propleural groove (Figure 17b,f) extends from near the cervical prominence to almost the posterior margin of the ventral propleural area. In the lateral propleural area (Figure 17c), the dorsal propleural margin (Figure 17a) extends from the cervical apodeme (Figure 17a–c) to the propleural arm (= proepimeral apodeme) (Figure 17c,d) in an approximately straight line; internally it is surrounded by the dorsal propleural ridge (Figure 17a,c) and externally by the anterior lamella of the dorsal propleural margin (Figure 17c). The propleural arm (Figure 17c,d) is approximately straight and bears a thin sheet (Figure 17c) on its posterior margin; the arm is located in the posteriormost propleural area; at its base it bears the posterior process of the dorsal propleural ridge (Figure 17a), which articulates with the anterior profurcal branch of the prosternum (Figure 17e). The posterior margin of the lateral propleural area extends to the lateral propleural margin (Figure 17c); together with the dorsal propleural margin (Figure 17c) it delimits the ventral propleural area (Figure 17a,b,f). The cervical prominence (Figure 17a–c,e) is located on the anteriormost area of the propleuron and forms the articulation of the propleuron with the postoccipital region of the head; one of its subcomponents, a protuberance with trichoid sensilla, is the cervical swelling

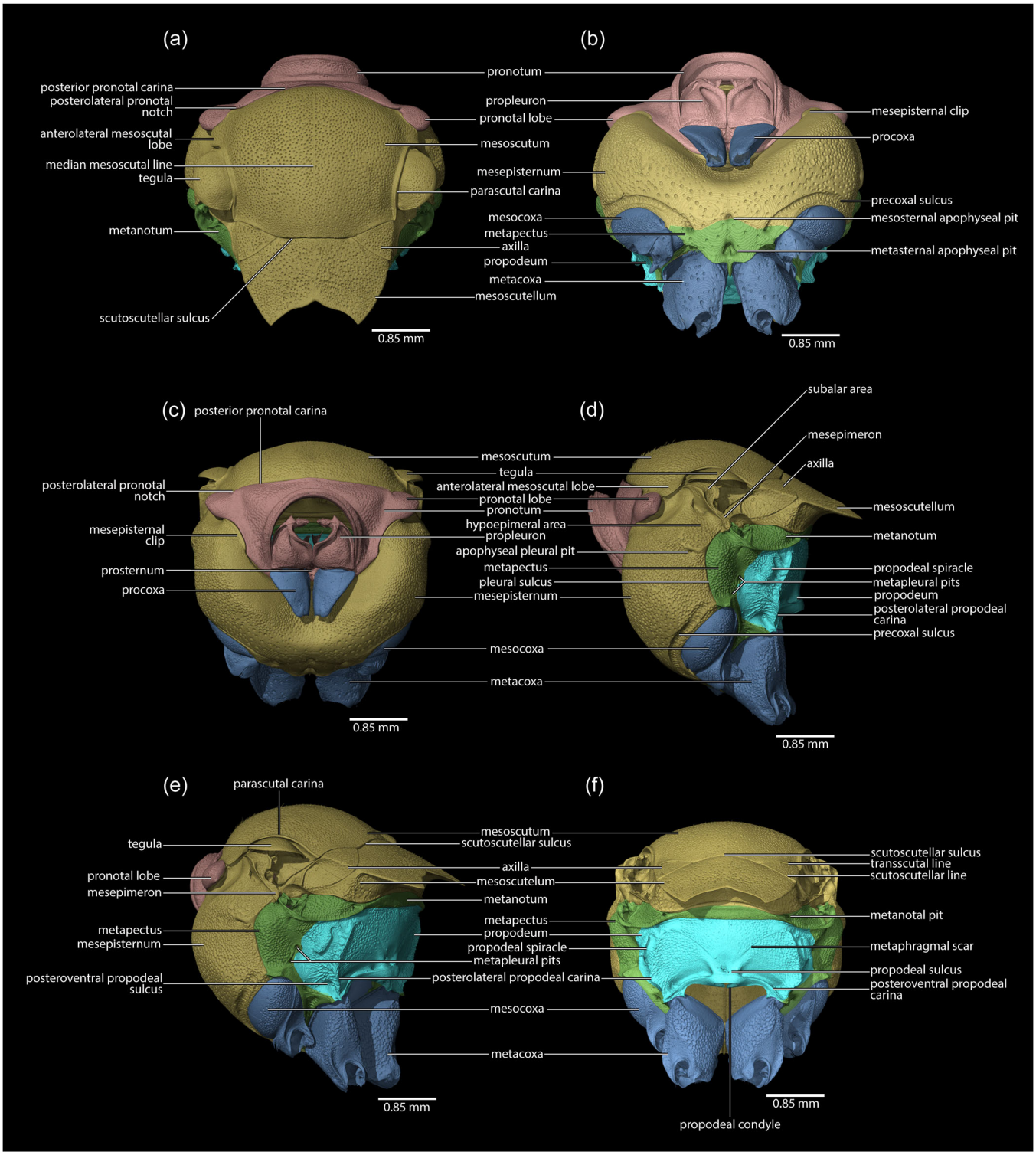

FIGURE 16 Mesosoma of *Thyreus albomaculatus*. (a) Dorsal view. (b) Ventral view. (c) Anterior view. (d) Lateral view. (e) Posterolateral view. (f) Posterior view.

(Figure 17a); anterior to this protuberance the cranial condyle (Figure 17a,b) forms the articulation of the propleuron with the head capsule; posterior to it the cervical apodeme (Figure 17a,c) receives the insertion of prothoracic muscles.

Propleural muscles (Figure 19a,b): **Idvm5a**, M. pronoto-cervicalis anterior primus (Sn: 46), **O**: dorsolaterally on the pronotum, **I**: posteriorly on the cervical apodeme of the propleuron on a tendon shared with Idvm5b; **Idvm5b**, M. pronoto-cervicalis anterior secundus (Sn: 47), **O**: dorsomedially on the pronotum, close to Itpm3, **I**: posteriorly on the cervical apodeme of the propleuron on a tendon shared with Idvm5a; **Itpm3**, M. pronoto-pleuralis anterior (Sn: 48), a relatively broad pronotal muscle, **O**: dorsomedially on the

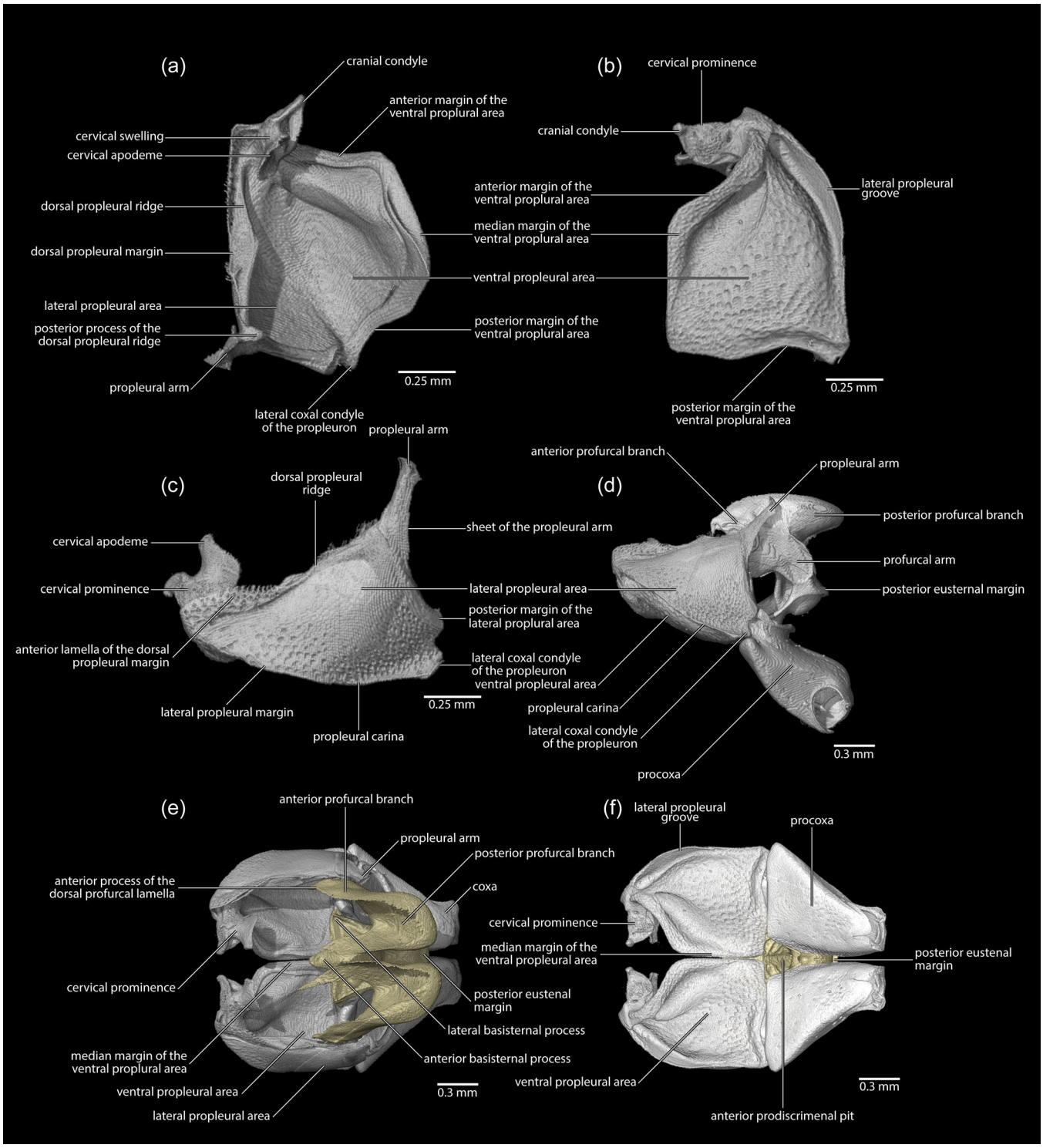

FIGURE 17 Propleuron and propectus (= pleurosternal complex) of *Thyreus albomaculatus*. (a) Propleuron, dorsal view. (b) Propleuron, ventral view. (c) Propleuron, lateral view. (d) Propectus, lateral view of propleuron. (e) Propectus, dorsal view of prosternum. (f) Propectus, ventral view of propleuron.

pronotum, close to the origin of Idvm5b, **I**: on the anterior lamella of the dorsal propleural margin; **Itpm4**, M. pronoto-apodemalis anterior (Sn: 49), a large pronotal muscle, **O**: anterolaterally on the pronotum, **I**: distally on the propleural arm of the propleuron, close to Itpm5; **Itpm5**, M. pronoto-apodemalis posterior (Sn: 50), a large pronotal muscle, **O**: posterolaterally on the pronotum, **I**: distally on the propleural arm of the propleuron, close to Itpm4; **Ivlm1**, M. profurca-cervicalis (Sn: 51), a broad cervical muscle, **O**: on the anteromedian profurcal process, **I**: posteriorly on the cervical apodeme of the propleuron.

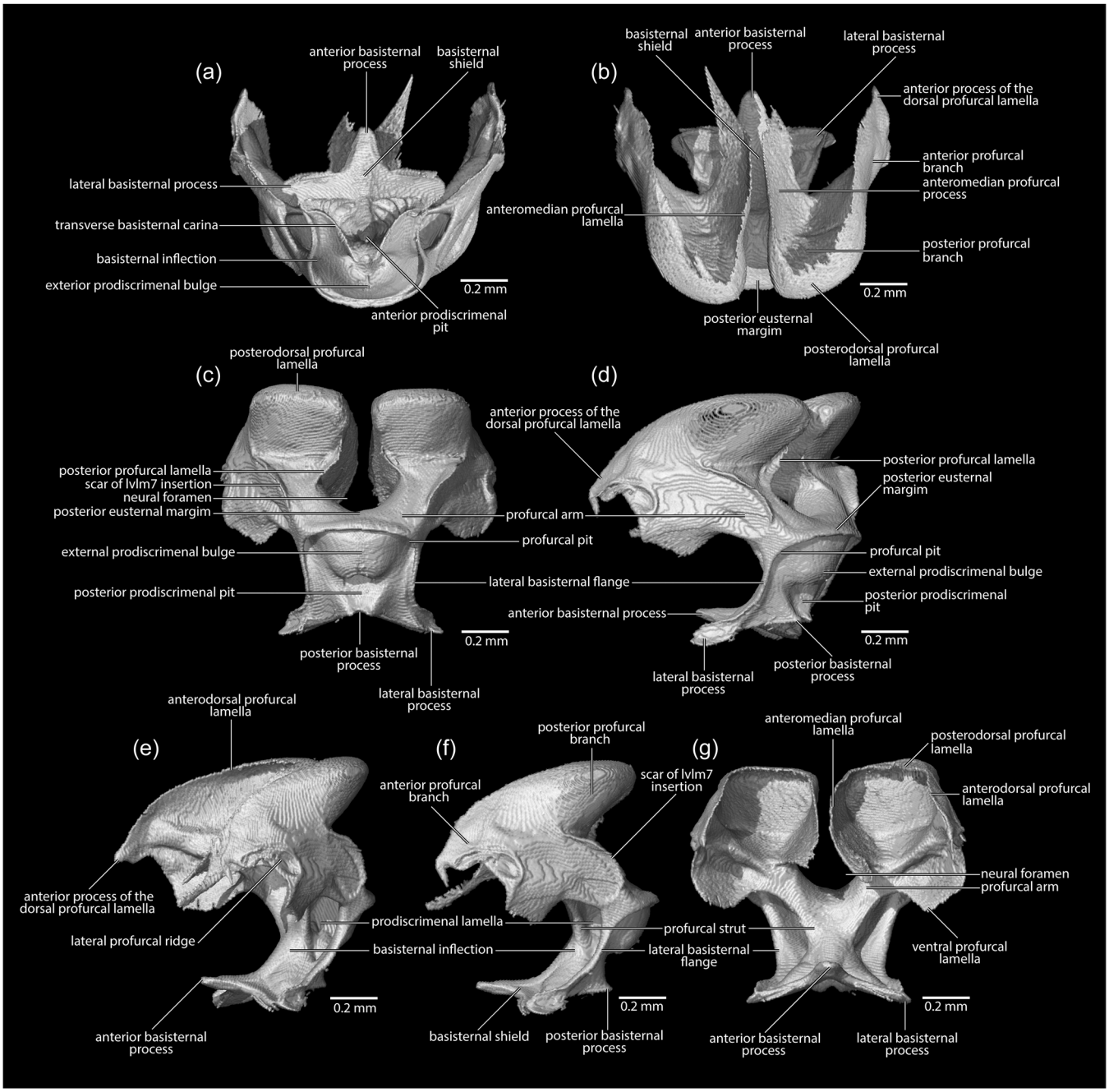

FIGURE 18 Prosternum of *Thyreus albomaculatus*. (a) Ventral view. (b) Dorsal view. (c) Posterior view. (d) Posterolateral view. (e) Anterolateral view. (f) Lateral view. (g) Anterior view.

Prosternum *(Figures 17e,f, 18a–g, and 19a)*

The prosternum, which is partially obscured by the propleurae as seen in external view (Figure 17e,f), forms the articulations with the procoxae posteriorly. In lateral view it is curved dorsad, forming the basisternal inflection (Figure 18e,f), which is separated from the basisternal shield (Figure 18a,b) by the transverse basisternal carina (Figure 18a). This carina also separates the anterior (Figure 18a) and posterior prodiscrimenal pits (Figure 18c), which are visible on the basisternal shield and basisternal inflection, respectively. The profurcal arms are not fused with each other, thus the neural foramen is open (Figure 18b,c,g). The prosternum is enclosed laterally by the lateral basisternal flanges (Figure 18c,d,f,g), and posteriorly by the posterior eusternal margin (Figure 18b–d). The basisternal shield (Figure 18a,b) is composed of the anterior (Figure 18a,b,d,e–g), lateral (Figure 18a,b,d,g), and posterior (Figure 18c–e) basisternal processes. The profurcal strut (Figure 18f,g) forms the anterior margin of the profurcal arm and is continuous with the ventral profurcal lamella (Figure 18g). The prodiscrimenal lamella (Figure 18e,f) lies posterad the profurcal strut. The basisternal inflection extends dorsad from the posterior

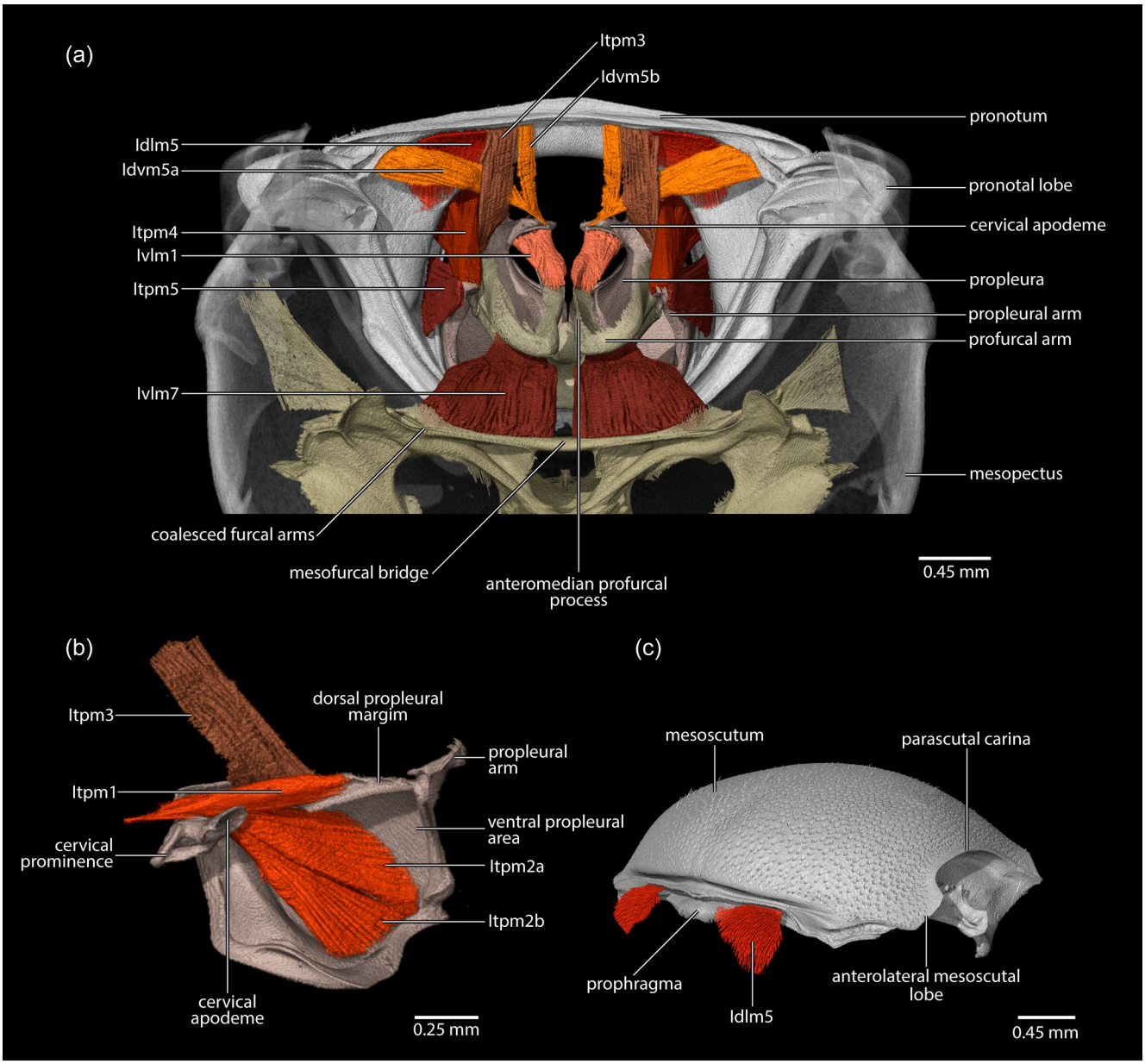

FIGURE 19 Muscles attached to the propectus and prophragma of *Thyreus albomaculatus*. (a) Muscles attached to the propectus, posterior view of the pronotum. (b) Propleural muscles, medial view of the propleuron. (c) Muscles attached to the prophragma, anterolateral view of the mesoscutum.

eusternal margin giving rise to the profurcal arms. Two profurcal pits (Figure 18c,d), the invagination sites of the profurcal arms, are clearly visible close to the posterior eusternal margin. The scar (Figure 18f) of the insertion of muscle lvlm7 (profurca-mesofurcalis) is located at the posterior margin of the profurcal arm, which is divided into the anterior (Figure 18f) and posterior profurcal branches (Figure 18f); the former extends ventrad into the ventral profurcal lamella (Figure 18d,f) and dorsally into the anterior process of the dorsal profurcal lamella (Figure 18d,e); the posterior profurcal branch bears the anteromedian (Figure 18b,g), anterodorsal (Figure 18e,g), posterodorsal (Figure 18b,c,g) and posterior (Figure 18c,d) profurcal lamellae.

Prosternal muscles (Figure 19a): **lvlm7**, M. profurca-mesofurcalis (Sn: 52), a broad intersegmental muscle, **O**: broadly on the mesofurcal bridge and the coalesced furcal arms, **I**: on the scar of the posterior margin of the profurcal arm.

3.2.2 | Mesothorax (Figure 16)

The mesothorax is by far the largest segment of the mesosoma in Hymenoptera and comprises the mesonotum, and mesopectus (mesepisternum + mesepimeron + mesothoracic endosternum i.e., the mesofurca).

Mesonotum (Figure 16a,c–e)

The mesonotum is divided into two main sclerotized regions: the broad anterior mesoscutum and the smaller posterior mesoscutellum. The mesoscutum is the largest part of the mesonotum and accounts for two-thirds of the total length of the mesosoma in dorsal view (Figure 16a); its sculpture consists of fine punctation. The median mesoscutal line (Figure 16a) extends between the anterior and posterior margins and thus completely divides the sclerite into two halves. On the anterior margin, the mesoscutum bears the well-developed prophragma (Figure 19c), which is produced ventrally and serves as an attachment area for muscles of the head, prothorax, and mesothorax. Laterally, the mesoscutum bears the longitudinal parascutal carina (Figures 16e and 19c) and articulates with the well-developed tegula (Figure 16a,c–e), which overlaps the mesoaxillary sclerites. A well-developed anterolateral mesoscutal lobe (Figures 16a,d and 19c) is located anterior to the tegula and posterior to the pronotal lobe. Posteriorly, the mesoscutum is divided from the mesoscutellum by the scutoscutellar sulcus, which is impressed between the axillae (Figure 16a,f). The axilla (Figures 16d–f and 24a) is the portion of the mesonotum that is anterolaterally separated from the mesoscutum by the transscutal line and posteriorly from the mesoscutellum by the scutoscutellar line; these two lines unite medially in the scutoscutellar sulcus. The mesoscutellum is produced posteriorly as a flat plate that has two acute posterior projections (Figure 16a) which conceal the metanotum and propodeum in dorsal view; it articulates anteriorly with the mesoscutum (Figure 16a), posteriorly with the metanotum (Figure 16d–f), and laterally (Figure 16e) with the dorsal area of the mesepimeron. Posteriorly on the ventral side, the mesoscutellum bears the scutoscutellar ridge that projects laterally as the axillary ridge and it is posteriorly delimited by the vertical apodemal lobe (Figure 25a).

The mesophragma (Figure 20b–d) reaches deeply into the propodeal cavity and articulates with the lateral area of the axilla (Figure 20b,c) (see also description and illustration of this condition in state 1 of char. 87 and fig. 47B of Vilhelmsen et al. [2010]). It has a middorsal notch (Figure 20e,f) and a pseudophragmal lobe (Figure 20f) at the anterodorsal margin (Figure 20e). The anterior face of this plate is distinguished by an arched mesophragmal pocket (Figure 20e), which extends laterally to form the mesolaterophragma (Figure 20f). On its posterior face, the mesophragma displays mesophragmal longitudinal and lateral ridges (Figure 20f). The mesosoma further provides attachment areas for the dorsal longitudinal indirect flight muscles anteriorly and a propodeal muscle posteriorly. Laterally, the mesophragma is connected to a small sclerite known as the axillary lever (also referred to as the accessory sclerite of the fourth axillary sclerite) (Figure 20c).

Prophragmal and mesophragmal muscles (Figures 19a,c and 20a,b,d). **Idlm5**, M. pronoto-phragmalis anterior (Sn: 45), a broad intersegmental pronotal muscle, **O**: lateral inner surface of the pronotum, **I**: laterally on the prophragma of the mesoscutum, close to Idlm1; **IIdlm1**, M. prophragma-mesophragmalis (Sn: 71), the large dorsal longitudinal indirect flight muscle, **O**: on the posterior face of the prophragma and medially on the ventral side of the mesoscutum, **I**: broadly on the anterior face of the mesophragma; **IIIdlm1**, M. mesophragma-metaphragmalis (Sn: 96), a longitudinal muscle of the mesophragma, **O**: on the propodeal ridge, **I**: on the posterior surface of mesophragma.

Mesopectus *(Figure 21)*

The lateral area of the mesothorax is composed of the small mesepimeron, the large mesepisternum, and the mesothoracic endosternal invaginations (mesofurca).

Externally (Figure 21a) the mesopectus displays densely arranged setal sockets in the μ-CT data. The small and narrow mesepimeron (Figure 21a,b) is located posterodorsally on the mesopectus and is separated from the mesepisternum by the pleural sulcus (Figure 21a). The mesepisternum articulates anteriorly with the pronotum; the **subspiracular area** close to this anterior margin bears the distinct **subspiracular ridge** (Figure 21b). Dorsally, the mesepisternum articulates with the anterior wing base and the second mesoaxillary sclerite via the pleural wing process (Figure 21a,b). The posterodorsal mesepisternal region is the hypoepimeral area (Figure 21a) that bears the **pleural apophyseal pit**, marking the invagination site of the pleural apophysis, and the **pleural apophyseal sulcus** (=scrobal suture of Michener [1944]) (Figure 21a), which might be produced as the **pleural apophyseal ridge** internally in other bee lineages (O. M. Meira, personal observation). The mesepisternum is in broad contact with the pronotum through its anterior margin (Figure 21a,b); an additional contact structure is present below the pronotal lobe, the mesepisternal clip (Rosa & Melo, 2023) (Figure 16b,c); it contacts the metapectus posteriorly through the pleural sulcus and ventrolaterally through the intercoxal lamella (Figure 23c). On the ventral surface, a well-developed pleural apophysis (= scrobe of Michener [1944]) (Figure 21b) is located close to the pleural ridge, which extends from the coxal process to the subspiracular ridge (see discussion section on the mesopectus); above it, the **subalar apophysis** delimits a cavity; ventrally a small **mesepisternal ridge** (Figure 21b) is present but does not reach the pleural apophysis. Ventromedially, the mesopectus extends into the mesosomal cavity as an invagination, thus forming the mesothoracic endosternum or mesofurca, which is fused with the metathoracic endosternum or metafurca (Figure 23a–c).

Mesopectal muscles *(Figure 22).* **IIdvm1**, M. mesonoto-sternalis (Sn: 72), a dorsoventral indirect flight muscle, **O**: laterally on the ventral side of the mesoscutum, laterad IIdlm1, **I**: ventrally on the mesepisternum, laterally to the mesofurca; **IIpspim1** M. mesanepisterno-spiracularis (Sn: 73), the only spiracular muscle of the mesothorax in bees, **O**: anterior margin of the subspiracular area, **I**: spiracular membrane on the spiracular aperture (note: we cannot resolve finer detail given the limitation of resolution in our μ-CT data set; see also Tonapi [1958]); **IItpm5**, M. mesonoto-pleuralis medialis (Sn: 75), **O**: broadly attached on the dorsolateral area of the mesepisternal region and on the pleural apophysis, posterior to IItpm7c and anterior to IIspm2, **I**: lateral margin of the mesoscutellum; **IItpm7**, M. mesanepisterno-axillaris (Sn: 76a, b, c), a broad muscle

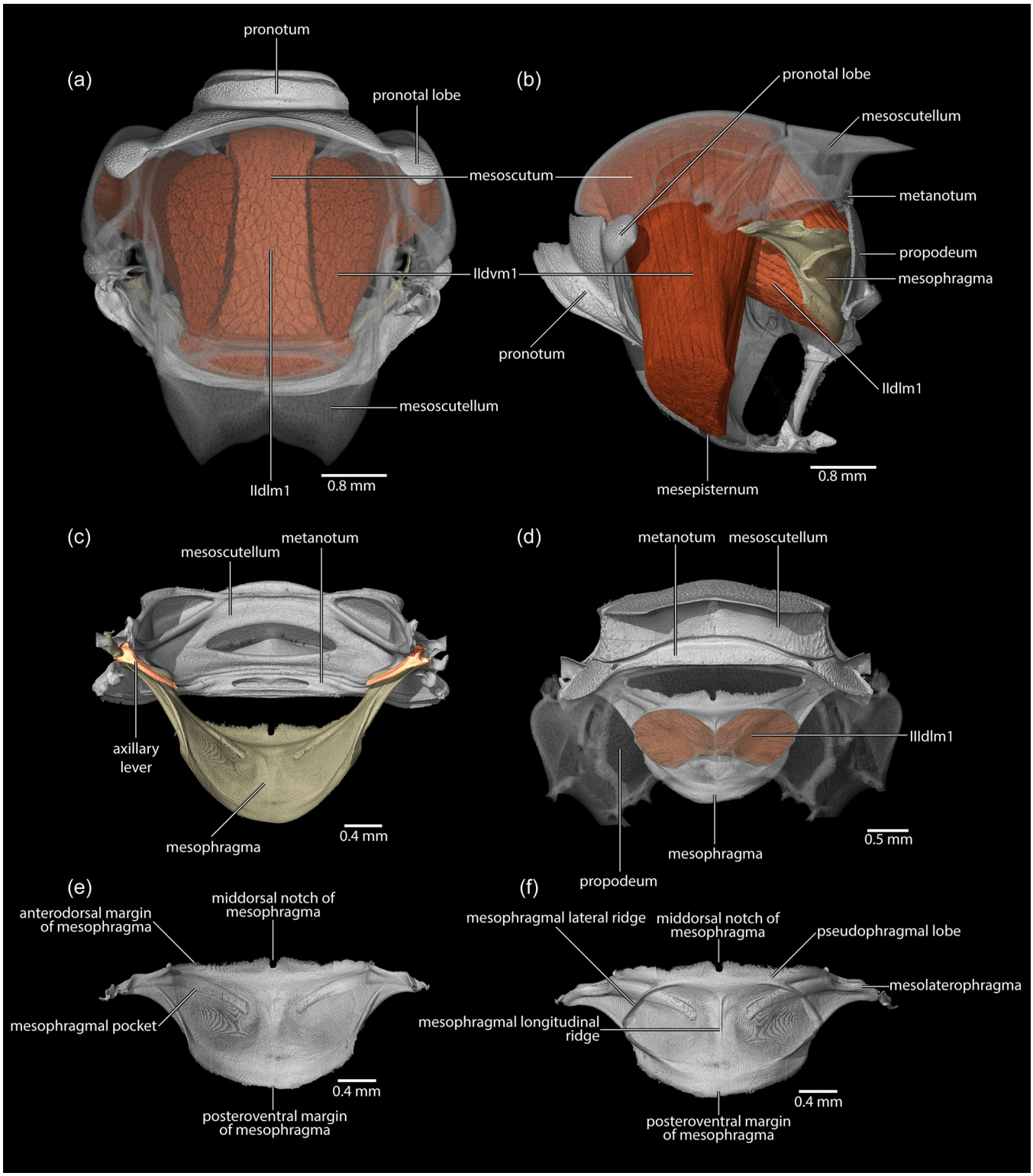

FIGURE 20 Muscles attached to the mesonotum and mesophragma of *Thyreus albomaculatus*. (a) Dorsoventral and longitudinal muscles, rendering of mesonotum semitransparent, dorsal view of the mesosoma. (b) Dorsoventral and longitudinal muscles, mesonotum semitransparent, lateral view of the mesosoma. (c) Articulation between mesoscutellum and mesophragma, ventral view of mesoscutellum. (d) Mesophragmal muscle (propodeum semitransparent), posterior view of the mesosoma. (e) Mesophragma, anterior view. (f) Mesophragma, posterior view.

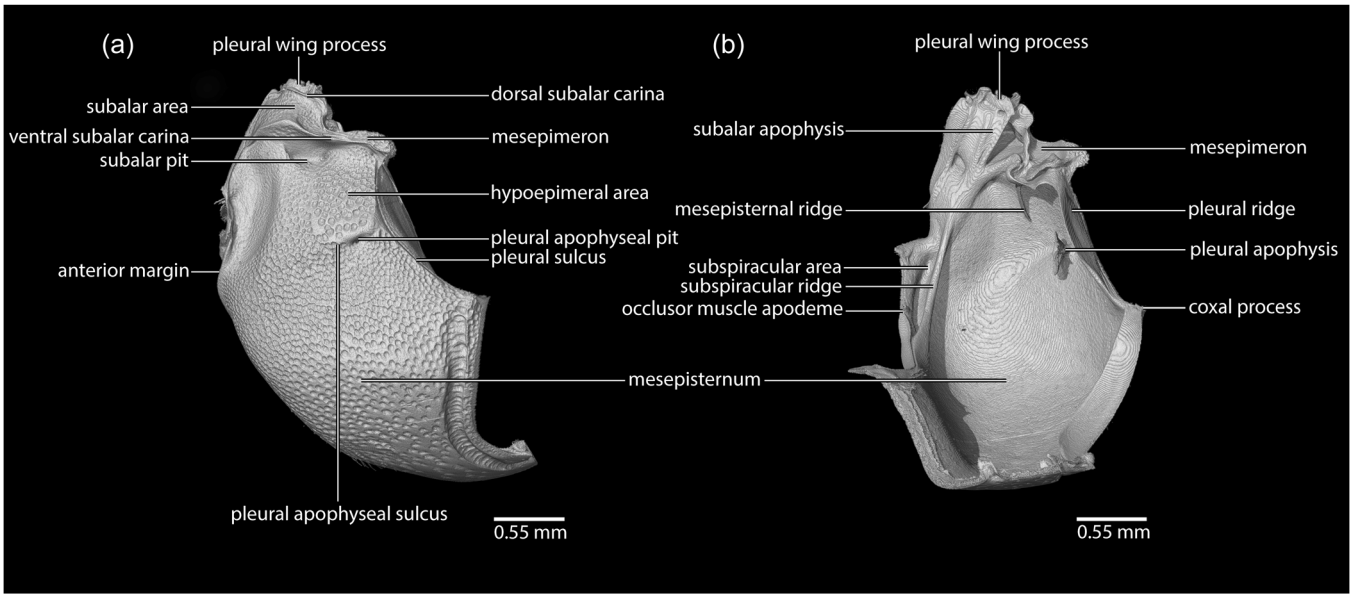

FIGURE 21 Mesopectus of *Thyreus albomaculatus*. (a) Lateral view. (b) Posteromedial view.

with 3 subcomponents, **IItpm7a** (Sn: 76a), **O**: on the subalar apophysis cavity, **I**: converging on a shared tendon that inserts on the third mesoaxillary sclerite; **IItpm7b** (Sn: 76b), **O**: laterally on the mesepisternal region, anterodorsad IItpm7c and posterior to IIspm1, **I**: converging on a shared tendon that inserts on the third mesoaxillary sclerite; **IItpm7c** (Sn: 76c), **O**: laterally on the mesepisternal region, posteroventrad IItpm7b and anterior to IItpm5, **I**: converging to a shared tendon that inserts on the third mesoaxillary sclerite; **IIspm1**, M. mesopleura-sternalis (Sn: 77), the mesobasalar muscle, **O**: ramified origin on the subspiracular area and anterior area of the mesepisternum, posterior to IIpspim1 and anterior to IItpm7a and IItpm7b, **I**: on the mesobasalar sclerite, below the tegula; **IIdvm8**, M. mesofurca-phragmalis (Sn: 78), **O**: broadly on the coalesced furcal arms and on the free distal portion of the mesofurcal arm, **I**: on the tip of the axillary lever; **IIspm2**, M. mesofurca-pleuralis (Sn: 79), the pleural-mesofurcal muscle, **O**: posterolaterally on the mesepisternal region, surrounding the pleural apophysis, posterior to IItpm5, **I**: on the tip of the free distal portion of the mesofurcal arm.

Meso-metafurca *(Figure 23)*

As the mesothoracic and metathoracic furcae (endosterna) are fused and form a structural unit in some bees and other Apoidea (Prentice, 1998; Vilhelmsen et al., 2010), both will be treated together. The meso/metafurcal complex (Figure 23a–c) is present as a horizontal plate forming a platform extending from the antemesofurcal area to the metadiscrimenal lamella (Figure 23a–c). On the dorsal surface of the horizontal plate, the free basal portion of the mesofurcal arms (Figure 23a,c) originates lateromedially as an invagination of the mesosternal apophyseal pit (Figure 23c) and extends to the mesofurcal bridge (Figure 23a,b). Laterad the mesofurcal bridge, an area of the meso-metafurcal fusion is formed by the coalesced furcal arms (Figure 23a–c). From this area, the free distal portion of the mesofurcal arms (Figure 23a–c) originates and extends towards the mesepisternal region, but without fusing with it. The metathoracic portion of the meso-metafurcal complex is similar in structure. The free basal portion of the metafurcal arms (Figure 23a,c) originates posterolaterally on the horizontal plate as an invagination of the metasternal apophyseal pit (Figure 23c) and extends to the mesofurcal bridge. The free distal portion of the metafurcal arms (Figure 23a,c) originates from the area of the coalesced arms; it extends to the metapectus and is attached to it; the dorsal metafurcal lamella is present shortly anterior to this attachment site. Below the horizontal plate (Figure 23c) the mesosternal and metasternal apophyseal pits are visible as invagination sites of the free basal portion of the meso- and metafurcal arms (Figure 23c). Medioventrad the horizontal plate, the intercoxal lamella (= paracoxal ridge) (Figure 23a–c) extends to the mesepisternal region and attaches to it, thus separating the mesodiscrimenal and metadiscrimenal lamellae (Figure 23c). Dorsally, the metadiscrimenal lamella is present as a robust median crest.

Axillary, basalar, and subalar sclerites (Figure 24)

Both the meso- and metathoracic regions contain specific sclerites that articulate with the mesepisternum and metapectus, respectively. With its larger size and the larger fore wings, the mesothorax is crucial in the context of flight, whereas the metathoracic region with the smaller hind wings plays a lesser role. In the following description, we will outline the wing articulation, leaving the interaction of the involved sclerotized elements with each other and with the surrounding membrane implied. The mesothorax bears five axillary sclerites and the metathorax four.

In the mesothorax, the mesobasalar sclerite (Figure 24a,b) articulates ventrally with the dorsal margin of the pleural wing

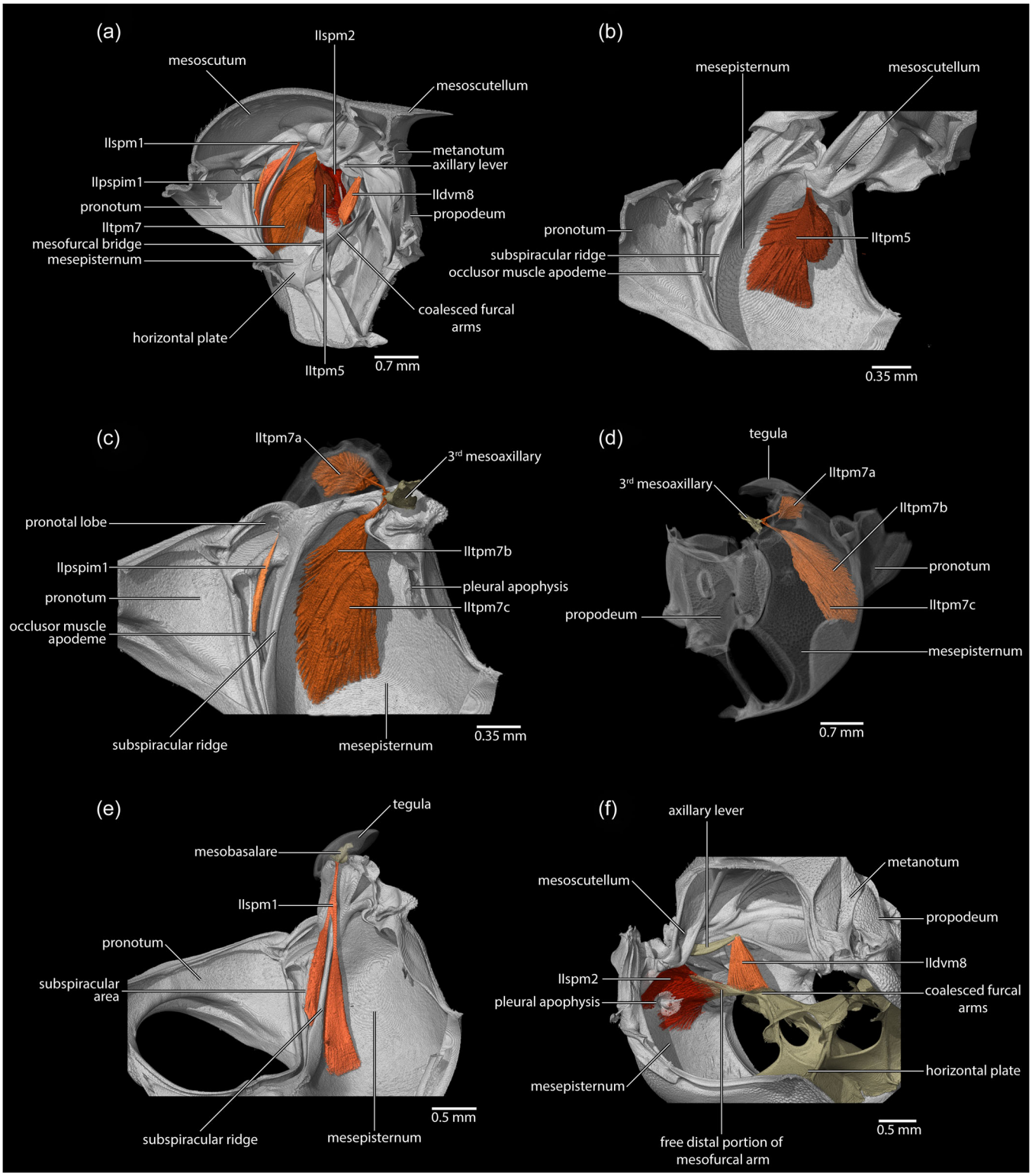

FIGURE 22 Mesopectal muscles of *Thyreus albomaculatus*. (a) Mesosoma and mesopectal muscles, medial view of the mesosoma. (b) Pronotum, mesopectus, and mesoscutellum, medial view of the mesopectus. (c) Pronotum and mesopectus, subalar area semitransparent, medial view of mesopectus. (d) Pronotum, mesopectus and propodeum, sclerites semitransparent, lateral view of the mesopectus. (e) Pronotum and mesopectus, tegula at low density, medial view of the mesopectus. (f) Mesosomal cavity, anteromedial view.

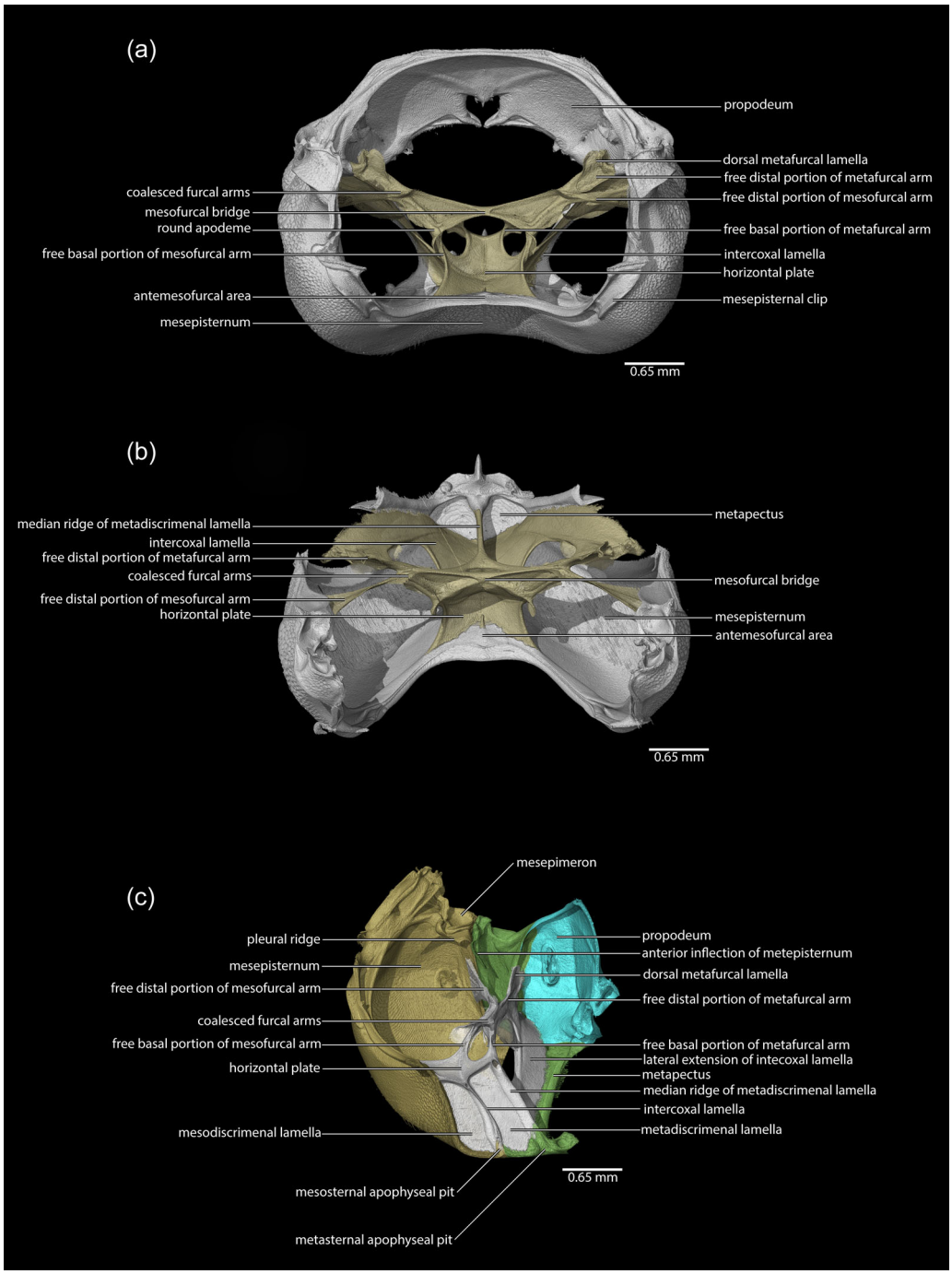

FIGURE 23 Meso-metafurcal complex of *Thyreus albomaculatus*. (a) Anterior view of the mesosoma. (b) Dorsal view of the mesosoma. (c) Medial view of the mesepisternum.

process and dorsally with the base of the forewing. The mesosubalar sclerite (Figure 24a,b) articulates ventrally with the dorsal margin of the mesepimeron. The first mesoaxillary sclerite (Figure 24a,b) is the largest, and its posterior margin articulates with the lateral margin of the mesoscutum, axilla, and base of the anterior wing. The second mesoaxillary sclerite (Figure 24a,b) is the only one that articulates through its ventral margin with the mesopectus through the posterodorsal margin of the pleural wing process; as the pivotal sclerite of the forewing, it also articulates anteriorly with the first mesoaxillary sclerite and posteriorly with the mesosubalar sclerite. The third mesoaxillary sclerite (Figure 24a,b) is the only one with a muscle insertion; it articulates with the base of the forewing. The fourth axillary sclerite (Figure 24a,b) is very small and articulates with the lateral margin of the axilla, the base of the anterior wing, and the axillary lever. The structure and configurations of the metabasalar, metasubalar, and metaxillary sclerites (Figure 24a,c) is similar to that of the mesothorax, except for the absence of the fourth axillary sclerite.

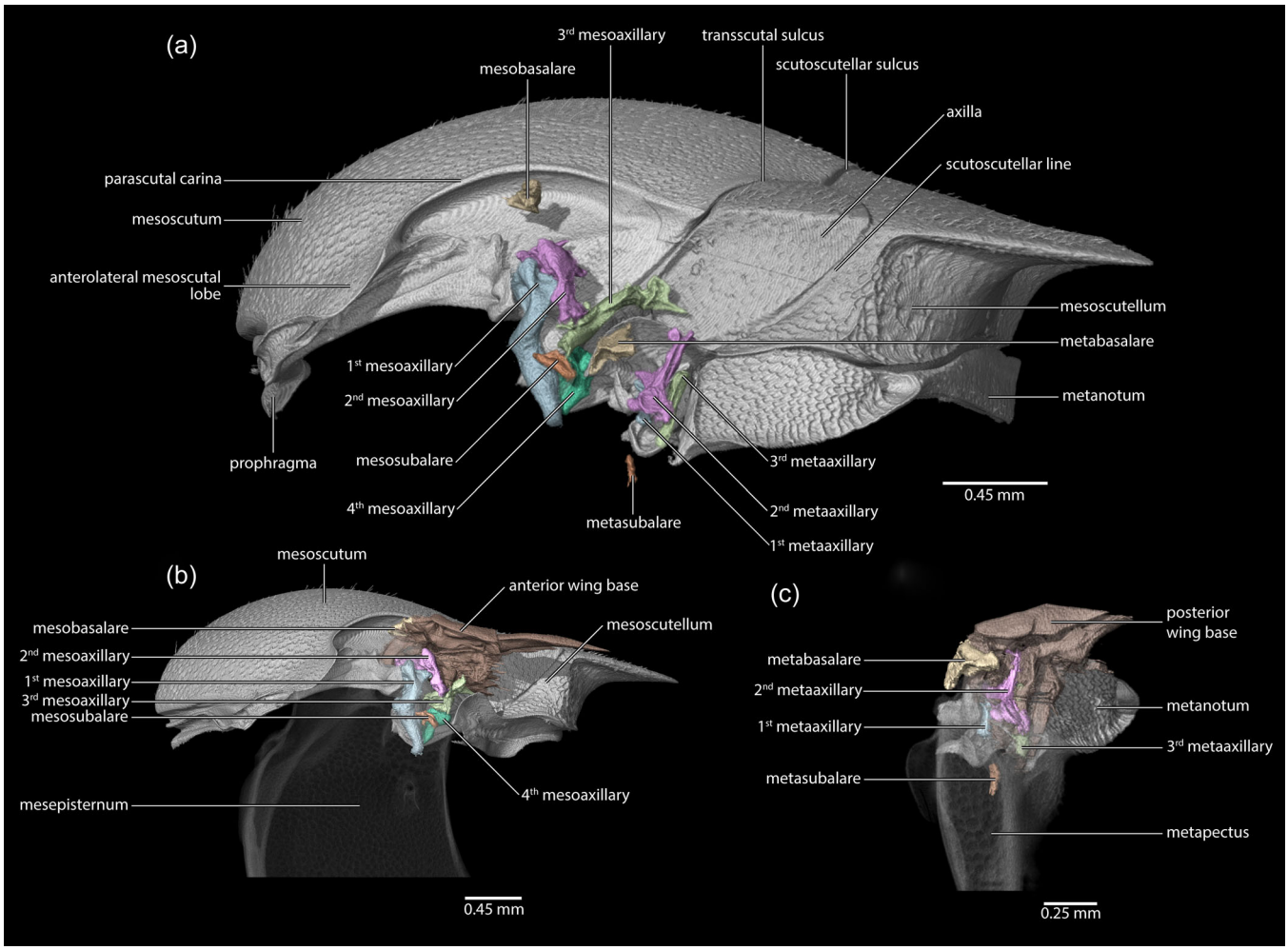

FIGURE 24 Axillary, basalar, and subalar sclerites of *Thyreus albomaculatus*. (a) Lateral view of the mesonotum. (b) Mesothoracic sclerites and mesopleura, semitransparent, lateral view of the mesonotum. (c) Metathoracic sclerites, metapectus semitransparent, lateral view of the metanotum.

3.2.3 | Metathorax (Figure 16)

The metathorax of bees and Hymenoptera is generally reduced in size and modified, appearing as dorsoventrally narrow plates or sclerite regions (Figure 16d–f). It is composed of the dorsal metanotum and the lateral metapectus (+ metathoracic endoskeleton; see meso-metafurca above).

Metanotum *(Figures 16d–f and 25a)*

The metanotum is a single transverse plate approximately less than half the size of the mesoscutellum. It is narrow medially but expands laterally, placed between the mesoscutellum anteriorly and the propodeum posteriorly (Figure 16d–f). Medially, the metanotum forms the chamber of the metanotum (Figure 25a); the insertion site of muscle IIIdlm3 is located laterad this chamber on the anterior surface of the internal metanotal ridge (Figure 25a), which extends laterally to the dorsolateral metanotal area (Figure 25a); a single small metanotal pit is located mesad this region (Figures 16f and 25a).

Metanotal muscles *(Figure 25a)*.

IIIdlm3, M. metascutello-scutellaris (Sn: 70), an intersegmental muscle, **O**: scutoscutellar ridge, **I**: anterior margin of the internal metanotal ridge.

Metapectus *(Figures 16d–f and 25b,c)*

The metapectus (= metepisternum *sensu*; Michener [1944]) is present as a narrow plate that extends ventrolaterad. The margin of the dorsal metapectal region (Figure 25c) articulates with the metanotum, the base of the posterior wing, and the metaaxillary sclerites. The most expanded portion of the metapectal region forms the lateral wall of the metathorax; it is also the area with the sites of origin of almost all metathoracic muscles and also the insertion site of the metafurcal arms (Figure 25c). Anteriorly, the anterior metepisternal inflection (Figure 25c) marks the limit between mesepisternum and metapectus. The separation of the margin of the metapectal region and the propodeum is not distinct externally but is indicated by the metapleural pits (Figure 16e); internally the separation can be traced by the posterior located metapleural ridge (Figure 25c). The

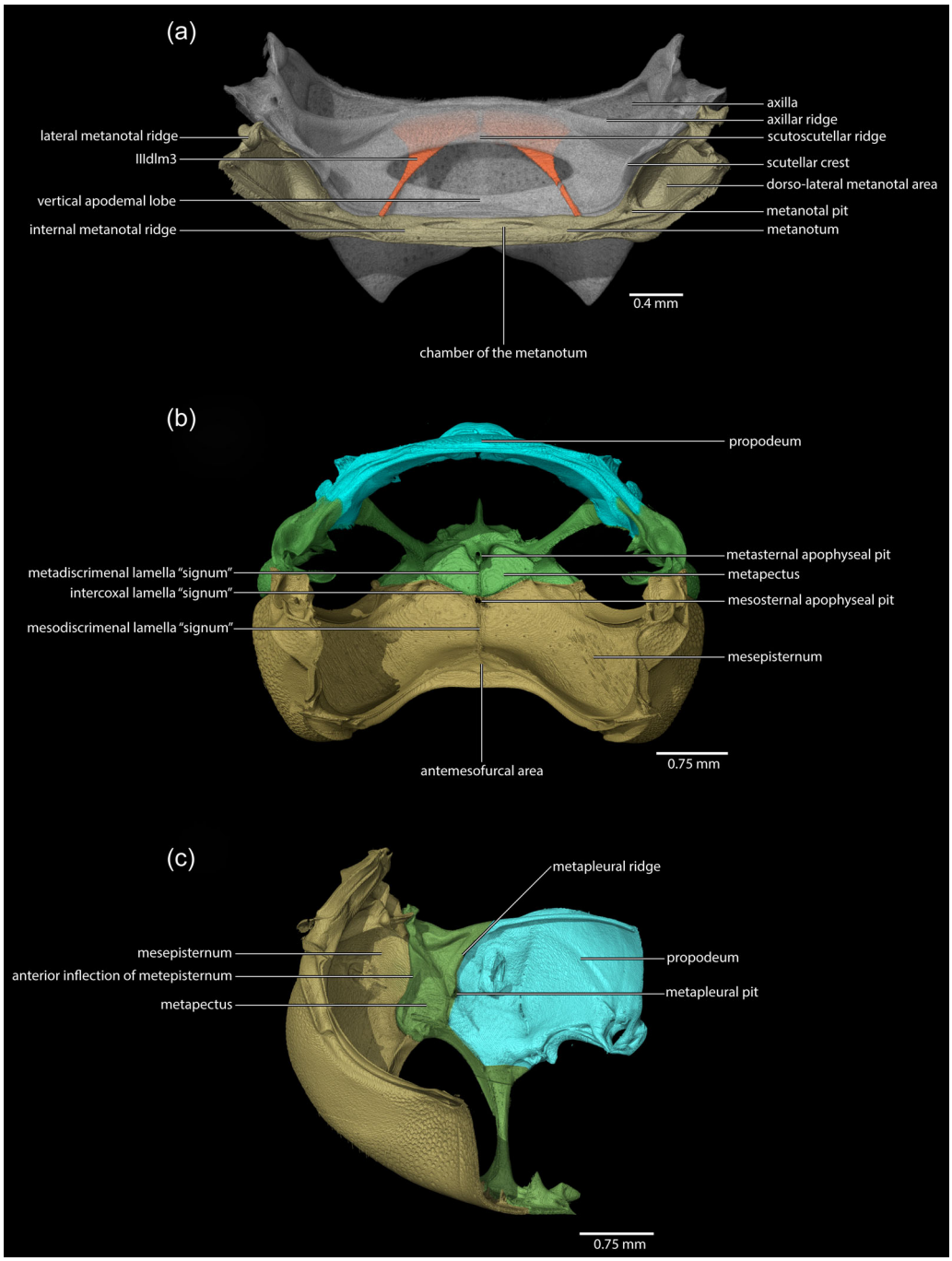

FIGURE 25 Metanotum, mesopectus and metapectus of *Thyreus albomaculatus*. (a) Metanotum and mesoscutellum, mesoscutellum semitransparent, ventral view of mesoscutellum. (b) Mesepisternum, metapectus and propodeum, dorsal view of the metapectus. (c) Mesepisternum, metapectus and propodeum, medial view of the metapectus.

metapectus extends ventrad and is continuous with the invagination of the metafurca on the metasternal apophyseal pit (see meso-metafurca above).

Metapectal muscles *(Figure 26)*. **IIItpm5**, M. metanoto-pleuralis medialis (Sn: 97), **O**: on the free distal portion of the metafurcal arm, and dorsal metafurcal lamella, **I**: tip of the dorsolateral metanotal area, medially to the insertion of IIItpm6; **IIItpm6**, M. metanoto-pleuralis posterior (Sn: 98), **O**: broadly on the dorsal metafurcal lamella, posterolateral to the IIItpm5 origin, **I**: tip of the dorsolateral metanotal area, posterior to the insertion of IIItpm5; **IIIdvm1**, M. metanoto-sternalis (Sn: 99), a broad and short muscle, **O**: broadly on the dorsolateral metanotal area, posterolaterad the origin of IIItpm6, **I**: on the filamentous process of the free distal portion of the metafurcal arm; **IIItpm7**, M. metanepisterno-axillaris (Sn: 100), a broad and short muscle, **O**: on the anterior inflection of

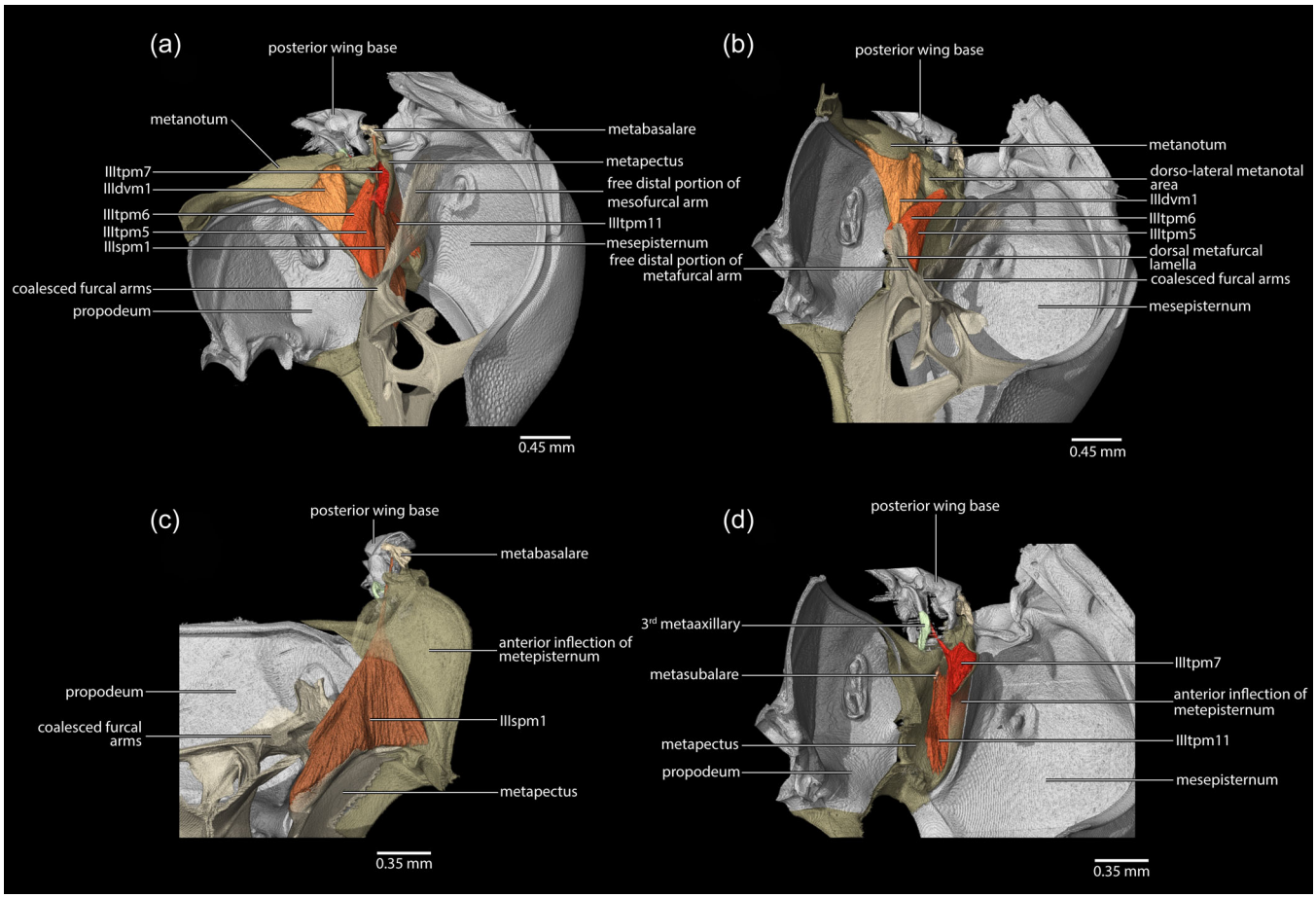

FIGURE 26 Metathoracic muscles of *Thyreus albomaculatus*. (a) Propodeum, metanotum, meso-metafurca and mesopectus, medial view of meso-metafurcal complex. (b) Propodeum, metanotum, meso-metafurca and mesopectus, medial view of the meso-metafurcal complex. (c) Metapectus, meso-metafurcal complex and propodeum, anterior view of the metapectus. (d) Propodeum, metanotum and mesopectus, medial view of the mesopectus.

metepisternum, **I**: on the third metaaxillary sclerite; **IIIspm1**, M. metapleura-sternalis (Sn: 101), **O**: ventral region of the metapectus, anterior to IIItpm5, **I**: metabasalar sclerite; **IIItpm11**, M. metapleura-subalaris (Sn: 102), **O**: anterior inflection of metepisternum, ventrad IIItpm7, **I**: metasubalar sclerite.

3.3 | The legs (Figures 27–29)

All pairs of legs are of a similar configuration, composed of coxa, trochanter, femur, tibia, tarsus, pretarsal claws, and a complex pretarsal arolium. The foreleg and the middle leg are of similar size, and the hind leg is the longest. The foreleg differs by the presence of a complex protibial-probasitarsal antenna cleaning device.

3.3.1 | Foreleg (Figure 27)

The protibial calcar and the basal part of the probasitarsus (= first tarsomere) form the complex antenna cleaner, a specialized structure formed by the modified inner surface of the probasitarsus and the large spur inserted at the distal end of the protibia (e.g., Basibuyuk & Quicke, 1995; Schönitzer, 1986). It is used for removing particles from the antennal sensilla. The procoxa is robust and roughly rectangular (Figure 16b,c). An articulatory membrane connects its bulging dorsal margin with the propectus, the lateral basisternal process, and the posterior margin of the ventral propleural area (Figures 17b and 26d). Posteriorly, the procoxa (Figures 16b,c and 27a–e) contacts the pronotum (Figure 27c). It articulates with the protrochanter distally (Figure 27a,b,e). The disticoxal foramen is open, that is, the distal procoxal membrane is exposed. The roughly rectangular protrochanter (Figure 27a,b,e,f) is slender, with subparallel dorsal and ventral margins; it is as long as the procoxa but distinctly narrower. A dicondylic articulation connects it with the procoxa. The basal articulatory piece is separated from the main portion of the protrochanter by a rounded proximal edge. Its oblique distal margin is connected with the profemur (Figure 27a,b,f), which is about as wide as the protrochanter, twice as long and slightly longer than the protibia. The trochantero-femoral articulation is dicondylic, with a limited

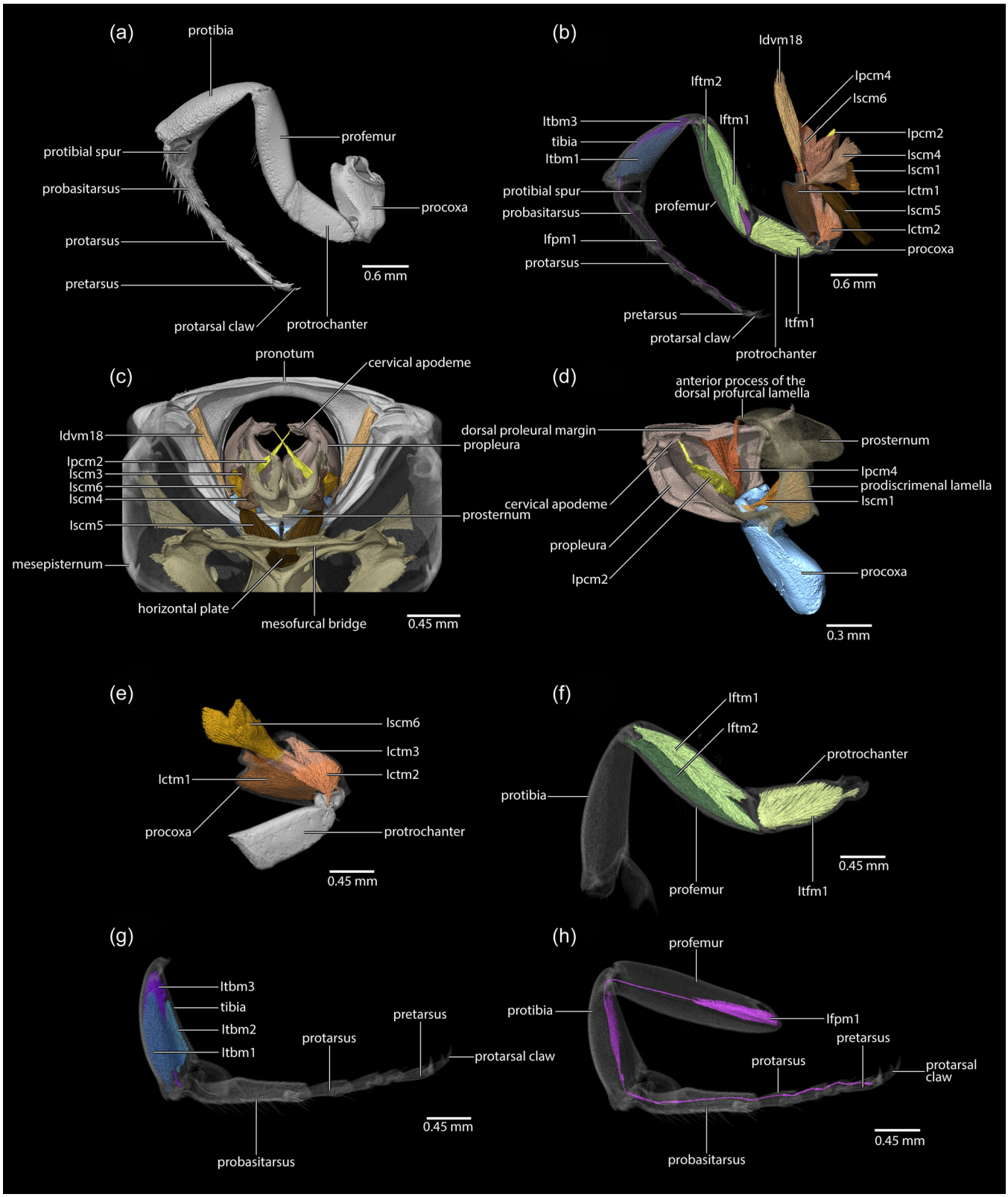

FIGURE 27 Left prothoracic leg of *Thyreus albomaculatus*. (a) Left prothoracic leg, posterior view. (b) Left prothoracic leg muscles, posterior view. (c) Insertion of extrinsic procoxal muscles, posterior view of pronotum. (d) Procoxal muscles attached to right propleuron and prosternum, prosternum semitransparent, medial view of propleuron. (e) Left protrochanteral muscles, procoxa semitransparent, posterior view of the procoxa. (f) Left profemoral and protibial muscles, sclerites semitransparent, posterior view of the profemur. (g) Left tarsal muscles, sclerites semitransparent, posteromedial view of protibia. (h) Tarsal muscle, sclerites semitransparent, posterior view of protibia.

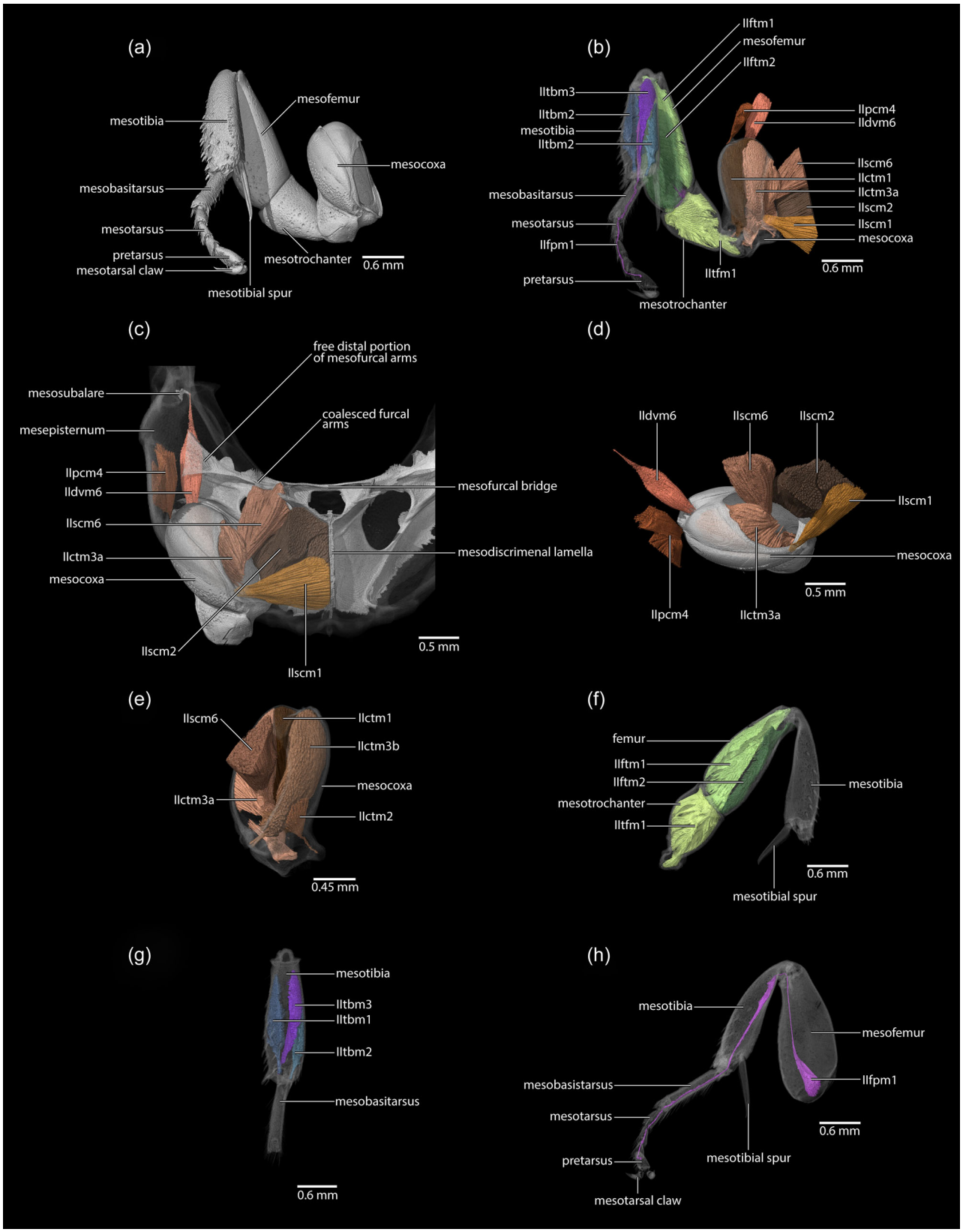

FIGURE 28 Right mesothoracic leg of *Thyreus albomaculatus*. (a) Right mesothoracic leg, anterior view. (b) Mesothoracic leg muscles, anterior view. (c) Insertions of extrinsic mesocoxal muscles, mesepisternum semitransparent, anteroventral view of meso/metafurca. (d) Right mesocoxal muscles, anterodorsal view of mesocoxa. (e) Right mesotrochanteral muscles, mesocoxa at low density, dorsal view of mesotrochanter. (f) Right mesofemoral and mesotibial muscles, sclerites semitransparent, posterior view of mesofemur. (g) Right tarsal muscles, sclerites semitransparent, dorsal view of mesotibia. (h) Right tarsal muscle, anterior view of mesotibia, sclerites semitransparent.

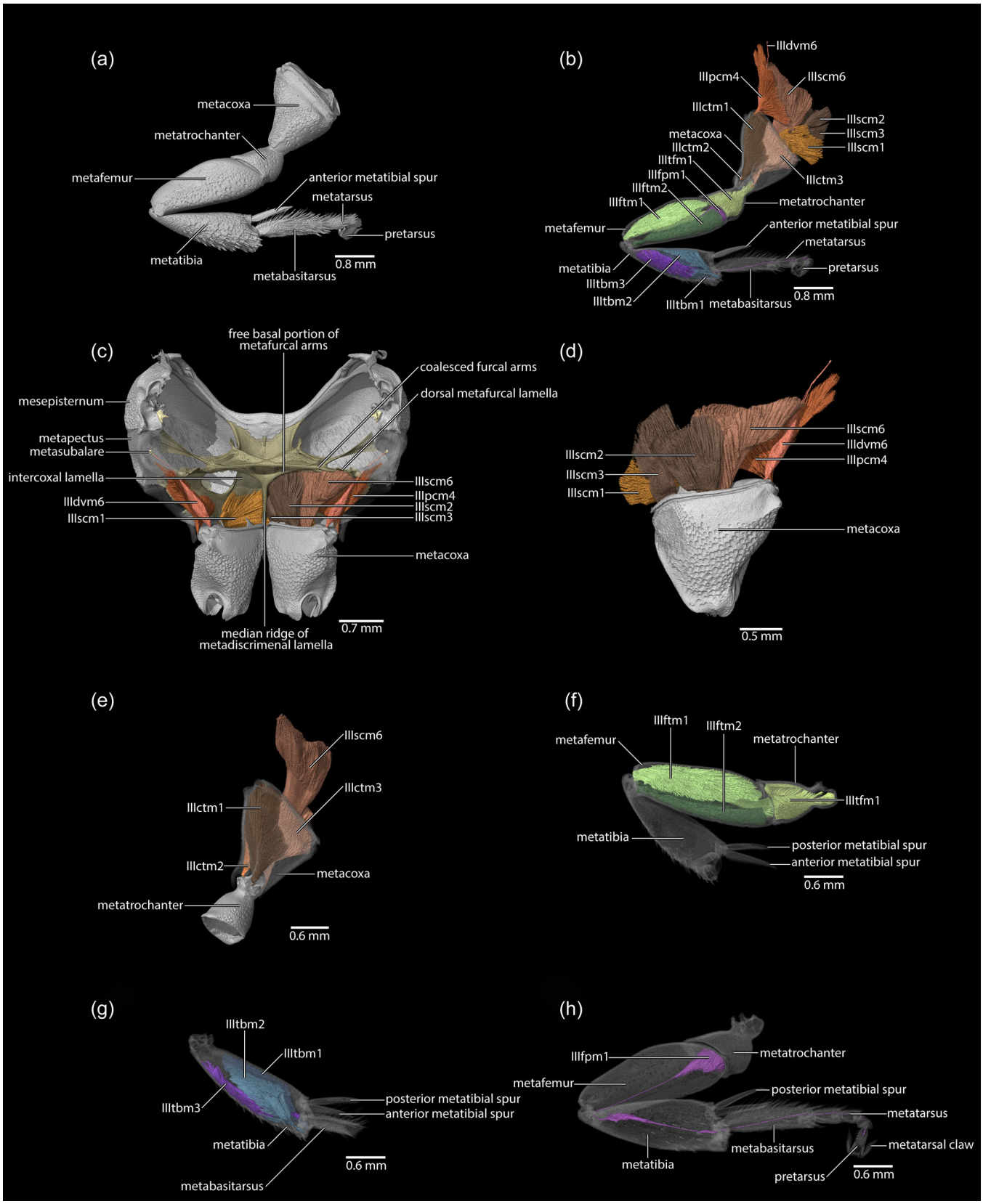

FIGURE 29 Right metathoracic leg of *Thyreus albomaculatus*. (a) Right metathoracic leg, anterior view. (b) Right metathoracic leg muscles, anterior view. (c) Right extrinsic metacoxal muscles insertions, metapectus semitransparent, dorsal view of meso/metafurca. (d) Right extrinsic metacoxal muscles, posterior view of metacoxa. (e) Right metatrochanteral muscles, metacoxa semitransparent, anterodorsal view of metacoxa. (f) Right metafemoral and metatibial muscles, sclerites semitransparent, anterodorsal view of metafemur. (g) Right tarsal muscles, sclerites semitransparent, anteroventral view of the metatibia. (h) Right tarsal muscle, sclerites semitransparent, anteroventral view of the metatibia.

flexibility. The protibia (Figure 27a,b,g,h) is slightly shorter than the profemur and about as wide. At its base, the femoro-tibial joint is dicondylic. The protibial spur, the proximal element of the antenna cleaner (= strigil *sensu* Michener [1944]), is inserted on the apex of the protibia and interacts with the probasitarsal comb. The tibio-tarsal joint is monocondylic. The protarsus (Figure 27a,b,g,h) is divided into five tarsomeres. The proximal probasitarsus is more elongated. The apical tarsomere bears the well-developed paired claws, which articulates with the unguitractor. A well-developed, sclerotized strap-shaped manubrium is inserted between the claws. The arolium is vestigial or absent (no membranous or sclerotized elements are recognizable in the data).

Foreleg muscles (Figure 27b–h)

Ipcm2, M. procoxa cervicalis transversalis (not described in Snodgrass [1942]), a transverse muscle, **O**: anteromedially on the cervical apodeme of the opposite side of the body, **I**: anterolaterally on the procoxal base, close to the insertion of Ipcm4; **Ipcm4**, M. propleuro-coxalis superior (Sn: 53), a branched muscle, **O**: broadly on the ventral surface of the dorsal propleural margin and on the anterior process of the dorsal profurcal lamella, **I**: anterolaterally on the procoxal base, anterior to the pleural articulation, close to the insertion of Ipcm2; **Iscm1**, M. profurca-coxalis anterior (Sn: 54), **O**: broadly on the prodiscrimenal lamella of the prosternum, **I**: anteromedially on the procoxal base; **Idvm18**, M. pronoto-coxalis lateralis (Sn: 55), a long muscle, **O**: laterally on the pronotum, anterior to the pronotal lobe, **I**: posterolaterally on the procoxal base, close to the insertion of Iscm4; **Iscm4**, M. profurca-coxalis lateralis (Sn: 56), a broad muscle, **O**: on the posterodorsal profurcal lamella of the profurcal arm, **I**: posterolaterally on the procoxal base, close to the insertion of Idvm18; **Iscm3**, M. profurca-coxalis medialis (Sn: 57), a thin muscle, **O**: on the sheet of the propleural arm (not on the profurca), **I**: posteromedially on the procoxal base; **Iscm5**, M. prospina-coxalis (Sn: 58), **O**: on the horizontal plate of the meso/metafurca, **I**: posteriorly on the procoxal base, mesad Iscm4; **Ictm1**, M. procoxa-trochanteralis anterior (Sn: 59), a broad muscle, **O**: anterolateral internal procoxal surface, laterad Ictm3, **I**: anteriorly on the protrochanteral articulation piece; **Ictm2**, M. procoxa-trochanteralis posterior (Sn: 60), a small muscle, **O**: posterior internal procoxal surface, posterior to Ictm1 and Ictm3, **I**: posteriorly on the coxo-trochanteral articulation piece; **Ictm3**, M. procoxa-trochanteralis medialis (Sn: 62), a broad muscle, **O**: broadly on the anteromedian internal procoxal surface, mesad Ictm1, **I**: depressor tendon of the protrochanter; **Iscm6**, M. profurca-trochanteralis (Sn: 61), a broad muscle, **O**: on the sheet of the propleural arm, **I**: depressor tendon of the protrochanter; **Itfm1**, M. trochantero-femoralis (Sn: 63), the only profemoral muscle, **O**: broadly on the protrochanter, **I**: posteroventrally on the profemoral base; **Iftm1**, M. femuro-tibialis dorsalis (Sn: 64), **O**: dorsally on the inner profemoral surface, **I**: dorsally on the protibial base; **Iftm2**, M. femuro-tibialis ventralis (Sn: 65), **O**: ventrally on the inner surface of profemur, **I**: ventrally on the protibial base; **Itbm1**, M. tibio-basitarsalis ventralis (Sn: 67), **O**: posteriorly on the inner protibial surface, **I**: posteriorly on the base of the probasitarsus; **Itbm2**, M. tibio-basitarsalis anterior (Sn: 66), **O**: anteroventrally on the inner protibial surface, **I**: anteriorly on base of the probasistarsus; **Itbm3**, M. tibio-basitarsalis posterior (Sn: 68), **O**: anterolaterally on the inner protibial surface, **I**: ventrally on the base of probasitarsus; **Ifpm1**, M. femuro-pretarsalis (Sn: 69), an extremely long muscle, **O**: anteriorly on the profemur and anteriorly on the protibia, **I**: base of the pretarsal apparatus.

3.3.2 | Middle leg (Figure 28)

The semicylindrical mesocoxa (Figures 16b,d,e and 28a–h) is robust and about twice as large as the procoxa (Figure 16b,d,e); its basicoxal region is grossly expanded and oriented dorsoventrally. An articulatory membrane connects it with the mesepisternum anteriorly and with the metapectus posteriorly (Figure 16e). The mesocoxa articulates distally with the mesotrochanter by a dicondylic joint (Figure 28a–c). The triangular mesotrochanter (Figure 28a,b,e,f) is about 2/3 the size of the mesocoxa. It is moderately narrowed proximally and distinctly widening distally. Its straight distal edge connects it with the mesofemur at the femuro-trochanteral joint which rotates in the axis of the leg relative to the coxo-trochanteral joint and is less flexible. The mesofemur (Figure 28a,b,f) is about as wide as the distal mesotrochanter, and about twice as long, and slightly longer than the mesotibia. The dicondylic articulation with the mesotrochanter has a limited flexibility. The mesotibia (Figure 28a,b,f–h) is slightly shorter and less wide than the mesofemur. A fairly dense vestiture of articulated chaetae (= traction setae) is present on its lateral surface. One spur is inserted on the mesotibial apex. The femuro-tibial joint is dicondylic. The tibio-tarsal joint is monocondylic. On the mesotarsus (Figure 28a,b,g,h), the first tarsomere, the mesobasitarsus, is more elongated than the other tarsal segments. The apical tarsomere bears the claws and the manubrium.

Middle leg muscles (Figure 28b–d)

IIpcm4, M. propleuro-coxalis posterior (Sn: 80), a branched muscle, **O**: laterally on the mesepisternum, close to IIspm2, **I**: laterally on the mesocoxal base; **IIscm1**, M. mesofurca-coxalis anterior (Sn: 81), **O**: posteroventrally on the mesodiscrimenal lamella, posterior to IIscm2, **I**: anteromedially on the mesocoxal base; **IIdvm6**, M. mesocoxa-subalaris (Sn: 82), a slender muscle, **O**: posterolaterally on the mesocoxal base, **I**: on the mesosubalar sclerite; **IIscm2**, M. mesofurca-coxalis posterior (Sn: 83), the largest mesocoxal muscle, **O**: anteroventrally on the mesodiscrimenal lamella, anterior to IIscm1, **I**: posteromedially on the base of the mesocoxa; **IIctm1**, M. mesocoxa-trochanteralis anterior (Sn: 84), a broad muscle, **O**: anterolateral internal surface of mesocoxa, laterad IIctm3, **I**: anteriorly on base of the mesotrochanter; **IIctm2**, M. mesocoxa-trochanteralis posterior (Sn: 85), a small muscle, **O**: posterior internal surface of mesocoxa, posterior to IIctm1 and IIctm3a, **I**: posteriorly on the base of the mesotrochanter; **IIctm3**, M. mesocoxa-trochanteralis medialis (Sn: 87 + 88), a broad muscle with two subcomponents; **IIctm3a**, M. mesocoxa-trochanteralis medialis primus (Sn: 87), **O**: anteriorly on the internal mesocoxal surface, medially to IIctm1, **I**:

depressor tendon of mesotrochanter; **IIctm3b**, M. mesocoxa-trochanteralis medialis secundus (Sn: 88), **O**: posteriorly on the internal mesocoxal surface, dorsally to IIctm2, **I**: depressor tendon of the mesotrochanter; **IIscm6**, M. mesofurca-trochanteralis (Sn: 86), a broad muscle, **O**: on the coalesced furcal arms, the free basal portion of mesofurcal arm, and the free distal portion of mesofurcal arm, **I**: depressor tendon of the mesotrochanter; **IItfm1**, M. trochantero-femoralis (Sn: 89), **O**: broadly on the mesotrochanter, **I**: posteroventrally on the mesofemoral base; **IIftm1**, M. femuro-tibialis dorsalis (Sn: 90), **O**: dorsally on the internal surface of mesofemur, **I**: dorsally on the base of mesotibia; **IIftm2**, M. femuro-tibialis ventralis (Sn: 91), **O**: ventrally on the internal surface of the mesofemur, **I**: ventrally at the base of the mesotibia; **IItbm1**, M. tibio-basitarsalis ventralis (Sn: 93), **O**: posteriorly on the internal surface of the mesotibia, **I**: posteriorly on base of the mesobasitarsus; **IItbm2**, M. tibio-basitarsalis anterior (Sn: 92), **O**: anteroventrally on the internal surface of the mesotibia, **I**: anteriorly on the base of the mesobasistarsus; **IItbm3**, M. tibio-basitarsalis posterior (Sn: 94), **O**: anterolaterally on the internal surface of the mesotibia, **I**: ventrally on the base of mesobasitarsus; **IIfpm1**, M. femuro-pretarsalis (Sn: 95), an extremely long muscle, **O**: anteriorly on the mesofemur and anteriorly on the mesotibia, **I**: base of the pretarsal apparatus.

3.3.3 | Hind leg (Figure 29)

The hind leg is larger than the middle leg; the setae are more densely arranged, especially on the metatibia and metatarsus. The metacoxa (Figures 16d–f and 29a–e) is larger than its pro- and mesothoracic equivalents. It appears cone-shaped and is about twice as long as the mesocoxa (Figure 16d–f). An articulatory membrane connects it anteriorly with the metapectus, and posteriorly with sternum II. Distally the metacoxa articulates with the metatrochanter (Figure 29a–e). The metatrochanter (Figure 29a,b,e,f) is about one-third the size of the metacoxa. It articulates through a dicondylic joint with the metacoxa. The metafemur is connected to its distal edge at the metatrochanteral joint with limited movability. The metafemur (Figure 29a,b,f) is about as wide as the metatrochanter and twice as long. It is slightly longer than the metatibia. The trochantero-femoral articulation is dicondylic with a limited flexibility. The metatibia (Figure 29a,b,f–h) is slightly shorter and less wide than the metafemur. The femuro-tibial joint is dicondylic. Two metatibial spurs are present apically. The tibio-tarsal joint is monocondylic. On the metatarsus (Figure 29a,b,g,h), the metabasitarsus is elongated and bears a dense vestiture of setae. The pretarsal elements are similar to those of the other legs.

Hind leg muscles (Figure 29)

IIIpcm4, M. metanepisterno-coxalis posterior (Sn: 103), **O**: broadly on the metapleural ridge and intercoxal lamella, **I**: anterolaterally on base of the metacoxa; **IIIscm1**, M. metafurca-coxalis anterior (Sn: 104), **O**: broadly on the free basal portion of metafurcal arm and metadiscrimenal lamella, **I**: anteriorly on the metacoxal base; **IIIdvm6**, M. metacoxa-subalaris (Sn: 105), **O**: posterolaterally on the base of the metacoxa, **I**: metasubalar sclerite; **IIIscm2**, M. metafurca-coxalis posterior (Sn: 106), **O**: broadly on the free basal portion of the metafurcal arm, laterally to IIIscm3, **I**: posteriorly at the metacoxal base; **IIIscm3**, M. metafurca-coxalis medialis (Sn: 106), **O**: metadiscrimenal lamella and free basal portion of metafurcal arm, medially to IIIscm2, **I**: posteromedially on the metacoxa; **IIIctm1**, M. metacoxa-trochanteralis anterior (Sn: 107), **O**: anterior internal metacoxal surface, **I**: anteriorly on the base of the metatrochanter; **IIIctm2**, M. metacoxa-trochanteralis posterior (Sn: 108), a small muscle, **O**: posterior internal surface of the metacoxa, **I**: posteriorly on the base of the metatrochanter; **IIIctm3**, M. metacoxa-trochanteralis medialis (Sn: 110), a broad muscle, **O**: ventrally on the internal surface of the metacoxa, **I**: depressor tendon of the metatrochanter; **IIIscm6**, M. metafurca-trochanteralis, (Sn: 109), **O**: posterior surface of the mesofurcal bridge and coalesced furcal arms, **I**: depressor tendon of the metatrochanter; **IIItfm1**, M. trochantero-femoralis (Sn: 111), the only metafemoral muscle, **O**: broadly on the metatrochanter, **I**: posteroventrally on the base of the metafemur; **IIIftm1**, M. femuro-tibialis dorsalis (Sn: 112), **O**: dorsally on the internal surface of the metafemur, **I**: dorsally on the base of the metatibia; **IIIftm2**, M. femuro-tibialis ventralis (Sn: 113), **O**: ventrally on the internal surface of the metafemur, **I**: ventrally at the base of the metatibia; **IIItbm1**, M. tibio-basitarsalis ventralis (Sn: 115), **O**: posteriorly on the internal surface of the metatibia, **I**: posteriorly on the base of the metabasitarsus; **IIItbm2**, M. tibio-basitarsalis anterior (Sn: 114), **O**: anteroventrally on the inner surface of the metatibia, **I**: anteriorly on the base of the metabasistarsus; **IIItbm3**, M. tibio-basitarsalis posterior (Sn: 116), **O**: anterolaterally on the inner surface of the metatibia, **I**: ventrally on the base of the metabasitarsus; **IIIfpm1**, M. femuro-pretarsalis (Sn: 117), an extremely long muscle, **O**: anteriorly on the metafemur and anteriorly on the metatibia, **I**: base of the pretarsal apparatus.

3.4 | Propodeum (abdominal segment I) (Figures 16 and 30)

The propodeum, the abdominal tergum I, is fused to the thorax. It is one of the largest areas of the mesosoma and forms the posteriormost part of this secondary tagma (Figure 16d–f). Anteriorly the propodeum presents the **propodeal antecosta** and articulates with the metanotum (Figures 16d–f and 30a,b); the propodeal spiracle, which is larger than any others, is located (Figures 16d–f and 30a) on the lateral propodeal region. The lateral propodeal areas are continuous externally with the metapectus, with the border indistinctly indicated by the metapleural pits (Figure 16d,e). Internally both regions are separated by the distinct metapleural ridge (Figure 25c) that runs alongside the metepisternal pits and the insertion of the metafurcal arms. Ventrally the marginal area of the propodeum (Figure 16f) forms the distinctly visible propodeal condyle (Figure 16f). Medially on the propodeum a v-shaped metaphragmal scar is present, culminating in the **propodeal sulcus**; this sulcus corresponds internally to the **propodeal ridge** (Figure 16f). A sternum associated with the propodeum is not present.

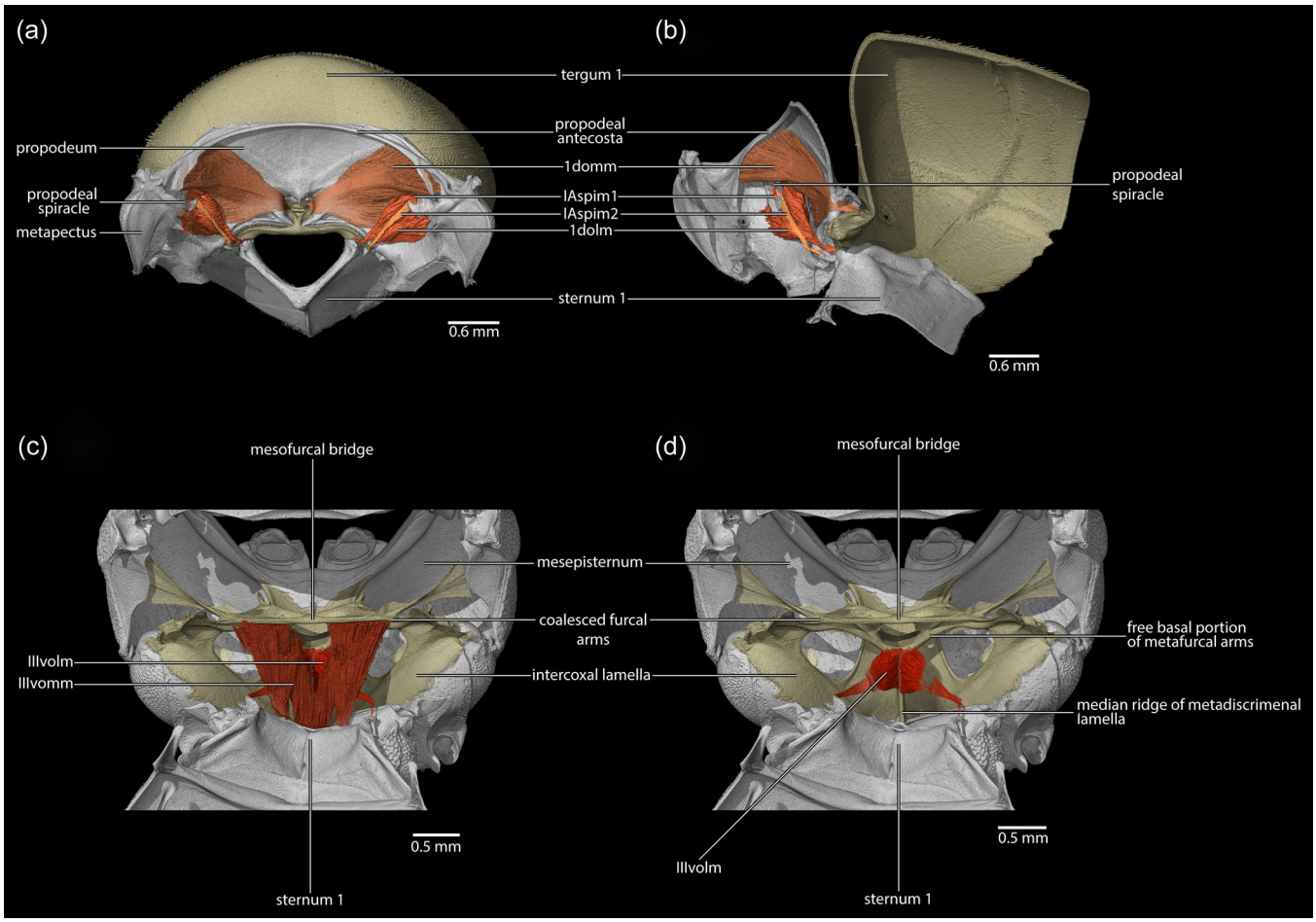

FIGURE 30 Propodeal musculature of *Thyreus albomaculatus*. (a) Propodeum and metasomal segment 1, anterior view of the propodeum. (b) Propodeum and metasomal segment 1, medial view of the propodeum. (c) Propodeal cavity, meso-metafurcal complex and metasomal segment 1, dorsal view of meso-metafurcal complex. (d) Propodeal cavity, meso-metafurcal complex and metasomal segment 1, dorsal view of meso-metafurcal complex.

3.4.1 | Propodeal muscles (Figure 30)

1domm, M. tergo-tergalis orthomedialis (Sn: 120), **O**: broadly on the anterior wall of the propodeum, **I**: medially on the constricted margin of tergum I; **1dolm**, M. tergo-tergalis ortholateralis (Sn: 121), **O**: broadly on the lateral region of the propodeum, below 1domm, **I**: laterally on the anterior margin of the tergum I; **lAspim1**, M. spiracularis I superior (Sn: 122), an intraspiracular muscle, **O**: sclerotized area above the propodeal spiracle, **I**: sclerotized area below the propodeal spiracle; **lAspim2**, M. spiracularis I posterior (Sn: 123), a thin spiracular muscle, **O**: small metapleural coxal process, **I**: sclerotized area below the propodeal spiracle; **IIIlvomm**, M. metafurca-abdominosternalis medialis, (Sn: 118), **O**: free basal portion of the metafurcal arm, posterior surface of the coalesced furcal arms, and mesofurcal bridge, **I**: medially on sternum 1; **IIIlvolm**, M. metafurca-abdominosternalis lateralis, (Sn: 119), **O**: metadiscrimenal lamella, **I**: laterally on sternum 1.

3.5 | Metasoma of *T. albomaculatus* (Figure 31)

The metasoma is the abdomen posterior to the propodeum (= abdominal segment I). It comprises six pregenital segments (= metasomal segments 1–6 = abdominal segments II–VII), the genitalia, and the proctiger (= anus-bearing segment complex posterad the genitalia) (Figure 31a,b). The pregenital tergites and sternites are laterally connected by narrow membranes, which are not visible externally. Sclerotized pleural elements are incorporated into the tergites and not visible as individual elements (Vilhelmsen, 1997, 2001). All exposed tergal and sternal plates are distinctly overlapping with the corresponding elements of the following segment, thus the metasoma forms a telescoping structure without exposed membranes. The metasomal spiracles (Figure 31a) are located on the lateroventral areas of terga 1–6; those of terga 2–6 are concealed by the preceding tergum. All metasomal terga lack laterotergites. Similar to the rest of the body, the surface of the cuticle, as documented in the μ-CT data, is covered with a fine pattern of setal sockets.

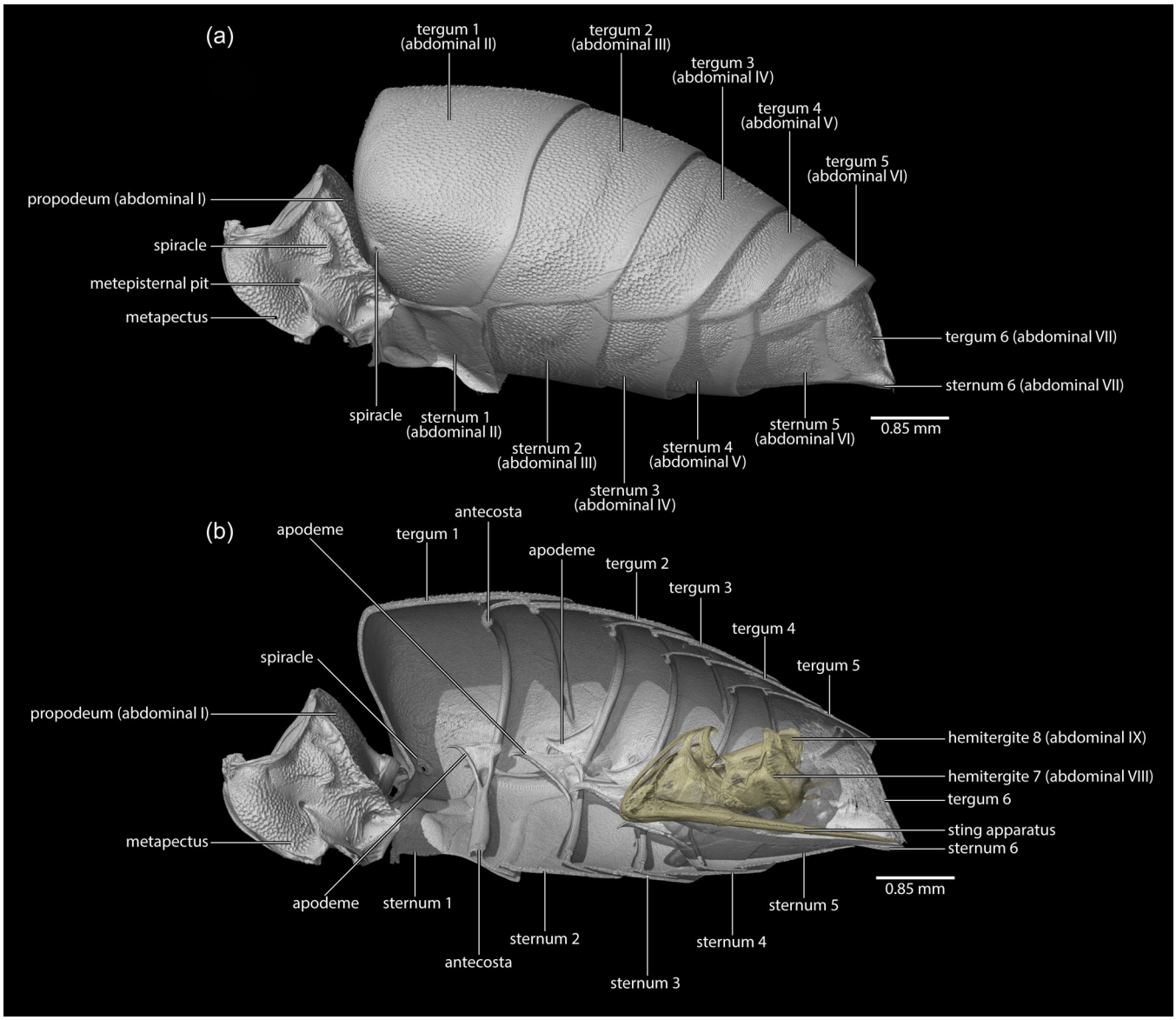

FIGURE 31 Metasoma and propodeum of *Thyreus albomaculatus*. (a) Lateral view of metasoma. (b) Medial view of metasoma.

The pregenital metasomal segments 1 and 2 are modified in correlation with their connection with the propodeum and share a similar skeletomuscular structure. The following metasomal segments 3–6 are similar in their configuration of sclerites and muscles. The pregenital and exposed part of the abdomen ends with metasomal segment 6 (tergum and sternum VII). The genital area is internalized and comprises metasomal segments 7 and 8, which contain the sting apparatus in females (Figure 31b).

3.5.1 | Metasomal segment 1 (abdominal segment II) (Figure 32)

The metasomal segment 1 comprises tergum and sternum 1 (abdominal tergum and sternum II) as sclerotized elements (Figures 31a,b and 32a,b).

Tergum 1, the largest tergal sclerite of the metasoma (Figure 31a), is a laterally and anteriorly inflected plate (Figure 32b); its posterior margin is connected with tergum 2 via a membrane and it articulates laterally with sternum 1 (Figure 31a). The anterior margin of tergum 1 is modified, constricted, and strengthened as the acrotergite ("pretergite") (Figure 32a,b), forming the metasomal articulation with the propodeum, the levator process (Figure 30a,b). Posterior to the acrotergite, the antecostal suture is visible externally (Figure 32a,b), but without a corresponding internal antecosta. The spiracle of tergum 1 (Figure 32a,b) is located ventrolaterally close to the connection with sternum 1. It lacks apodemes.

Sternum 1 is distinctly smaller than the corresponding tergite; it is posteriorly connected with sternum 2 and laterally with tergum 1 (Figure 31a) via membranes; its surface has a complex shape, with anterior, lateral, and median carinae; the median carina is longitudinally

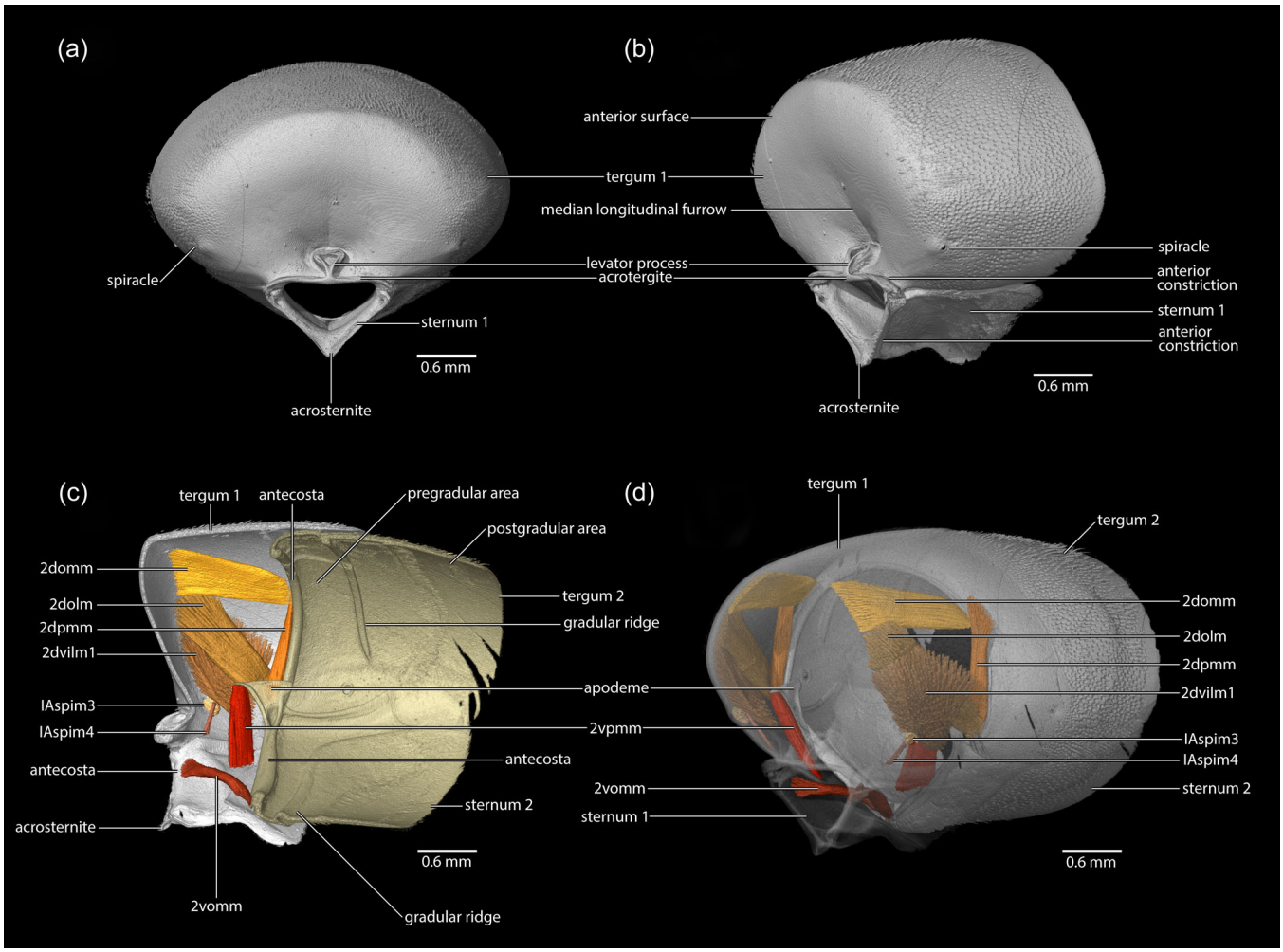

FIGURE 32 Metasomal segments 1 and 2 of *Thyreus albomaculatus*. (a) Segment 1, anterior view. (b) Segment 1, anterolateral view. (c) Segments 1 and 2, and muscles of segment 1, medial view of tergum 1. (d) Segments 1 and 2 and muscles of segment 1, sclerites of segment 1 semitransparent, anterolateral view of tergum 1.

oriented, developed as a flange, and unevenly sinuate along its length. Anteriorly, the acrosternite connects sternum 1 with the propodeum (Figure 32a,b). Posterior to the acrosternite, the antecosta (Figure 32a–c) is well developed internally, as an attachment area for muscles; externally it is visibly as the antecostal furrow (Figure 32a,b). The lateral surface, laterad the lateral carina, contacts and contours to terga 1 and 2. Similar to tergum 1, sternum 1 lacks apodemes.

Metasomal segment 1 muscles *(Figure 32c,d)*

2domm, M. tergo-tergalis orthomedialis (Sn: 124), **O**: dorsolaterally on the anterior area of tergum 1, above 2dolm origin, **I**: dorsolaterally on the antecosta of tergum 2; **2dolm**, M. tergo-tergalis ortholateralis (Sn: 125), **O**: dorsolaterally on the anterior area of tergum 1, below the origin of 2domm, **I**: anteroventrally on the antecosta of tergum 2, below the insertion of 2dpmm; **2dpmm**, M. tergo-tergalis paramedialis (Sn: 126), **O**: dorsolaterally on the posterior area of tergum 1, **I**: anteroventrally on the antecosta of tergum 2, above the insertion of 2dolm; **2dvilm1**, M. tergo-sternalis interior lateralis primus (Sn: 129), **O**: laterally on the anterior area of tergum 2, below the origin of 2dpmm, **I**: laterally on sternum 1, laterally to the origin of 2vpmm; **2vpmm**, sterno-sternalis paramedialis (Sn: 132), **O**: lateromedially on sternum 1, medially to the insertion of 2dvilm, **I**: anteriorly on the apodeme of sternum 2; **2vomm**, M. sterno-sternalis orthomedialis (Sn: 130), **O**: laterally on the antecosta of sternum 1, **I**: medially on the antecosta of sternum 2; **lAspim3**, M. spiracularis II superior (Sn: 127), **O**: sclerotized area above the spiracle of tergum 1, **I**: sclerotized area below the spiracle of tergum 1; **lAspim4**, M. spiracularis II posterior (Sn: 128), **O**: laterally on the anterior margin of sternum 1, **I**: sclerotized area below the spiracle of metasomal segment 1.

3.5.2 | Metasomal segment 2 (abdominal segment III) (Figure 33)

Metasomal segment 2 differs distinctly from segment 1 in terms of sclerites and muscles; it is composed of the plate-like tergum and sternum 2 (abdominal tergum and sternum III) (Figure 31a,b). Tergum 2 is about as large as the posterior portion of tergum 1 (Figure 31b)

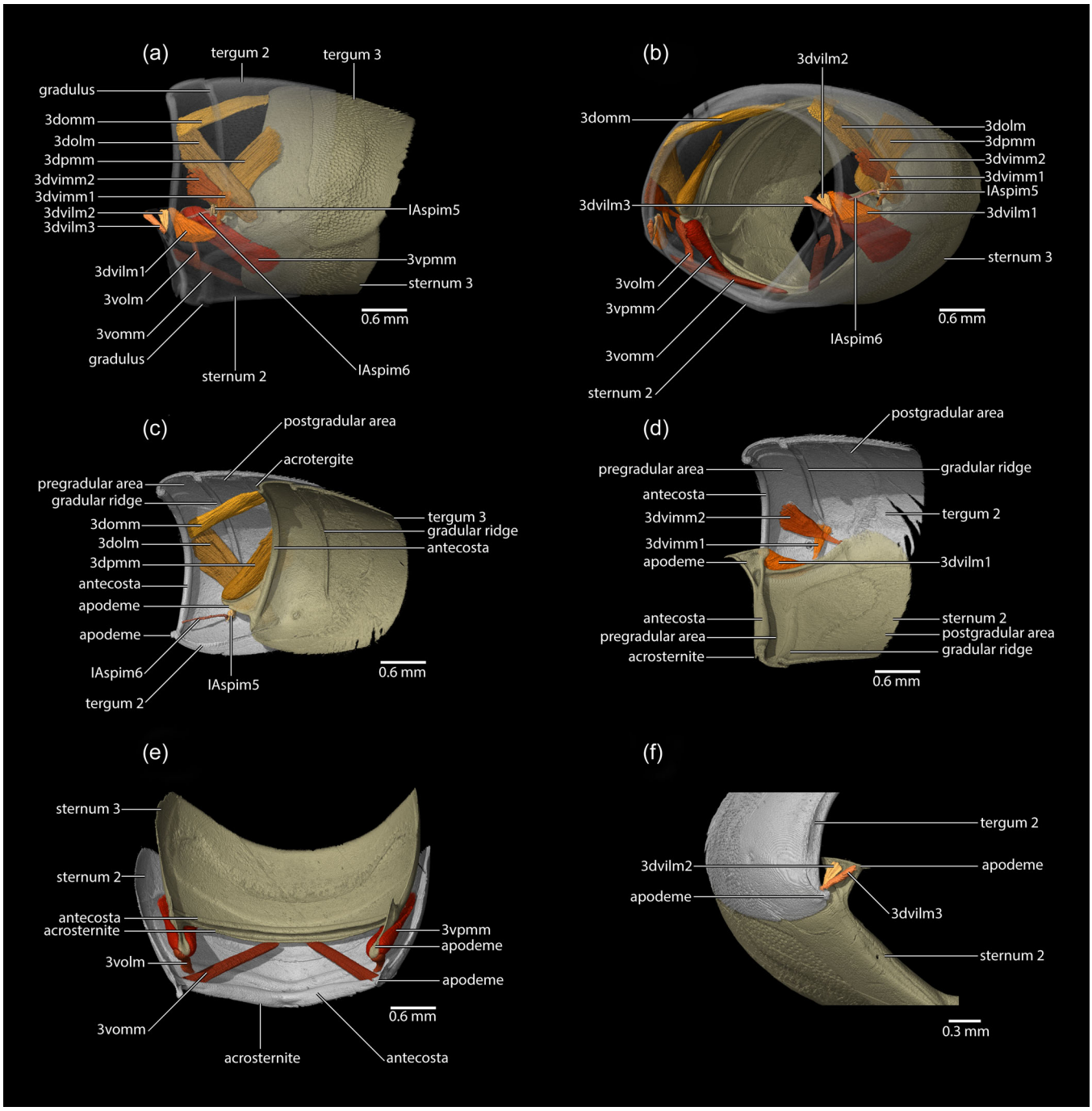

FIGURE 33 Metasomal segments 2 and 3 of *Thyreus albomaculatus*. (a) Segments 2 and 3, sclerites of segment 2 semitransparent, lateral view of tergum 2. (b) Segments 2 and 3 sclerites of segment 2 semitransparent, anterolateral view of tergum 2. (c) Tergum 2 and 3, and muscles of segment 2, medial view of tergum 2. (d) Muscles of segment 2, medial view of tergum 2. (e) Muscles of sternum 2 and 3, anterodorsal view of sternum 2. (f) Segment 2 with muscles, anterolateral view of sternum 2.

but lacks a constricted and modified anterior margin. It is posteriorly connected with tergum 3 via membrane, and laterally with sternum 2 (Figure 31a,b). Anteriorly, an antecosta is present on tergum 2 but an acrotergite is lacking (Figure 33c,d). Near the anterior margin, tergum 2 bears the gradulus (Figure 33a), which is a distinct external line that extends towards the lateral margins but does not reach these; it divides the sclerite into a smaller anterior pregradular region and a more extensive postgradular region (Figure 33d). Internally, the gradulus is marked by a well-developed internal ridge (**gradular ridge**) (Figure 33c,d). The spiracle (Figure 33c) of tergum 2 is located laterally on the pregradular area, close to the gradular ridge. The moderately developed apodeme of tergum 2 (Figure 33c,f) is located at the anteroventral margin of the antecosta. Sternum 2 is similar in size to sternum 1 (Figure 32c). Posteriorly, it connects with sternum 3

and laterally with tergum 2 (Figure 31a,b). The gradulus near its lateral apex (Figure 33a) corresponds with a well-developed internal gradular ridge (Figure 33d), similar to the tergum of this segment. The well-developed antecosta of sternum 2 (Figure 33d,e) bears a visible acrosternite anteriorly; distinctly developed apodemes of sternum 2 (Figure 33d,f) are located laterally on this structure.

Metasomal segment 2 muscles *(Figure 33a–f)*

3domm, M. tergo-tergalis orthomedialis (Sn: 133), **O**: dorsolaterally on the antecosta of tergum 2, above the origin of 3dolm, **I**: dorsomedially on the antecosta of tergum 3; **3dolm**, M. tergo-tergalis ortholateralis (Sn: 134), **O**: dorsolaterally on the antecosta of tergum 2, below the origin of 3domm, **I**: anteroventrally on the anterior margin of tergum 3, below the insertion of 3dvimm2; **3dpmm**, M. tergo-tergalis paramedialis (Sn: 135), **O**: dorsolaterally on the postgradular area of tergum 2, **I**: anteriorly on the apodeme of tergum 3; **3dvilm**, M. tergo-sternalis interior lateralis, a muscle with three subcomponents, **3dvilm1**, M. tergo-sternalis interior lateralis primus (Sn: 138), **O**: anteroventrally on the pregradular area of tergum 2, **I**: tip of apodeme of sternum 2, posterior to the origin of 3dvilm2; **3dvilm2**, M. tergo-sternalis interior lateralis secundus (not observed by Snodgrass [1942]), **O**: tip of the apodeme of sternum 2, anterior to the insertion of 3dvilm1, **I**: apodeme of tergum 2, close to the insertion of 3dvilm3; **3dvilm3**, M. tergo-sternalis interior lateralis tertius (not observed by Snodgrass [1942]), **O**: tip of the apodeme of sternum 2, anterior to the origin of 3dvilm2, **I**: apodeme of tergum 2, close to the insertion of 3dvilm2; **3dvimm**, a muscle with two subcomponents, **3dvimm1**, M. tergo-sternalis interior anteromedialis (Sn: 139), **O**: below the lateral end of the gradular ridge of tergum 2, **I**: medially on the lateral margin of sternum 2, anterior to the insertion of 3dvimm2; **3dvimm2**, M. tergo-sternalis interior posteromedialis (Sn: 140), **O**: ventrally on the pregradular area of tergum 2, **I**: posteriorly on the lateral margin of sternum 2, posterior to the insertion of 3dvimm1; **3vpmm**, M. sterno-sternalis paramedialis, (Sn: 143), **O**: laterally on the postgradular area of sternum 2, **I**: ventrally on the apodeme of sternum 3, posterior to the insertion of 3volm; **3vomm**, M. sterno-sternalis orthomedialis (Sn: 141), **O**: laterally on the antecosta of sternum 2 anterior to the origin of 3volm, **I**: medially on the acrosternite of sternum 3; **3volm**, M. sterno-sternalis ortholateralis (Sn: 142), **O**: anterolaterally on the pregradular area of sternum 2, posterior to the origin of 3vomm, **I**: tip of the apodeme of sternum 3, anterior to the insertion of 3vpmm; **lAspim5**, M. spiracularis III superior (Sn: 136), **O**: sclerotized area above the spiracle of tergum 2, **I**: sclerotized area below the spiracle of tergum 2; **lAspim6**, M. spiracularis III posterior (Sn: 137), **O**: laterally on the anterior margin of sternum 2, **I**: sclerotized area below the spiracle of metasomal segment 2.

3.5.3 | Metasomal segment 3 (abdominal IV) (Figure 34)

Metasomal segment 3 (Figure 31a,b) is similar in its structure to segment 2. Tergum 3 (Figure 34) is somewhat smaller than tergum 2 (Figure 31b). Laterally, it connects with sternum 3 and posteriorly with tergum 4 (Figure 31a,b). On the anterior margin, the antecosta and acrotergite are visible (Figure 34c). A distinct gradulus (externally) and gradular ridge (internally) (Figure 34d) separate the smaller pregradular area (Figure 34d), from the larger postgradular area (Figure 34d). Spiracle 3 (Figure 34c) is located laterally on the pregradular area, close to the gradular ridge. The apodeme (Figure 34c) of tergum 3 is more developed than that of the preceding tergum. Sternum 3, which is slightly smaller than sternum 3 (Figure 31a,b), is posteriorly connected with sternum 4. The antecosta and acrosternite are present on the anterior margin (Figure 34e). Unlike in sternum 2, the gradular ridge (Figure 34d) is restricted to the lateral sternal areas. The apodeme (Figure 34d,e) is well developed.

Metasomal segment 3 muscles *(Figure 34a–e)*

4domm, M. tergo-tergalis orthomedialis (Sn: 144), **O**: dorsolaterally on the antecosta of tergum 3, above the origin of 4dolm, **I**: dorsomedially on the acrotergite of tergum 4; **4dolm**, M. tergo-tergalis ortholateralis (Sn: 145), **O**: dorsolaterally on the antecosta of tergum 3, below the origin of 4domm, **I**: ventrally on the anterior margin of tergum 4, below the insertion of 4dvimm2; **4dpmm**, M. tergo-tergalis paramedialis (Sn: 146), **O**: dorsolaterally on the postgradular area of tergum 3, **I**: apodeme of tergum 4; **4dvilm1**, M. tergo-sternalis interior lateralis primus (Sn: 149), **O**: ventrally on the pregradular area of tergum 3, **I**: tip of apodeme of sternum 3; **4dvimm1**, M. tergo-sternalis interior anteromedialis (Sn: 150), **O**: posteroventrally on the pregradular area of tergum 3, **I**: medially on the lateral margin of sternum 3, anterior to the insertion of 4dvimm2; **4dvimm2**, M. tergo-sternalis interior posteromedialis (Sn: 151), **O**: anteroventrally on the pregradular area of tergum 3, **I**: posteriorly on the lateral margin of sternum 3, posterior to the insertion of 4dvimm1; **4volm**, M. sterno-sternalis ortholateralis (Sn: 153), **O**: anterolaterally on sternum 3, posterolateral to the of origin 4vomm, **I**: tip of the apodeme of sternum 4, anterior to the insertion of 4vpmm; **4vpmm**, M. sterno-sternalis paramedialis (Sn: 154), **O**: posterolaterally on the sternum 3, **I**: ventrally on the apodeme of sternum 4, posterior to the insertion of 4volm; **4vomm**, M. sterno-sternalis orthomedialis (Sn: 152), **O**: laterally on the antecosta of sternum 3, anteromedially to the origin of 4volm, **I**: medially on the acrosternite of sternum 4; **lAspim7**, M. spiracularis IV superior (Sn: 147), **O**: sclerotized area above the spiracle of tergum 3, **I**: sclerotized area below the spiracle of tergum 3; **lAspim8**, M. spiracularis IV posterior (Sn: 148), **O**: laterally on the anterior margin of sternum 3, **I**: sclerotized area below the spiracle of metasomal segment 3.

3.5.4 | Metasomal segment 4 (abdominal segment V) (Figure 35)

Metasomal segment 4 (Figure 31a,b) is similar to segment 3. Tergum 4 (Figure 31a,b) is smaller than the preceding one and connected with the adjacent sclerites in the usual manner. Antecosta and acrotergite are present anteriorly (Figure 35c) and also a distinct gradular ridge (Figure 35d) separating the pregradular (Figure 35d) from the

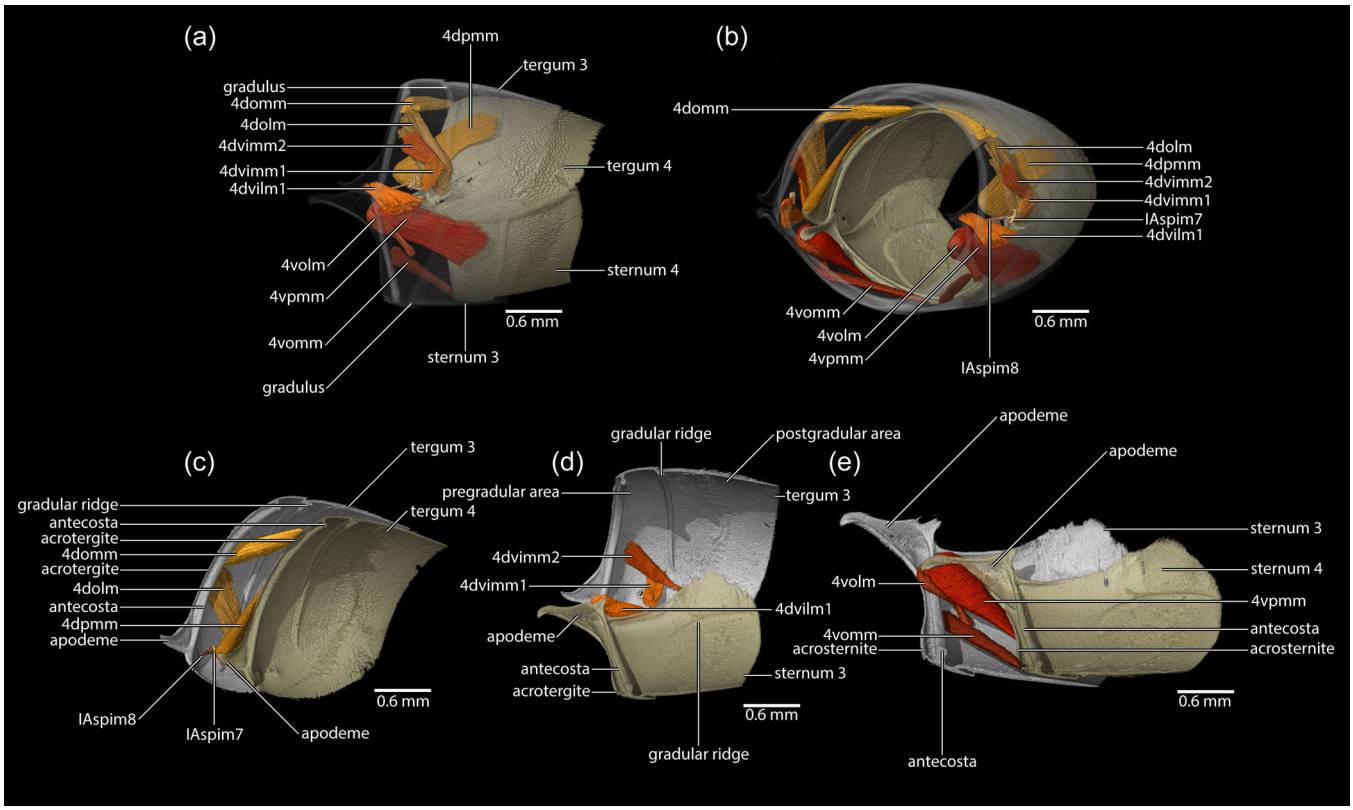

FIGURE 34 Metasomal segments 3 and 4 of *Thyreus albomaculatus*. (a) Segments 3 and 4, sclerites of segment 3 semitransparent, lateral view of tergum 3. (b) Segments 3 and 4, sclerites of segment 3 semitransparent, anterolateral view of tergum 3. (c) Tergum 4, 5, and muscles of segment 3, anteromedial view of tergum 3. (d) Muscles of segment 3, medial view of tergum 3. (e) Sternum 3, 4 and muscles of segment 3, medial view of sternum 3.

postgradular area (Figure 35d). The spiracle (Figure 35c) is located ventrolaterally on the pregradular area, and the apodeme (Figure 35c) anteroventrally on the acrotergite of tergum 4. Sternum 4 bears the antecosta and acrosternite (Figure 35c) on the anterior margin; similar to sternum 3 it also bears a gradulus and gradular ridge which are restricted to the lateral areas of the sternum; the apodeme is well developed (Figure 35c,d).

Metasomal segment 4 muscles *(Figure 35a–e)*

5domm, M. tergo-tergalis orthomedialis (Sn: 155), **O**: dorsolaterally on the antecosta of tergum 4, dorsally to 5dolm origin, **I**: dorsomedially on the acrotergite of tergum 5; **5dolm1**, M. tergo-tergalis ortholateralis minor (Sn: 156), **O**: lateroventrally on the antecosta of tergum 4, below the origin of 5dolm2, **I**: anteroventrally on the anterior margin of tergum 5, below the insertion 5dolm2; **5dolm2**, M. tergo-tergalis ortholateralis major (Sn: 156), **O**: laterally on the antecosta of tergum 4, dorsad the origin of 5dolm1, **I**: anteroventrally on the anterior margin of tergum 5, dorsad the insertion 5dolm1; **5dpmm**, M. tergo-tergalis paramedialis (Sn: 157), **O**: dorsolaterally on the postgradular area of tergum 4, **I**: apodeme of tergum 5; **5dvilm1**, M. tergo-sternalis interior lateralis primus (Sn: 160), **O**: ventrally on the pregradular area of tergum 4, **I**: posterior tip of apodeme of sternum 4; **5dvimm1**, M. tergo-sternalis interior anteromedialis (Sn: 161), **O**: posteroventrally on the pregradular area of tergum 4; **I**: medially on the lateral margin of sternum 4, anterior to the insertion of 5dvimm2; **5dvimm2**, M. tergo-sternalis interior posteromedialis (Sn: 162), **O**: anteroventrally on the pregradular area of tergum 4, close to the dorsal branch of 5dolm, **I**: posteriorly on the lateral margin of sternum 4, posterior to the insertion of 5dvimm1; **5volm**, M. sterno-sternalis ortholateralis (Sn: 164), **O**: laterally on the anterior area of sternum 4, posterior to 5vomm origin, **I**: dorsally on apodeme of sternum 5, laterad the insertion of 5vpmm; **5vpmm**, M. sterno-sternalis paramedialis (Sn: 165), **O**: laterally on the posterior area of sternum 4, **I**: ventrally on the apodeme of sternum 5, laterad the insertion of 5volm; **5vomm**, M. sterno-sternalis orthomedialis (Sn: 163), **O**: laterally on the antecosta of sternum 4, anteromediad the origin of 5volm, **I**: medially on the acrosternite of sternum 5; **lAspim9**, M. spiracularis III superior (Sn: 158), **O**: sclerotized area above the spiracle of tergum 4, **I**: sclerotized area below the spiracle of tergum 4; **lAspim10**, M. spiracularis III posterior (Sn: 159), **O**: laterally on the anterior margin of sternum 4, **I**: sclerotized area below the spiracle of metasomal segment 4.

3.5.5 | Metasomal segment 5 (abdominal VI) (Figure 36)

Metasomal segment 5 (Figure 31a,b) is similar in structure to segment 4. Tergum 5 articulates with the adjacent sclerites in the typical

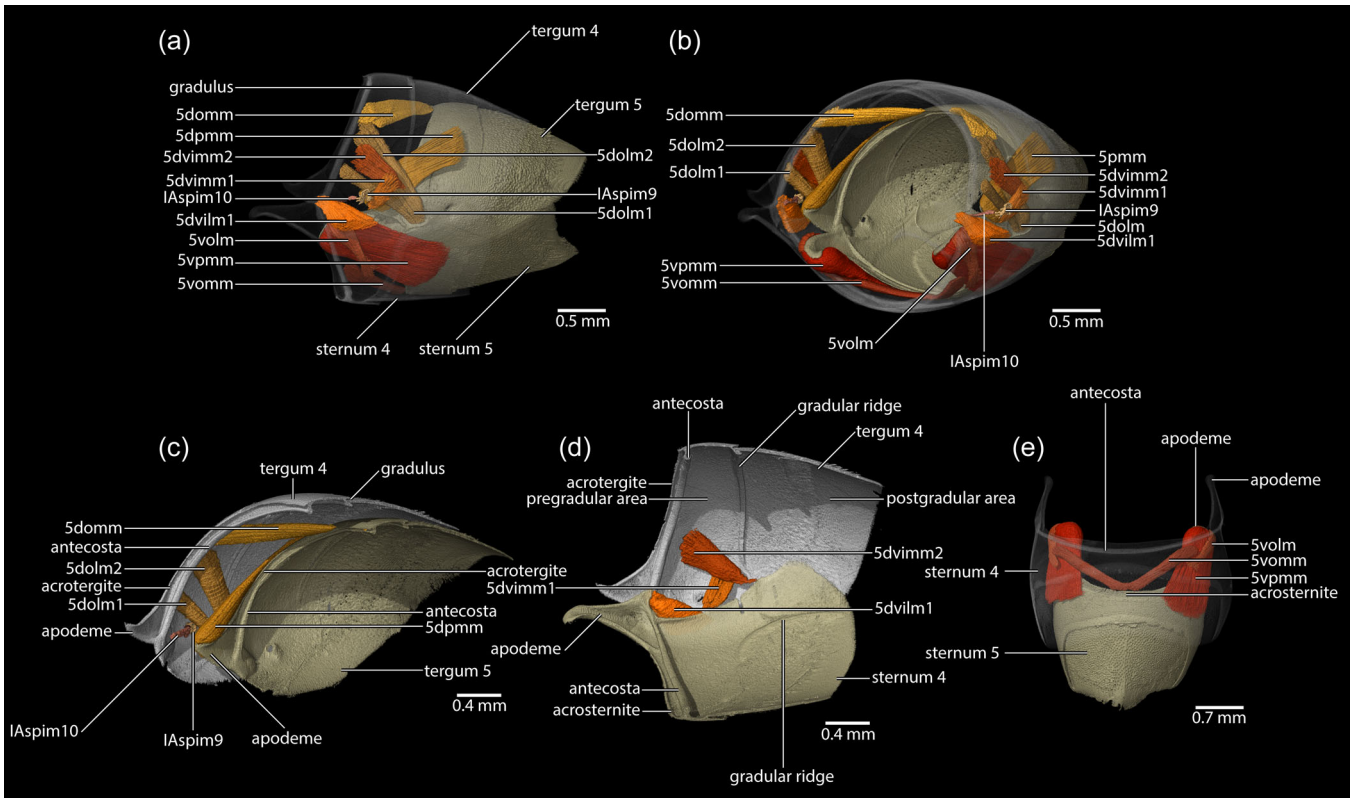

FIGURE 35 Metasomal segments 4 and 5 of *Thyreus albomaculatus*. (a) Segments 4 and 5, sclerites of segment 4 semitransparent, lateral view of tergum 4. (b) Segments 4 and 5, sclerites of segment 4 semitransparent, anterolateral view of tergum 4. (c) Tergum 4, 5, and muscles of segment 3, anteromedial view of tergum 4. (d) Muscles of segment 4 muscles, medial view of tergum 4. (e) Sternum 4, 5 and muscles of segment 4, sternum 4 semitransparent, ventral view of sternum 4.

manner (Figure 31a,b). It is smaller than tergum 4 (Figure 31a,b) but similar in its general structure, with a gradular ridge separating the pregradular and postgradular areas (Figure 36d). The spiracle (Figure 36c) of tergum 5 is located ventrally on the pregradular area. The well-developed apodeme (Figure 36c,d) is located ventrally on the antecosta of tergum 5. Sternum 5 displays a well-developed gradular ridge (Figure 36d) separating the pregradular and postgradular areas. The apodeme (Figure 36d) is laterally located on the antecosta of sternum 5.

Metasomal segment 5 muscles (Figure 36a–e)

6domm, M. tergo-tergalis orthomedialis (Sn: 166), **O**: laterally on the antecosta of tergum 5, above the origin of 6dolm, **I**: dorsomedially on the acrotergite of tergum 6; **6dolm**, M. tergo-tergalis ortholateralis (Sn: 167), **O**: ventrally on the antecosta of tergum 5, below the origin of 6domm, **I**: ventrally on the anterior margin of tergum 6, below the insertion of 6dvimm2; **6dpmm**, M. tergo-tergalis paramedialis (Sn: 168), **O**: dorsolaterally on the postgradular area of tergum 5, **I**: apodeme of tergum 6; **6dvilm1**, M. tergo-sternalis interior lateralis primus (Sn: 171), **O**: ventrolaterally on the pregradular area of tergum 5, **I**: posterior tip of the apodeme of sternum 5; **6dvimm1**, M. tergo-sternalis interior anteromedialis (Sn: 172), **O**: ventrally on the pregradular area of tergum 5, **I**: medially on the lateral margin of sternum 5, anterior to the insertion of 6dvimm2; **6dvimm2**, M. tergo-sternalis interior posteromedialis (Sn: 173), **O**: anteroventrally on the pregradular area of tergum 5, **I**: posteriorly on the lateral margin of sternum 5, posterior to the insertion of 5dvimm1; **6volm**, M. sterno-sternalis ortholateralis (Sn: 175), **O**: laterally on the pregradular area of sternum 5, **I**: laterally on the apodeme of sternum 6, laterad the insertion of 6vpmm; **6vpmm**, M. sterno-sternalis paramedialis (Sn: 176), **O**: laterally on the postgradular area of sternum 5, **I**: medially on the apodeme of sternum 6, mediad the insertion of 6volm; **6vomm**, M. sterno-sternalis orthomedialis (Sn: 174), **O**: on the apodeme of sternum 5, **I**: medially on the acrosternite of sternum 6; **lAspim11**, M. spiracularis III superior (Sn: 169), **O**: sclerotized area above the spiracle of tergum 5, **I**: sclerotized area below the spiracle of tergum 5; **lAspim12**, M. spiracularis III posterior (Sn: 170), **O**: laterally on the anterior margin of sternum 5, **I**: sclerotized area below the spiracle of metasomal segment 5.

3.5.6 | Metasomal segment 6 (abdominal VII) (Figure 37)

Metasomal segment 6 (Figure 31a,b) is the last complete and exposed segment. It is structurally different from the preceding segments as the posterior margins of the tergum and sternum that compose it form the near-complete closure of the apex of the metasoma, leaving only the narrow opening for the genital apparatus (in females

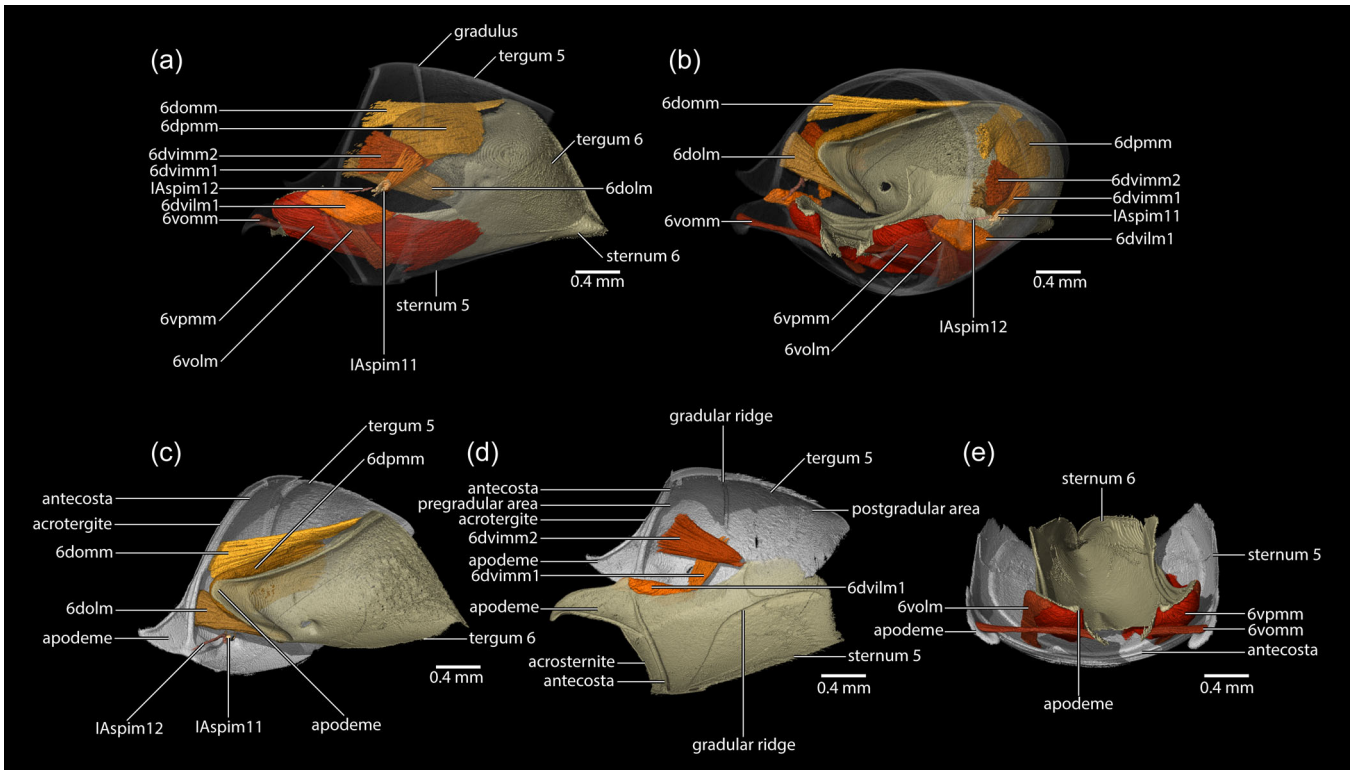

FIGURE 36 Metasomal segments 5 and 6 of *Thyreus albomaculatus*. (a) Segments 5 and 6, sclerites of segment 5 semitransparent, lateral view of tergum 5. (b) Segments 5 and 6, sclerites of segment 5 semitransparent, anterolateral view of tergum 5. (c) Tergum 5 and 6 and muscles of segment 5, anteromedial view of tergum 5. (d) Muscles of segment 5, medial view of tergum 5. (e) Sternum 5 and 6 and muscles of segment 5, anterodorsal view of sternum 5.

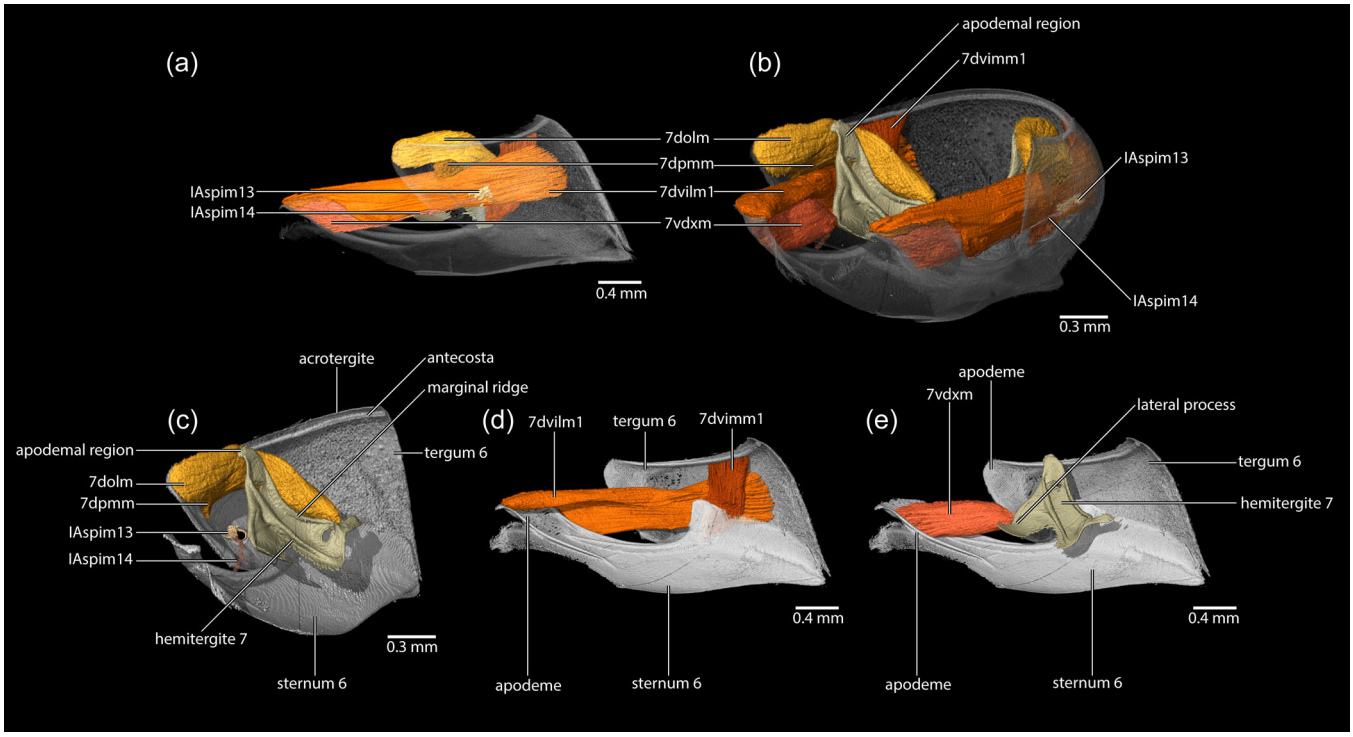

FIGURE 37 Metasomal segments 6 and hemitergite 7 of *Thyreus albomaculatus*. (a) Segment 6 and hemitergite 7, sclerites of segment 6 semitransparent, lateral view of tergum 6. (b) Segment 6 and hemitergite 7, sclerites of segment 6 semitransparent, anterolateral view of tergum 6. (c) Segment 6, hemitergite 7, and muscles of segment 6, anteromedial view of tergum 6. (d) Muscles of segment 6, medial view of tergum 6. (e) Segment 6, hemitergite 7, and muscles of segment 6, medial view of tergum 6.

hemitergites 7 and 8 and sting apparatus). Tergum 6 (Figure 37) is a posteriorly arched plate, which lacks a gradular ridge but bears well-developed apodemes anteriorly on the antecosta (Figure 37c,d). The arched sternum 6 (Figure 37) bears well-elongated apodemes (Figure 37e) but completely lacks a gradular ridge (Figure 37c).

Metasomal segment 6 muscles (Figure 37a–e)

7dolm, M. tergo-tergalis ortholateralis (Sn: 178), **O**: anterior tip of the apodeme of tergum 6, above the origin of 7dpmm, **I**: posteriorly on the marginal ridge of hemitergite 7; **7dpmm**, M. tergo-tergalis paramedialis (Sn: 179), **O**: anterior tip of the apodeme of tergum 6, below 7dolm, **I**: apodemal region of hemitergite 7; **7dvilm1**, M. tergo-sternalis interior lateralis primus (Sn: 182), **O**: tip of the apodeme of sternum 6, anterior to 7vdxm, **I**: posteriorly on tergum 6; **7vdxm**, M. sterno-tergalis exterior (Sn: 184), **O**: tip of the apodeme of sternum 6, posterior to 7dvilm1, **I**: lateral process of hemitergite 7; **7dvimm1**, M. tergo-sternalis interior anteromedialis (Sn: 183), **O**: laterally on the antecosta of tergum 6, above 7dvilm1, **I**: medially on the lateral margin of sternum 6; **lAspim13**, M. spiracularis III superior (Sn: 180), **O**: sclerotized area above the spiracle of tergum 6, **I**: sclerotized area below the spiracle of tergum 6; **lAspim14**, M. spiracularis III posterior (Sn: 181), **O**: laterally on the anterior margin of sternum 6, **I**: sclerotized area below the spiracle of metasomal segment 6.

3.5.7 | Hemitergites 7 and 8 (abdominal VIII and IX) (Figure 38)

The metasomal segments 7 and 8 are both invaginated and strongly modified; the terga are subdivided longitudinally into

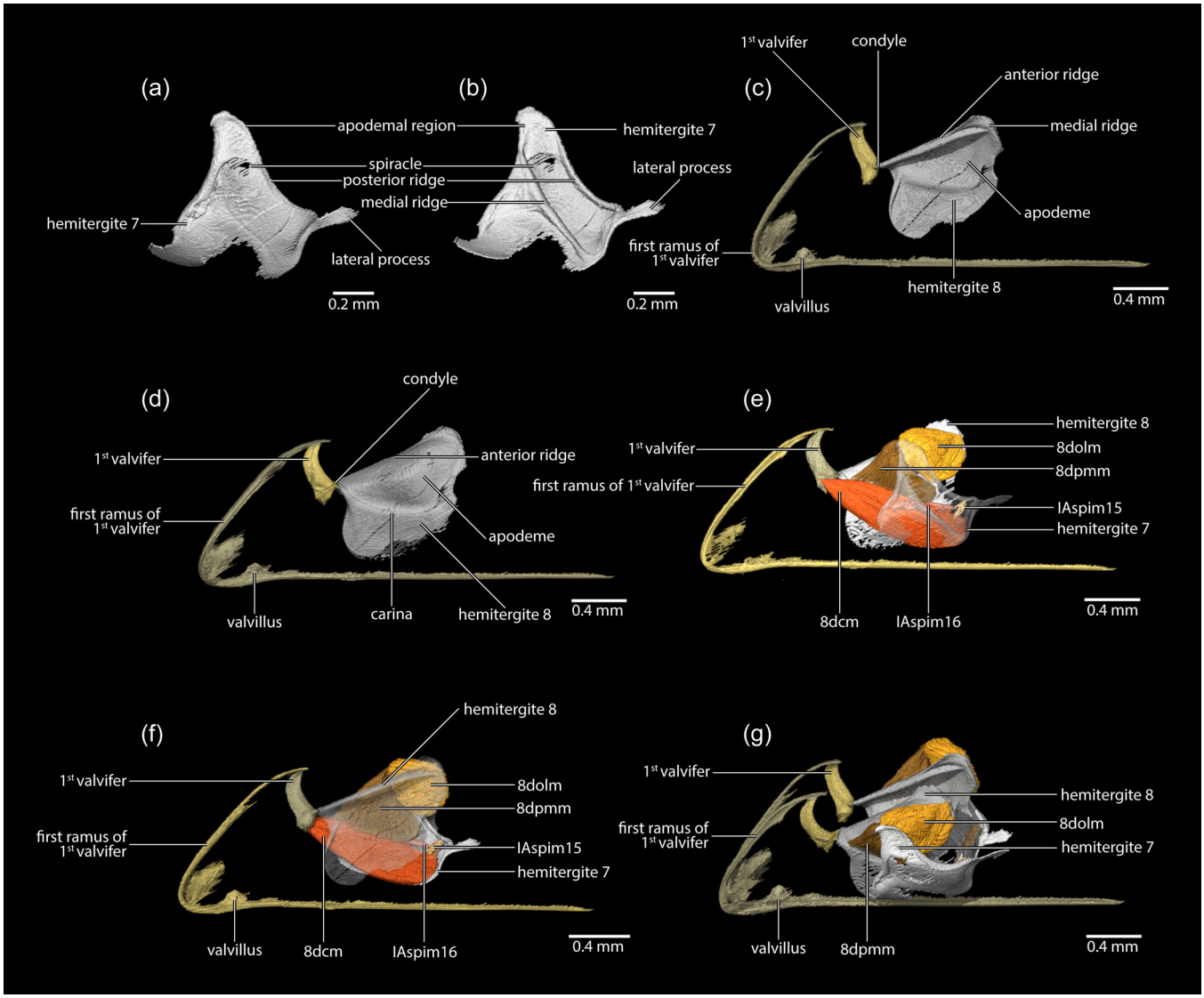

FIGURE 38 Hemitergites 7 and 8 of *Thyreus albomaculatus*. (a) Hemitergite 7, lateral view. (b) Hemitergite 7, medial view. (c) Hemitergite 8 and first valvifer, medial view of hemitergite 8. (d) Hemitergite 8 and first valvifer, lateral view of hemitergite 8. (e) Hemitergite 7, 8, first valvifer and muscles, hemitergite 7 semitransparent, lateral view of hemitergite 7. (f) Hemitergite 7, 8, first valvifer and muscles, hemitergite 8 semitransparent, inner view of hemitergite 8. (g) Hemitergite 7, 8, first valvifer and muscles, dorsolateral view of hemitergite 7.

lateral plates, the hemitergites 7 and 8 (Figure 38). The hemitergites 7 bear a spiracle (Figure 38a) and pronounced medial and marginal ridges (Figure 38b); anteriorly they display the apodemal region (Figure 38a,b) and a distinct lateral process of hemitergite 7 is present laterally (Figure 38a). Hemitergite 7 is located laterally to the sting apparatus (Figure 38g) and to hemitergite 8. Hemitergite 8 (Figures 38–40) is less structurally complex than hemitergite 7; it bears a distinct carina medially (Figure 38d) and a condyle of it anteriorly articulates with the first valvifer (Figure 38c,d). Hemitergites 8 are enclosed by hemitergites 7 (Figure 38g).

Hemitergite muscles *(Figure 38)*

8dolm, M. tergo-tergalis ortholateralis (Sn: 188), **O**: apodemal region of hemitergite 7, posterior to 8dpmm, **I**: posterodorsally on hemitergite 8; **8dpmm**, M. tergo-tergalis paramedialis (Sn: 187), **O**: apodemal region of hemitergite 7, anterior to 8dolm, **I**: carina of hemitergite 8; **8dcm**, M. tergo-coxalis (solus) (Sn: 192), **O**: posteroventrally on hemitergite 7, **I**: posteriorly on the first valvifer; **IAspim15**, M. spiracularis III superior (Sn: 189), **O**: sclerotized area above the spiracle of hemitergite 7, **I**: sclerotized area below the spiracle of hemitergite 7; **IAspim16**, M. spiracularis III posterior (Sn: 190), **O**: laterally on the medial area of hemitergite 7, **I**: sclerotized area below the spiracle of hemitergite 7.

3.5.8 | Sting apparatus (Figures 39 and 40)

The sting apparatus (Figure 39) is about 2.5 mm long and comprises the appendages of abdominal segments VIII and IX (note: the terminologies of both Michener (and its derivatives) and Lieberman are used in parallel to facilitate understanding). The paired appendages of segment VIII comprise the proximally located first valvifer (= gonocoxa 8, gcx8) (Figures 38c–g, 39, and 40d,f) and distally located first ramus (= gonapophysis 8, gap8) (Figures 38c–g, 39, and 40a–d,f); those of segment IX comprise the proximally located second valvifer (= gonocoxa 9, gcx9) (Figures 39b–d and 40b–f) and two distal rami, the lateral being the third valvula (= gonostylus 9, gst9) (Figures 39 and 40) and the medial being the second ramus (= gonapophysis 9, gap9) (Figures 39b–d and 40b–f). The first valvifer (gcx8) (Figure 38c–g) is a triangular structure that articulates anteriorly with the condyle of hemitergite 8 (Figure 38c,d) and extends posteriorly with its first ramus (gap8) on the sides of the sting shaft (Figure 39c,d). The valvillus is present as a chitinous flap slightly anterior to the middle of the extension of the first ramus (gap8) (Figure 38c,d,f,g). The second valvifer (gcx9) is more robust (Figure 39c,d) and has the second ramus (gap9) extending on the sides of the sting shaft and furcula (Figure 39c,d); it is mainly composed of the apodeme which dorsally forms the apodemal ridge and extends posteriorly as the third valvula (gst9) (Figure 39a,c,d).

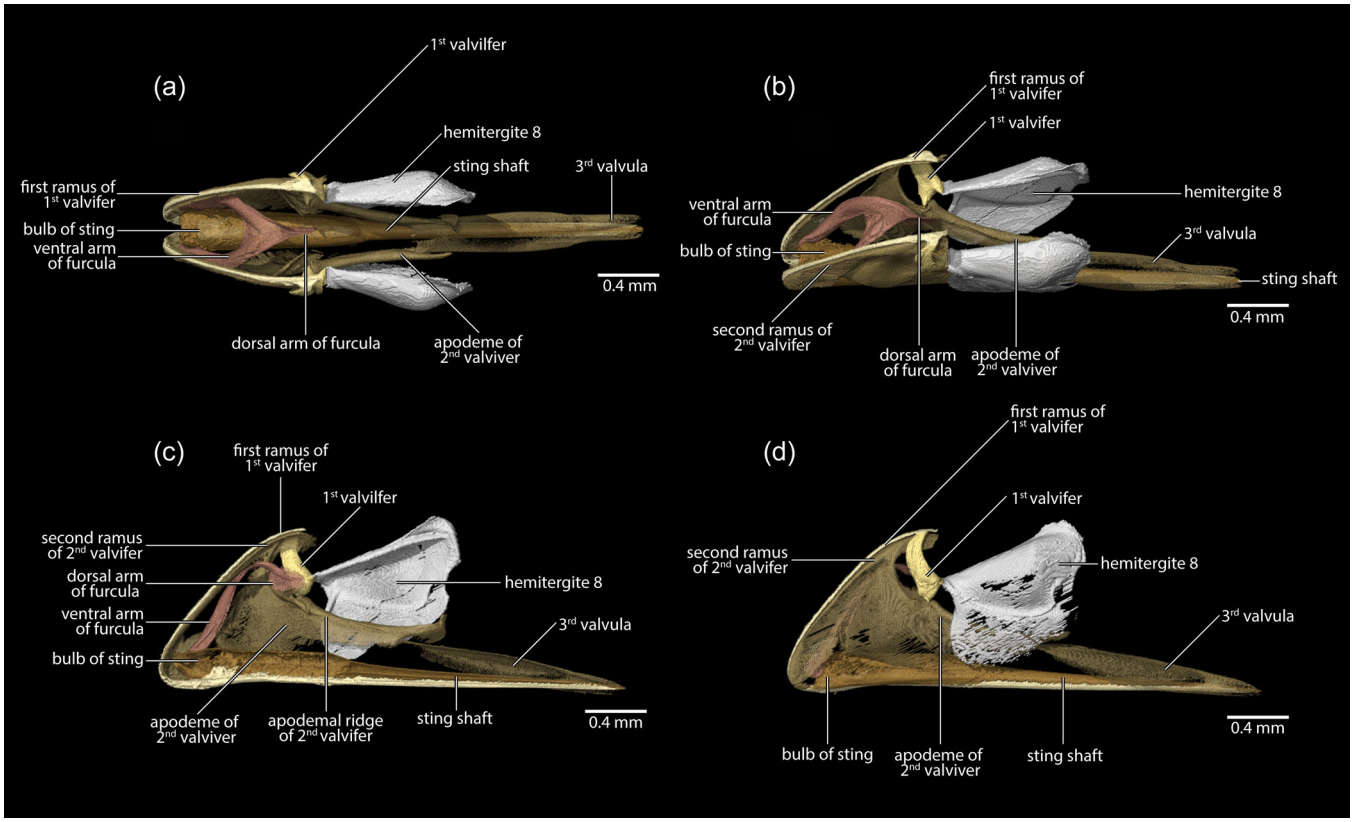

FIGURE 39 Sting apparatus of *Thyreus albomaculatus*. (a) Dorsal view of the sting shaft. (b) Dorsolateral view of the sting shaft. (c) Medial view of the sting shaft. (d) Lateral view of the sting shaft.

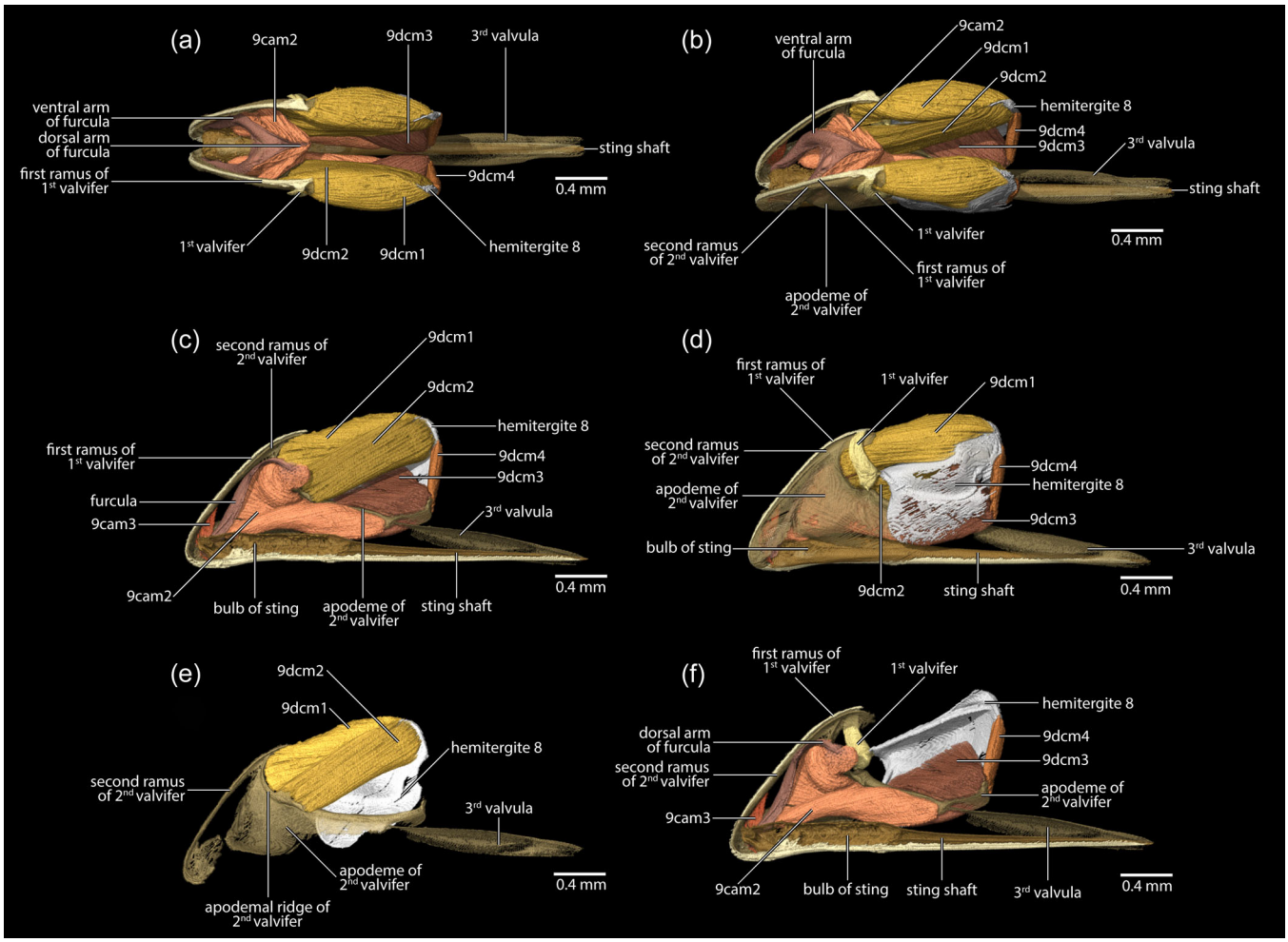

FIGURE 40 Sting apparatus and associated muscles of *Thyreus albomaculatus*. (a) Dorsal view of the sting shaft. (b) Dorsolateral view of the sting shaft. (c) Medial view of the sting shaft. (d) Lateral view of the sting shaft. (e) Medial view of the second valvifer. (f) Medial view of the sting shaft.

The second ramus (gap9) extends on the sides of the sting shaft and furcula (Figure 39c,d). The furcula (Figure 39a–c) is a Y-shaped structure that articulates directly with the bulb of the sting shaft by the ventral arms of furcula (Figure 39a–c). The bulb of the long and sharp sting shaft (Figure 39c,d) articulates with the furcula, and the entire sting apparatus through most of its length by the first and second valvifers (gcx8, 9) (Figure 39c).

Sting apparatus muscles (Figures 40 and 41)

9cam2, M. coxo-apophysealis major posterior (Sn: 197), **O**: internally on the posterior part of apodemal ridge of the second valvifer, posterior to 9dcm2 origin, **I**: broadly on furcula; **9cam3**, M. coxo-apophysealis minor (Sn: 196), **O**: middle of the second ramus of the second valvifer, **I**: base of bulb of sting; **9dcm1**, M. tergo-coxalis anterior externalis (Sn: 198a), **O**: dorsally on the anteriormost part of the apodemal ridge of the second valvifer, anterior to 9dcm2, **I**: dorsally on hemitergite 8; **9dcm2**, M. tergo-coxalis anterior internalis (Sn: 198b), **O**: dorsally on the anterior part of the apodemal ridge of the second valvifer, posterior to 9dcm1, **I**: dorsally on hemitergite 8; **9dcm3**, tergo-coxalis lateralis (Sn: 199), **O**: ventrally on hemitergite 8, below the origin of 9dcm1 and 9dcm2, **I**: tip of the apodeme of the second valvifer, anterior to the origin of 9dcm4; **9dcm4**, M. tergo-coxalis medialis (not observed by Snodgrass [1942]), **O**: posterodorsally on hemitergite 8, posterior to the insertion of 9dcm2, **I**: tip of the apodeme of the second valvifer, posterior to 9dcm3; **9domm**, tergo-tergalis orthomedialis (Sn: 201), **O**: apodemal region of hemitergite 7, **I**: medially on the membranous area of the proctiger (not shown in the figure), internally to tergum 6; **9dolm**, tergo-tergalis ortholateralis (Sn: 200), **O**: apodemal region of hemitergite 7, **I**: laterally on the membranous area of the proctiger (not shown in the figure).

4 | DISCUSSION

4.1 | Bee morphology so far

The morphological study of bees became consolidated as one of the widely studied areas of insect anatomy, contributing to a solid application of terms for the group (e.g., Michener, 2007). Four characteristics define the structure of this morphological study to

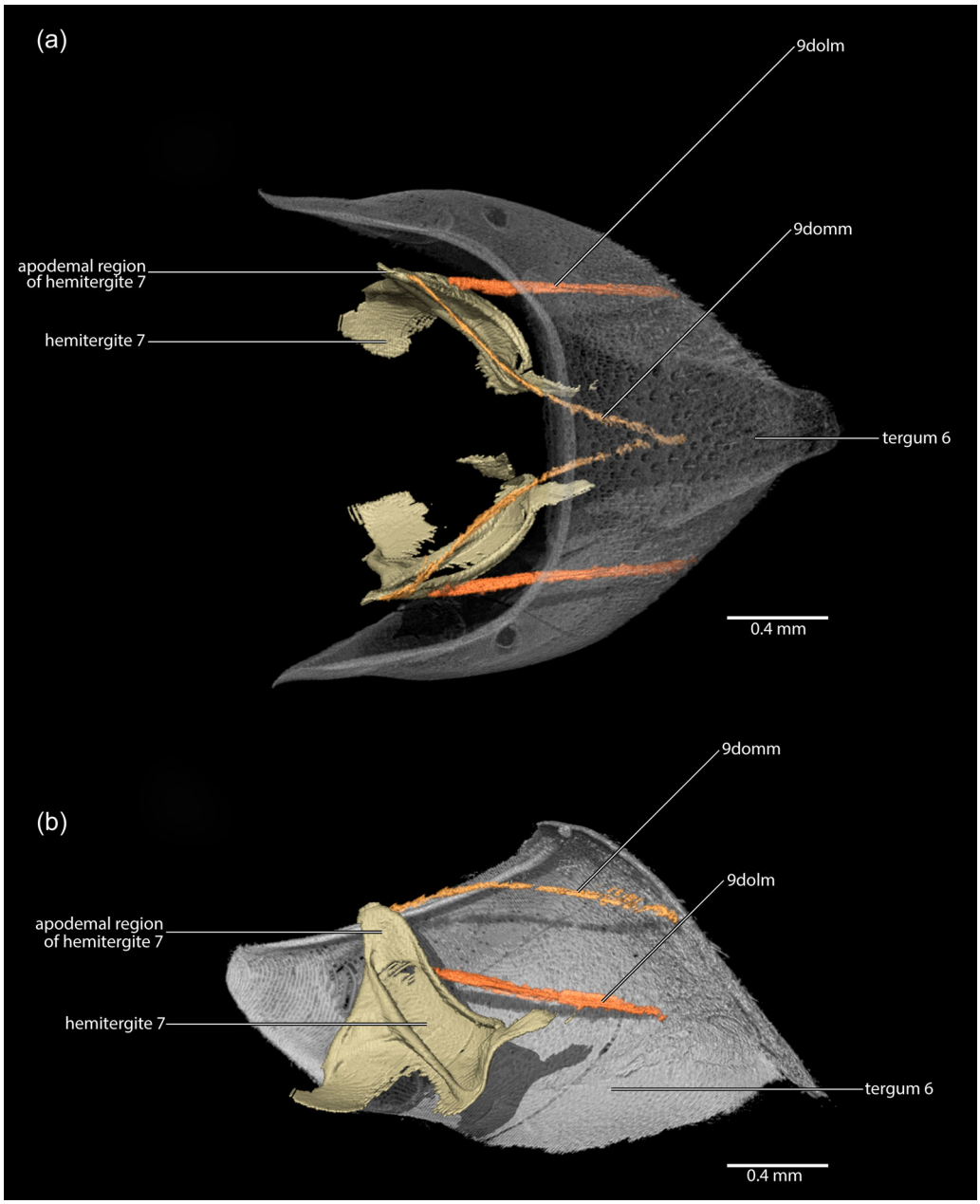

FIGURE 41 Tergum 6, hemitergite 7 and associated musculature of *Thyreus albomaculatus*. (a) Tergum 6 semitransparent, ventral view of tergum 6. (b) Medial view of tergum 6.

date: (1) we have a species that has been studied in detail in many of its aspects, namely the honey bee (*A. mellifera* Linnaeus), and this is not the case for any other of the more than 20,000 species of bees described so far; (2) with the exception of the in-depth treatments for *A. mellifera*, almost nothing, or very little, has been done on the study of musculature in bees and their intimate association with skeletal structures; (3) unlike ants, bees and other groups of Hymenoptera have been studied very little in light of new imaging technologies, we only have a few very specific treatments for the group, and this is especially true when we think about the skeletal-muscular association; and finally, (4), this vast literature generated in bees, especially for skeletal structures, ended up creating a very specific terminology only used for this group. In many cases, point (4) makes communication with researchers of other groups of Hymenoptera (and insects in general) difficult. Thus, given the present bee-specific system, it is difficult to make clear comparisons and to derive homology inferences; this also limits the understanding of the structures themselves and their evolution. With these characteristics in mind, we present here a comprehensive atlas of the skeletomusculature in bees and a baseline for future comparison studies on the anatomical and functional morphology throughout the Apoidea, aiming furthermore to ease the comparability of bees to other Hymenoptera and other groups of insects. In this context, some of the limitations of µ-CT are important to recognize. For instance, histological properties of

tissues, ultrastructure on the cellular level, fine details of cuticular surfaces, and membranous or semimembranosus elements are not or at least not fully accessible with this technique. This can be due to insufficient resolution of the scan relative to body size, or inadequate contrast (sometimes due to inadequate technique), or to the suboptimal preservation of the specimen. Additional techniques are required to fully document the anatomy on different levels, such as histological sections, transmission electron microscopy, scanning electron microscopy (SEM), or confocal laser scanning microscopy (CLSM).

4.2 | Refining bee morphology: A comprehensive anatomical vocabulary and reference system

The present study provides a reconstruction of the entire skeletomusculature of a single bee species (and individual) based on synchrotron μ-CT data. To date, works have either been restricted to individual tagmata or particular structural complexes. In total, we identified 199 muscle groups; 36 of these were in the head, 88 in the mesosoma, and 75 in the metasoma.

4.2.1 | Head

We identified most of the structures described in the literature and agree with most previous assessments. However, we present a different interpretation of the postoccipital region and endoskeleton, recognizing a number of structures for the first time, for which we provide new terminology.

Mouthparts

One special case of homology–terminology conflict is that of the labial parts in bees, with conflict both among authorities and within the sequential works of these authors (Table 1). The labium of bees comprises four recognized sclerotic elements. From distal to proximal, Snodgrass (1925) recognized three of these as the "mentum," the "submentum," and "lorum," which he later referred to as the "prementum," "postmentum," and "lorum" (Snodgrass, 1942, 1956). Likewise, Michener (1944) recognized the "prementum," "mentum," and "submentum," conflicting with all three of Snodgrass's treatments, and later Michener (1984, 2007) replaced his "submentum" with "lorum." In contrast, Plant and Paulus (1987, 2016) recognized the labium as the prementum and postmentum, with the postmentum being present as one single sclerite or subdivided into mentum and lorum (= submentum).

We agree with the interpretation of Plant and Paulus (1987, 2016) that the labium is subdivided into prementum and postmentum, but we disagree with the interpretation of a subdivided postmentum in bees. In the groundplan of Hymenoptera, the postmentum (comprising the mentum and submentum) is a relatively small single sclerite, if present at all (Beutel & Vilhelmsen, 2007; Vilhelmsen, 1996: figs. 5c and 9b). This condition is present in bees, but the postmentum can also be secondarily subdivided, in this case composed of the main **median portion of the postmentum** and the lorum. This interpretation differs from that of Plant and Paulus (1987, 2016), who postulated a postmentum subdivided into mentum and lorum, the latter consequently corresponding to the submentum of other groups of Hymenoptera. In contrast, we do not recognize a mentum but instead a median portion of the postmentum and a lorum as a novel postmental subdivision. In this context, it is important to note that the submentum in Hymenoptera is never connected with the maxilla nor is it present as an individual element, as the lorum sclerite is. This specific condition is likely a novelty for bees with such a subdivision, as noted by Plant and Paulus (1987, 2016). Table 1 summarizes the terminology correspondence for the labial sclerites in bees and our label usage herein.

Maxilla

A derived feature of *T. albomaculatus* is the reduced maxillary palpus. During the examination and segmentation of the data, no associated muscle was found in this structure. Snodgrass (1942) described one muscle attached to the maxillary palpus (Muscle 14, muscle of the maxillary palpus, Snodgrass [1942]), while Youssef (1971) described two muscles, musculus stipiti-maxillopalpualis I (likely correspondent to muscle of the maxillary palpus of Snodgrass [1942]) and musculus stipiti-maxillopalpualis II, a single fiber muscle.

Postocciput

In the postoccipital region, some structures lacked descriptions even in detailed previous works on the group. We now offer a documentation covering new features, such as the lip-like structures

TABLE 1 Applied morphological ontology correspondence for the labial parts.

Snodgrass (1925)	Snodgrass (1942, 1956)	Michener (1944)	Michener (1984, 2007)	Plant and Paulus (1987)	This work
Mentum	Prementum	Prementum	Prementum	Prementum	Prementum
–	–	–	–	Postmentum	Postmentum
Submentum	Postmentum	Mentum	Mentum	Mentum	Median portion of postmentum
Lorum	Lorum	Submentum	Submentum	Lorum (= submentum)	Lorum (subdivision of postmentum)

located lateral to the occipital foramen. We identify the supratentorial invagination above the occipital foramen that forms the supratentorial carina delimiting the postoccipital region together with the postoccipital sulcus. We also provide a reinterpretation of the postoccipital sulcus, which, in our study, is interpreted as a depression encompassing both the posterior tentorial pit and the newly described tentorio-tentorial bridge pit. The latter is an invagination of the tentorial structure itself, and so far, we can confirm its presence only in *T. albomaculatus*, because it was not observed in *Lasioglossum* and *Andrena*.

Cephalic endoskeleton

The cephalic endoskeleton in bees has been interpreted in different ways by different authors such as Snodgrass (1942), Michener (1944), and the very comprehensive study by Porto et al. (2016). In our study we present different interpretations for some structures and regions. Given the intricate connection between the hypostoma, the tentorium and the epistomal ridge in bees, this structure proves to be a challenging region for interpretation and inference. In relation to the tentorial bridges recognized in bees, in this work we describe three of them: the tentorio-tentorial bridge corresponding to the primary tentorial bridge of Michener (1944), the tentorio-postgenal bridge, and the tentorio-hypostomal bridge. Additionally, we recognize the composite lamella of the tentorium and postgenal region, a structure corresponding to the secondary tentorial bridge of Porto et al. (2016). However, in an in-depth analysis of our data, and comparison with other bees, a composite origin for this structure seems likely. Included are likely elements of the tentorium (more specifically the anterior tentorial arm) and remnants of the postgena (reduced to a ridge in our individual).

0md6, M. tentorio-mandibularis

We represent muscle 0md6 for the first-time using CT-scan data. This muscle was overlooked by Snodgrass (1942) but recorded by Youssef (1971) as the musculus tentorio-mandibularis. It corresponds to M. hypopharyngo-mandibularis observed in *Macroxyela* of Xyelidae (0md4; Beutel & Vilhelmsen, 2007). In this study M. hypopharyngomandibularis (M. 13) originates from the tentorium and not from the hypopharynx as the name suggests. Zimmermann and Vilhelmsen (2016) describe two muscles, 0md6 and 0md8, but they only illustrate 0md8 (which matches the structural pattern for origin and insertion that we see in bees for muscle 0md6) and mistakenly state that Youssef (1971) described two muscles (0md6 and 0md8) in *A. mellifera* (he only described one muscle, M. tentorio-mandibularis, that we believe, corresponds to 0md6). Additionally, muscle 0md8 in ants (Richter et al., 2020, 2021, 2023) does not correspond to 0md6 in bees which might indicate that 0md6 was overlooked in ants so far (personal observation Brendon E. Boudinot).

0mx4, M. tentoriostipitalis anterior and 0mx5, M. tentoriostipitalis posterior

We also registered the shared point of attachment of 0mx4 and 0mx5; this was a condition already indicated in some bees by Meira and Gonçalves (2021; character 05 state 0).

4.2.2 | Mesosoma

Prothorax

Our main distinction in relation to literature occurs in the interpretation and description of the eusternum. We understand the prosternum as a combined element comprising the eusternum + the spinasternum (absent in the taxon sampling). The eusternum is composed of the basisternal shield and basisternal inflection with the profurca originating from the latter.

Subspiracular area and prepectus

Both Snodgrass (1942) and Michener (1944) did not describe the prepectus in the anterior region of the mesopectus. This structure, as pointed out by Brothers (1975), Gibson (1985, 1999), Gibson et al. (1999), Melo (1999), and Vilhelmsen et al. (2010), may be present in the suborder Apocrita as a free, large (e.g., Chalcidoidea, Stephanoidea, and others Vilhelmsen et al. [2010]) or small sclerite (part of the intersegmentalia), or in a fused form with the mesepisternum and with the external suture obliterated, which is evident in *T. albomaculatus*. We observe considerable variation in our preliminary SR-μ-CT datasets, which raises the level of uncertainty to the point that we cannot confirm the existence of the prepectus in *Thyreus* or indeed, in many other taxa. For example, in a trigonalyid (scan: BB044), the anterior branch of the mesobasalare muscle (IIspm1) and the spiracular occlusor muscle (IIpspim1) attach to the pronotum posteriorly, while there is no indication of a prepectus (this condition was also observed in Ceraphronoidea, Cynipoidea, and others [Vilhelmsen et al., 2010]). At the same time, we observe the definitive subspiracular ridge and area in the trigonalyid specimen. Furthermore, we observed in cross-sectional data of an ampulicid (scan: BEB033) that the occlusor muscle attaches to a very small apodeme situated at the extreme anterodorsal region of the subspiracular area, which was also separated from the remainder of the mesopectus by an extremely small groove. This raises the question whether this could be the vestige of the prepectus. We cannot be sure of that either, as we also observe a discrete and also extremely small sclerite between this occlusor muscle apodeme and the pronotal lobe, the same pattern we observe in *Thyreus*. In other words, with the submicron-scale resolution of our SR-μ-CT data, we observe a complex of anatomical entities in the intersegmental region of different hymenopterans, all of which need to be explicitly conceived and accounted for. Therefore, in the present work, we remain agnostic about the prepectus in *Thyreus*, which we presently consider to be indistinguishable. Whether this means that it is "absent" or "fused" is up to future study to resolve, and we refer to the area between the anterior margin of the mesepisternum and the subspiracular ridge as subspiracular area.

Mesopectus

In bees there is a certain dissonance in the terminology applied to the ventrolateral region of the mesopectus (mesosoma excluding mesoscutum). Michener (1944) described this region as the mesopleura (pleural area of the mesosome excluding the endosternum).

Snodgrass (1942) described this region as the pterothoracic pleura, similar to Michener (1944). Furthermore, Camargo et al. (1967) referred to the lateral area of the mesosoma as the mesopectus (composed of the mesepisternum and mesopleura (mesepimeron plus subalar area). However, in the present study, this term does not encompass the mesosomal endosternum. Here, we refer to the lateral region of the mesothorax as the mesopectus, encompassing, in addition to the pleural areas (mesepisternum and mesepimerom), the mesosomal endosternum (mesofurca). In fact, this concept has been previously used (e.g., Vilhelmsen et al., 2010). Between the mesepisternum and the metapectus, we recognize the presence of the pleural sulcus (correspondent to a pleural ridge internally), different from Michener (1944) who considered this integumental line to be a suture. Additionally, we realize that there is a conflict in the homology interpretation of the pleural ridge between Snodgrass (1935, 1942), which has further muddied the waters of comparative anatomy of the mesopectus. Specifically, Snodgrass (1935, p. 165) defines the pleural ridge as an internal carina that extends from the coxopleural articulation to the pleural wing process. In contrast, Snodgrass (1942, fig. 17A,B) labeled this carina (our "pleural ridge") as "f," or the "internal ridge of the recurrent groove." Our observations suggest that this "ridge of the recurrent groove" extends from the pleurocoxal articulation to the pleural wing process (see our Figure 21), and that the structure that Snodgrass (1942) labeled as his "pleural ridge" is a secondary ridge extending ventrad from the pleural ridge to the pleural apophysis (our "mesepisternal ridge").

Scrobal sulcus/scrobe

We treat the "scrobe" and "scrobal sulcus" of the mesopectus differently from prior authors. We prefer to restrict the term "scrobe" to concave contact surfaces, that is, formative elements that receive body parts when those parts are flexed (see Boudinot et al., 2022). Rather, we recognize that the mesopectus externally bears the **pleural apophyseal pit** (= scrobe from Michener [1944]) and also **pleural apophyseal sulcus** (= scrobal sulcus from Michener [1944]), which correspond internally to the pleural apophysis (Snodgrass, 1942) and **pleural apophyseal ridge**.

Metapectus

In agreement with the terminology applied to the mesothorax, we apply the term metapectus to the lateral area of the metathorax plus the endosternal metathoracic element (metafurca).

Itpm1, M. pleurocrista-occipitalis, Itpm2a, M. propleuro-occipitalis dorsal and Itpm2b, M. propleuro-occipitalis ventral

Snodgrass (1942) described muscle 42 (the pleural levator or rotator of the head), a three-branched muscle with origins in the ventral area and the dorsal propleural ridge that unite on a tendon inserting onto the postocciput. We found the same pattern but we differ in terms of the interpretation of this muscle, which we interpret as a bipartite group, comprising Itpm1, m. pleurocrista-occipitalis (which originates on the dorsal propleural ridge) and Itpm2, m. propleuro-occipitalis (which originates on the ventral area of the propleuron). Itpm2 is here subdivided into Itpm2a, m. propleuro-occipitalis dorsally and Itpm2b, m. propleuro-occipitalis ventrally. This is based on the interpretation of the topology of these muscles correlating with the general muscular concept for Neoptera (Friedrich & Beutel, 2008a) as well as on Vilhelmsen et al. (2010), where muscles Itpm1 and Itpm2 are described in positions very similar to the topology found in *T. albomaculatus*.

Aibekova et al. (2022) described two muscles that originate on the propleuron and insert on the postocciput: Itpm1 and Itpm2. We interpreted Itpm1 of Aibekova et al. (2022) as corresponding to our Itpm2a, and their Itpm2 as corresponding to our Itpm2b. This interpretation is based on the topology described by Aibekova et al. (2022) and as implied in Friedrich and Beutel (2008a), as both muscles originate on the ventral area of the propleuron (a common pattern for Itpm2) and none on the propleural ridge (as it would be expected for Itpm1).

Idvm5a, M. pronoto-cervicalis anterior primus and Idvm5b, M. pronoto-cervicalis anterior secundus

We suggest that muscles 46 and 47 of Snodgrass (1942) correspond to our muscles Idvm5a, M. pronoto-cervicalis anterior primus and Idvm5b, Idvm5b, M. pronoto-cervicalis anterior secundus. Snodgrass (1942) described his number 46 as the "phragmatopleural muscle of the prothorax," indicating that the origin of this muscle was on the prophragma, and the same seems to be true for muscle 47 judging by his Figure 12a (Snodgrass, 1942). Our data indicate that Idvm5a and Idvm5b actually attach on the anterior margin of the mesoscutum.

Ipcm2, M. procoxa cervicalis transversalis

Ipcm2 was not identified in the honey bee by Snodgrass (1942), but it was described and partially illustrated by Daly (1964), and also presented and documented by OMM (unpublished observations) in the same species. It is a muscle documented in other Hymenoptera such as Scelionidae (Mikó et al., 2007) and Formicidae (Aibekova et al., 2022). In bees it appears to share the insertion point on the procoxa with one of the branches of Ipcm4.

Ipcm4, M. propleuro-coxalis superior

This was described by Snodgrass (1942) as a muscle that originates on the episternum (propleuron) and is inserted onto the procoxa. Porto et al. (2016) described the anterior process of the dorsal profurcal lamella, a digitiform process located on the anterior profurcal branch. We now know, based on data from this study and also unpublished observations by OMM, that this is possibly an additional origin for this muscle, in addition to the one on the dorsal propleural margin.

The metapostnotum and the propodeal triangle

The Apoidea have been historically thought to be synapomorphically defined by modification of the metapostnotum, namely that this structure is expanded posteriorly into the propodeum, thus forming the propodeal triangle (Brothers, 1976), a condition also assumed to exist in Bethylidae (e.g., Kawada et al., 2015). However, based on our

observations, we reject this homology hypothesis for the propodeal triangle (as well as for the "metapostnotum" of Bethylidae).

With the groundplan of the Neoptera (Beutel et al., 2014) as the primary reference point and definitional source, the metapostnotum is the posterior portion of the metanotum, anterior to the propodeum of Hymenoptera, and more specifically, anterior to the propodeal antecosta. It is fused to the first abdominal tergum in Hymenoptera (Friedrich & Beutel, 2010; Whitfield et al., 1989), and separated from the metanotum by a membrane. However, it is still separated from the remainder of the first abdominal tergum in its free and fused form (= propodeum) by the tergal antecosta. Because the antecosta of the sampled bees (plus evaluation of unpublished scans of Bethylidae) is complete and comes into close proximity (nearly touching) the propodeum anteriorly without curving posteriorly, we draw the following conclusion: The metapostnotum is not a part of the propodeum, ergo the "metapostnotum" of Bethylidae is a subdivision of the propodeum and not the metapostnotum, and the propodeal triangle of Apoidea is also not equivalent with the metapostnotum. In both Bethylidae and Apoidea, the propodeal antecosta forms a continuous rim in tight association with the metanotal-propodeal articulation. The medial region of the propodeum lacks muscular attachment, and the lateral margins may be marked internally and/or externally by sulci or ridges. In contrast between the two, the phragmophragmal muscle (IIIdlm1, ph2-ph3) in Apoidea has migrated posteromedially from the anterolateral margins of the propodeum. It is possible that the lateromedial division lines of the propodeum in Apoidea are "scars" resulting from the migration of these muscles. Alternatively, these lines may be secondarily derived as some boundary element between the musculated and unmusculated portions of the propodeum.

4.2.3 | Metasoma

The metasomal structure is very similar to what was described in the literature for other bees (Michener, 1944; Snodgrass, 1942).

The petiole

The term "petiole" has been applied to the anterior constriction of the anterior margin of the first metasomal tergum in bees, in analogy to the botanical usage of "petiole" for the stems of leaves. This contrasts with the usage of this term for other Hymenoptera, where "petiole" refers to the entire first metasomal segment. Because of this conflict, we decided not to use the term petiole for *Thyreus* and recognized, instead, the "levator process" of the first metasomal tergum.

IIIdlm3, M. metascutello-scutellaris

This muscle was indicated by Snodgrass (1942) as the "external longitudinal dorsal muscle of the mesothorax," being a transverse muscle of the mesoscutellum. However, as suggested by Daly (1964) and the data presented here, this muscle actually runs from the mesoscutellum to a small insertion point on the metanotum.

IIIscm2, M. metafurca-coxalis posterior and IIIscm3, M. metafurca-coxalis medialis

Snodgrass (1942) described muscle 106 as the mesal retractor of the hind coxa, indicating its origin on the metafurca and its insertion by a broad tendon on the posterior margin of the hind coxa. However, as noted by Wille (1956), some bees have two muscles in this region (or a subdivision of the same muscle). Although not indicated by Snodgrass (1942), the presence of this same condition was also confirmed in *A. mellifera* (personal observation Odair M. Meira). In this way, we understand that muscle 106 of Snodgrass (1942) corresponds to muscles IIIscm2 and IIIscm3.

2dvilm1, M. tergo-sternalis interior lateralis

In his study, Snodgrass (1942) suggested that muscle 129 (named as lateral muscle of abdominal segment II), would be equivalent to the third lateral muscle of the other abdominal segments. However, that muscle, as described by him, is, in fact, an intersegmental muscle (from tergum 3 to sternum 4, and so on), while Snodgrass (1942) described muscle 129 as an intrasegmental muscle (from tergum 2 to sternum 2). In this way, we suggest that muscle 129 of Snodgrass (1942) actually corresponds with the M. tergo-sternalis interior lateralis (2dvilm1; Lieberman et al., 2022).

3dvilm2, M. tergo-sternalis interior lateralis secundus and 3dvilm3, M. tergo-sternalis interior lateralis tertius

These two muscles are not recorded in bees or other groups in Hymenoptera. It is conceivable that they would easily go unnoticed in dissection due to their very small size. Both originate on the apodeme of sternum 2 and are inserted at the same point close to the apodeme of tergum 2. Unlike some of the serial muscles of the metasoma (which are very similar throughout the metasomal segments), both these muscles are only present in the metasomal segment 2.

9dcm4, M. tergo-coxalis medialis

This muscle is not represented by Snodgrass (1942) but is very distinct in *T. albomaculatus*. This muscle connects the posterior margin of hemitergite 8 to the apodeme of the second valvifer on the sting apparatus.

5 | CONCLUSION

By comparing our observations and interpretations with those of Snodgrass (1942), Michener (1944), and others, we were able to resolve a number of homology problems—the head endoskeleton and propodeal triangle are sclerotic highlights—while also establishing new anatomical concepts for several structural complexes, including the postocciput and dorsal mesopectal region. In this process, we recognized that we had to limit the scope of our work, as we are yet unable to complete the homologization of the ventral mesosoma without detailed comparisons across the Hymenoptera and Holometabola, for example. Further, we have found through this and prior studies (e.g., Boudinot et al., 2021; Richter et al., 2022) that the level

of structural detail that needs to be evaluated for a comprehensive study is spectacular. Thus, we have chosen to develop the present study as a stepping stone on the way to realizing a truly complete atlas of anatomy, which will ideally be enhanced by multimodal sampling of the phenotype, that is, via macrophotography, SEM, histology, and CLSM. Regardless, it is clear that despite the contemporary limitations of μ-CT technology, the advantage of digital dissections and ad libitum documentation via volume renders grossly outweighs the cost of manual reconstruction. Without a doubt, future anatomical studies of other Hymenoptera will reveal broad fields of heretofore hidden biodiversity and will lay the foundation for a comparative phenomic approach to insect functional morphology, paleontology, and phylogenetics.

AUTHOR CONTRIBUTIONS

Odair M. Meira: Conceptualization; formal analysis; writing—original draft preparation; project administration. **Rolf G. Beutel**: Conceptualization, formal analysis; supervision; writing—review and editing. **Hans Pohl**: Resources; formal analysis; supervision; writing—review and editing. **Thomas van de Kamp**: Resources; writing—review and editing. **Eduardo A. B. Almeida**: Conceptualization; funding acquisition; resources; supervision; writing—review and editing. **Brendon E. Boudinot**: Conceptualization, resources; supervision; formal analysis; writing—review and editing; supervision.

ACKNOWLEDGMENTS

This work was supported by the São Paulo Research Foundation (FAPESP grants 2018/09666-5, 2019/09215-6, 2021/07258-0, 2022/11349-3) and by Coordenação de Aperfeiçoamento de Pessoal de Nível Superior—Brasil (CAPES)—Finance Code 001. Brendon E. Boudinot was supported by research fellowships from Alexander von Humboldt Stiftung (2020–2022) and the Peter S. Buck fund of the Smithsonian Institution (2022–2023). The authors thank Tomás Faragó for tomographic reconstruction and Angelica Cecilia and Marcus Zuber for the assistance at the beamline. The authors acknowledge the KIT Light Source for the provision of instruments at their beamlines, and we would like to thank the Institute for Beam Physics and Technology (IBPT) for the operation of the storage ring, the Karlsruhe Research Accelerator (KARA). The authors are grateful to Diego S. Porto, Lars Vilhelmsen, and one anonymous reviewer for their valuable comments and suggestions. The authors also thank Anderson Lepeco, Daniel Tröger, and Michael Weingardt for insightful discussions and support with renders and figures, and Laurence Packer for his assistance in making a habitus photograph of a *T. albomaculatus* bee shown in the graphical abstract.

CONFLICT OF INTEREST STATEMENT

The authors declare no conflicts of interest.

DATA AVAILABILITY STATEMENT

The data that support the findings of this study are openly available in Zenodo at https://zenodo.org, reference number https://doi.org/10.5281/zenodo.11636631.

ORCID

Odair M. Meira http://orcid.org/0000-0003-3495-5262
Hans Pohl http://orcid.org/0000-0002-7090-6612
Thomas van de Kamp http://orcid.org/0000-0001-7390-1318
Eduardo A. B. Almeida http://orcid.org/0000-0001-6017-6364
Brendon E. Boudinot http://orcid.org/0000-0002-4588-0430

REFERENCES

Aibekova, L., Boudinot, B. E., Georg Beutel, R., Richter, A., Keller, R. A., Hita-Garcia, F., & Economo, E. P. (2022). The skeletomuscular system of the mesosoma of *Formica rufa* workers (Hymenoptera: Formicidae). *Insect Systematics and Diversity*, *6*(2), 1–26. https://doi.org/10.1093/isd/ixac002

Alba-Tercedor, J., & Alba-Alejandre, I. (2019). Comparing micro-CT results of insects with classical anatomical studies: The European honey bee (*Apis mellifera* Linnaeus, 1758) as a benchmark (Insecta: Hymenoptera, Apidae). *Microscopy*, *40*, 12–15.

Alexander, B. A., & Michener, C. D. (1995). Phylogenetic studies of the families of short-tongued bees (Hymenoptera: Apoidea). *University of Kansas Science Bulletin, Lawrence*, *55*, 377–424.

Almeida, E. A. B., Bossert, S., Danforth, B. N., Porto, D. S., Freitas, F. V., Davis, C. C., Murray, E. A., Blaimer, B. B., Spasojevic, T., Ströher, P. R., Orr, M. C., Packer, L., Brady, S. G., Kuhlmann, M., Branstetter, M. G., & Pie, M. R. (2023). The evolutionary history of bees in time and space. *Current Biology*, *33*(16), 3409–3422. https://doi.org/10.1016/j.cub.2023.07.005

Basibuyuk, H. H., & Quicke, D. L. J. (1995). Morphology of the antenna cleaner in the Hymenoptera with particular reference to non-aculeate families (Insecta). *Zoologica Scripta*, *24*, 157–177.

Berry, R. P., & Ibbotson, M. R. (2010). A three-dimensional atlas of the honeybee neck. *PLoS One*, *5*(5), e10771.

Beutel, R. G., Friedrich, F., Yang, X.-K., & Ge, S.-Q. (2014). *Insect morphology and phylogeny: A textbook for students of entomology*. De Gruyter. https://doi.org/10.1515/9783110264043

Beutel, R. G., & Vilhelmsen, L. (2007). Head anatomy of Xyelidae (Hexapoda: Hymenoptera) and phylogenetic implications. *Organisms Diversity & Evolution*, *7*(3), 207–230.

Bitsch, C., & Bitsch, J. (2002). The endoskeletal structures in arthropods: Cytology, morphology and evolution. *Arthropod Structure & Development*, *30*(3), 159–177.

Blanke, A., Rühr, P. T., Mokso, R., Villanueva, P., Wilde, F., Stampanoni, M., Uesugi, K., Machida, R., & Misof, B. (2015). Structural mouthpart interaction evolved already in the earliest lineages of insects. *Proceedings of the Royal Society B: Biological Sciences*, *282*(1812), 20151033.

Booher, D. B., Gibson, J. C., Liu, C., Longino, J. T., Fisher, B. L., Janda, M., Narula, N., Toulkeridou, E., Mikheyev, A. S., Suarez, A. V., & Economo, E. P. (2021). Functional innovation promotes diversification of form in the evolution of an ultrafast trap-jaw mechanism in ants. *PLoS Biology*, *19*(3), e3001031.

Boudinot, B. E., Moosdorf, O. T. D., Beutel, R. G., & Richter, A. (2021). Anatomy and evolution of the head of *Dorylus helvolus* (Formicidae: Dorylinae): Patterns of sex- and caste-limited traits in the sausagefly and the driver ant. *Journal of Morphology*, *282*, 1616–1658. https://doi.org/10.1002/jmor.21410

Boudinot, B. E., Richter, A., Katzke, J., Chaul, J. C. M., Keller, R. A., Economo, E. P., Beutel, R. G., & Yamamoto, S. (2022). Evidence for the evolution of eusociality in stem ants and a systematic revision of † *Gerontoformica* (Hymenoptera: Formicidae). *Zoological Journal of the Linnean Society*, *195*(4), 1355–1389. https://doi.org/10.1093/zoolinnean/zlab097

Brock, F., Southwell, R., Hazell, Z., Wessling, R., Green, M., & Davis, D. (2022). Using high-resolution digital photography and micro-CT

scanning to investigate deathwatch beetle damage to an historic timber from HMS Victory. *Environmental Archaeology*, *29*(1), 80–96. https://doi.org/10.1080/14614103.2021.2024689

Brothers, D. J. (1975). Phylogeny and classification of the aculeate Hymenoptera, with special reference to Mutillidae. *University of Kansas Science Bulletin*, *50*, 483–648.

Brothers, D. J. (1976). Modifications of the metapostnotum and origin of the 'propodeal triangle' in Hymenoptera Aculeata. *Systematic Entomology*, *1*, 177–182. https://doi.org/10.1111/j.1365-3113.1976.tb00036.x

Camargo, J. M. F., Kerr, W. E., & Lopes, C. R. (1967). Morfologia externa de *Melipona* (*Melipona*) *marginata* Lepeletier (Hymenoptera, Apoidea). *Papéis Avulsos de Zoologia*, *20*, 229–258. https://doi.org/10.11606/0031-1049.1967.20p229-258

Cecilia, A., Rack, A., Douissard, P.-A., Martin, T., dos Santos Rolo, T., Vagovič, P., Hamann, E., van de Kamp, T., Riedel, A., Fiederle, M., & Baumbach, T. (2011). LPE grown LSO: Tb scintillator films for high-resolution X-ray imaging applications at synchrotron light sources. *Nuclear Instruments and Methods in Physics Research Section A: Accelerators, Spectrometers, Detectors and Associated Equipment*, *648*, S321–S323.

Daly, H. V. (1964). Skeleto-muscular morphogenesis of the thorax and wings of the honey bee *Apis mellifera* (Hymenoptera: Apidae). *University of California Publublications in Entomology*, *39*, 1–77.

Danforth, B. N., Cardinal, S., Praz, C., Almeida, E. A. B., & Michez, D. (2013). The impact of molecular data on our understanding of bee phylogeny and evolution. *Annual Review of Entomology*, *58*, 57–78. https://doi.org/10.1146/annurev-ento-120811-153633

Danforth, B. N., Minckley, R. L., & Neff, J. L. (2019). *The Solitary bees. Biology, evolution, conservation*. Princeton University Press. https://doi.org/10.2307/j.ctvd1c929

Douissard, P.-A., Cecilia, A., Rochet, X., Chapel, X., Martin, T., Kamp, T., Helfen, L., Baumbach, T., Luquot, L., Xiao, X., Meinhardt, J., & Rack, A. (2012). A versatile indirect detector design for hard X-ray microimaging. *Journal of Instrumentation*, *7*, P09016.

Engelkes, K., Friedrich, F., Hammel, J. U., & Haas, A. (2018). A simple setup for episcopic microtomy and a digital image processing workflow to acquire high-quality volume data and 3D surface models of small vertebrates. *Zoomorphology*, *137*(1), 213–228. https://doi.org/10.1007/s00435-017-0386-3

Faragó, T., Gasilov, S., Emslie, I., Zuber, M., Helfen, L., Vogelgesang, M., & Baumbach, T. (2022). Tofu: A fast, versatile and user-friendly image processing toolkit for computed tomography. *Journal of Synchrotron Radiation*, *29*(3), 916–927.

Friedrich, F., & Beutel, R. G. (2008a). The thorax of *Zorotypus* (Hexapoda, Zoraptera) and a new nomenclature for the musculature of Neoptera. *Arthropod Structure and Development*, *37*, 29–54.

Friedrich, F., & Beutel, R. G. (2008b). Micro-computer tomography and a renaissance of insect morphology. *SPIE: Developments in X-ray Tomography VI*, *7078*, 545–550.

Friedrich, F., & Beutel, R. G. (2010). The thoracic morphology of *Nannochorista* (Nannochoristidae) and its implications for the phylogeny of Mecoptera and Antliophora. *Journal of Zoological Systematics and Evolutionary Research*, *48*, 50–74. https://doi.org/10.1111/j.1439-0469.2009.00535.x

Friedrich, F., Matsumura, Y., Pohl, H., Bai, M., Hörnschemeyer, T., & Beutel, R. G. (2014). Insect morphology in the age of phylogenomics: Innovative techniques and its future role in systematics. *Entomological Science*, *17*(1), 1–24.

Gibson, G. A. P. (1985). Some pro- and mesothoracic structures important for phylogenetic analysis of Hymenoptera, with a review of terms used for the structures. *The Canadian Entomologist*, *117*(11), 1395–1443. https://doi.org/10.4039/Ent1171395-11

Gibson, G. A. P. (1999). Sister-group relationships of the Platygastroidea and Chalcidoidea (Hymenoptera) an alternate hypothesis to Rasnitsyn (1988). *Zoologica Scripta*, *28*, 125–138.

Gibson, G. A. P., Heraty, J. M., & Woolley, J. B. (1999). Phylogenetics and classification of Chalcidoidea and Mymarommatoidea a review of current concepts (Hymenoptera, Apocrita). *Zoologica Scripta*, *28*, 87–124.

Girón, J. C., Tarasov, S., González Montaña, L. A., Matentzoglu, N., Smith, A. D., Koch, M., Boudinot, B. E., Bouchard, P., Burks, R., Vogt, L., Yoder, M., Osumi-Sutherland, D., Friedrich, F., Beutel, R. G., & Mikó, I. (2023). Formalizing invertebrate morphological data: A descriptive model for cuticle-based skeleto-muscular systems, an ontology for insect anatomy, and their potential applications in biodiversity research and informatics. *Systematic Biology*, *72*(5), 1084–1100. https://doi.org/10.1093/sysbio/syad025

Gonçalves, R. B., De Meira, O. M., & Rosa, B. B. (2022). Total-evidence dating and morphological partitioning: A novel approach to understand the phylogeny and biogeography of augochlorine bees (Hymenoptera: Apoidea. *Zoological Journal of the Linnean Society*, *195*(4), 1390–1406. https://doi.org/10.1093/zoolinnean/zlab098

Graf, V. (1965). Contribuição ao estudo da anatomia da cabeça dos Apoidea—A musculatura do complexo lábio-maxilar de *Xylocopa* Latreille, 1802 (Hymenoptera-Apoidea). *Boletim Da Universidade Federal Do Paraná, Zoologia*, *2*(7), 93–100.

Griebenow, Z. H., Richter, A., van de Kamp, T., Economo, E. P., & Liebermann, Z. E. (2023). Comparative morphology of male genital skeletomusculature in the Leptanillinae (Hymenoptera: Formicidae), with a standardized muscular terminology for the male genitalia of Hymenoptera. *Arthropod Systematics & Phylogeny*, *81*, 945–1018.

Herman, G. T. (2009). *Fundamentals of computed tomography, image reconstruction from projections* (2nd ed.). Springer.

Hillen, A. P., Foley, IV, J. R., Salcedo, M. K., Socha, J. J., & Salom, S. M. (2023). 3D X-ray analysis of the subterranean burrowing depth and pupal chamber size of *Laricobius* (Coleoptera: Derodontidae), a specialist predator of *Adelges tsugae* (Hemiptera: Adelgidae). *Journal of Insect Science (Online)*, *23*(3), 19.

Hörnschemeyer, T., Beutel, R. G., & Pasop, F. (2002). Head structures of Priacma serrataleconte (coleptera, archostemata) inferred from X-ray tomography. *Journal of Morphology*, *252*, 298–314.

van de Kamp, T., Mikó, I., Staniczek, A. H., Eggs, B., Bajerlein, D., Faragó, T., Hagelstein, L., Hamann, E., Spiecker, R., Baumbach, T., Janšta, P., & Krogmann, L. (2022). Evolution of flexible biting in hyperdiverse parasitoid wasps. *Proceedings of the Royal Society B: Biological Sciences*, *289*, 20212086.

van de Kamp, T., dos Santos Rolo, T., Vagovič, P., Baumbach, T., & Riedel, A. (2014). Three-dimensional reconstructions come to life—Interactive 3D PDF animations in functional morphology. *PLoS One*, *9*, e102355.

van de Kamp, T., Schwermann, A. H., dos Santos Rolo, T., Lösel, P. D., Engler, T., Etter, W., Faragó, T., Göttlicher, J., Heuveline, V., Kopmann, A., Mähler, B., Mörs, T., Odar, J., Rust, J., Tan Jerome, N., Vogelgesang, M., Baumbach, T., & Krogmann, L. (2018). Parasitoid biology preserved in mineralized fossils. *Nature Communications*, *9*, 3325.

van de Kamp, T., Vagovič, P., Baumbach, T., & Riedel, A. (2011). A biological screw in a beetle's leg. *Science*, *333*, 52.

Kawada, R., Lanes, G. O., & Azevedo, C. O. (2015). Evolution of metapostnotum in flat wasps (Hymenoptera, Bethylidae): Implications for Homology Assessments in Chrysidoidea. *PLoS One*, *10*(10), e0140051.

Klunk, C. L., Argenta, M. A., Rosumek, F. B., Schmelzle, S., van de Kamp, T., Hammel, J. U., Pie, M. R., & Heethoff, M. (2023). Simulated biomechanical performance of morphologically disparate ant mandibles under bite loading. *Scientific Reports*, *13*, 16833.

Lieberman, Z. E., Billen, J., van de Kamp, T., & Boudinot, B. E. (2022). The ant abdomen: the skeletomuscular and soft tissue anatomy of *Amblyopone australis* workers (Hymenoptera: Formicidae). *Journal of Morphology*, *283*, 693–770.

Litman, J. R. (2019). Under the radar: Detection avoidance in brood parasitic bees. *Philosophical Transactions of the Royal Society, B: Biological Sciences*, *374*, 20180196.

Liu, S.-P., Richter, A., Stoessel, A., & Beutel, R. G. (2019). The mesosomal anatomy of *Myrmecia nigrocincta* workers and evolutionary transformations in Formicidae (Hymenoptera). *Arthropod Systematics & Phylogeny*, *77*(1), 1–19.

Meira, O. M., & Gonçalves, R. B. (2018). The relevance of the mesosomal internal structures to the phylogeny of Augochlorini bees (Hymenoptera: Halictinae). *Zoologica Scripta*, *47*, 197–205. https://doi.org/10.1111/zsc.12270

Meira, O. M., & Gonçalves, R. B. (2021). Comparative morphology and evolution of the cranial musculature in bees (Hymenoptera: Apoidea). *Arthropod Structure & Development*, *65*, 101112. https://doi.org/10.1016/j.asd.2021.101112

Melo, G. A. R. (1999). Phylogenetic relationships and classification of the major lineages of Apoidea (Hymenoptera), with emphasis on the crabronid wasps. *Scientific Papers, Natural History Museum of the University of Kansas, Lawrence*, *14*, 1–55.

Michener, C. D. (1944). Comparative external morphology, phylogeny, and a classification of the bees (Hymenoptera). *Bulletin of the American Museum of Natural History*, *82*, 151–326.

Michener, C. D. (1984). A comparative study of the mentum and lorum of bees (Hymenoptera: Apoidea). *Journal of the Kansas Entomological Society*, *57*(4), 705–714.

Michener, C. D. (2007). *The bees of the world*. Johns Hopkins University Press.

Mikó, I., Vilhelmsen, L., Johnson, N. F., Masner, L., & Pénzes, Z. (2007). Skeletomusculature of Scelionidae (Hymenoptera: Platygastroidea): Head and mesosoma. *Zootaxa*, *1571*, 178.

Packer, L. (2003). Comparative morphology of the skeletal parts of the sting apparatus of bees (Hymenoptera: Apoidea). *Zoological Journal of the Linnean Society*, *138*, 1–38.

Paganin, D., Mayo, S. C., Gureyev, T. E., Miller, P. R., & Wilkins, S. W. (2002). Simultaneous phase and amplitude extraction from a single defocused image of a homogeneous object. *Journal of Microscopy*, *206*, 33–40.

de Paula, J. C., Doello, K., Mesas, C., Kapravelou, G., Cornet-Gómez, A., Orantes, F. J., Martínez, R., Linares, F., Prados, J. C., Porres, J. M., Osuna, A., & de Pablos, L. M. (2022). Exploring honeybee abdominal anatomy through micro-CT and novel multi-staining approaches. *Insects*, *13*(6), 556.

Plant, J. D., & Paulus, H. F. (1987). Comparative morphology of the postmentum of bees (Hymenoptera: Apoidea) with special remarks on the evolution of the lorum. *Journal of Zoological Systematics and Evolutionary Research*, *25*, 81–103. https://doi.org/10.1111/j.1439-0469.1987.tb00594.x

Plant, J. D., & Paulus, H. F. (2016). Evolution and phylogeny of bees. Review and cladistic analysis in light of morphological evidence (Hymenoptera, Apoidea). *Zoologica*, *161*, 7–21.

Porto, D. S., & Almeida, E. (2019). A comparative study of the pharyngeal plate of Apoidea (Hymenoptera: Aculeata), with implications for the understanding of phylogenetic relationships of bees. *Arthropod Structure & Development*, *50*, 64–77. https://doi.org/10.1016/j.asd.2019.04.002

Porto, D. S., & Almeida, E. A. B. (2021). Corbiculate bees (Hymenoptera: Apidae): exploring the limits of morphological data to solve a hard phylogenetic problem. *Insect Systematics and Diversity*, *5*, 32. https://doi.org/10.1093/isd/ixab008

Porto, D. S., Almeida, E. A. B., & Vilhelmsen, L. (2017). Comparative morphology of internal structures of the mesosoma of bees with an emphasis on the corbiculate clade (Apidae: Apini). *Zoological Journal of the Linnean Society*, *179*, 303–337. https://doi.org/10.1111/zoj.12466

Porto, D. S., Vilhelmsen, L., & Almeida, E. A. B. (2016). Comparative morphology of the mandibles and head structures of corbiculate bees (Hymenoptera: Apidae: Apini). *Systematic Entomology*, *41*, 339–368. https://doi.org/10.1111/syen.12156

Prentice, M. A. (1998). *The comparative morphology and phylogeny of apoid wasps (Hymenoptera: Apoidea)* [PhD Dissertation]. University of California.

Püffel, F., Pouget, A., Liu, X., Zuber, M., van de Kamp, T., Roces, F., & Labonte, D. (2021). Morphological determinants of bite force capacity in insects: A biomechanical analysis of polymorphic leaf-cutter ants. *Journal of the Royal Society Interface*, *18*, 20210424.

Ramirez-Esquivel, F., & Ravi, S. (2023). Functional anatomy of the worker honeybee stinger (*Apis mellifera*). *Iscience*, *26*(7), 107103.

Ribi, W., Senden, T. J., Sakellariou, A., Limaye, A., & Zhang, S. (2008). Imaging honey bee brain anatomy with micro-X-ray-computed tomography. *Journal of Neuroscience Methods*, *171*(1), 93–97.

Richter, A., Boudinot, B., Yamamoto, S., Katzke, J., & Beutel, R. G. (2022). The first reconstruction of the head anatomy of a Cretaceous insect, †*Gerontoformica gracilis* (Hymenoptera: Formicidae), and the early evolution of ants. *Insect Systematics and Diversity*, *6*(5), 4.

Richter, A., Boudinot, B. E., Garcia, F. H., Billen, J., Economo, E. P., & Beutel, R. G. (2023). Wonderfully weird: The head anatomy of the armadillo ant, *Tatuidris tatusia* (Hymenoptera: Formicidae: Agroecomyrmecinae), with evolutionary implications. *Myrmecological News*, *33*, 35–75.

Richter, A., Garcia, F. H., Keller, R. A., Billen, J., Economo, E. P., & Beutel, R. G. (2020). Comparative analysis of worker head anatomy of *Formica* and *Brachyponera* (Hymenoptera: Formicidae). *Arthropod Systematics & Phylogeny*, *78*, 133–170.

Richter, A., Garcia, F. H., Keller, R. A., Billen, J., Katzke, J., Boudinot, B. E., Economo, E. P., & Beutel, R. G. (2021). The head anatomy of *Protanilla lini* (Hymenoptera: Formicidae: Leptanillinae), with a hypothesis of their mandibular movement. *Myrmecological News*, *31*, 85–114.

Roig-Alsina, A., & Michener, C. D. (1993). Studies of the phylogeny and classification of long-tongued bees (Hymenoptera: Apoidea). *The University of Kansas Science Bulletin*, *55*, 123–162.

Rosa, B. B., & Melo, G. A. R. (2023). A new fossil family of aculeate wasp sheds light on early evolution of Apoidea (Hymenoptera). *Systematic Entomology*, *48*(3), 402–421. https://doi.org/10.1111/syen.12584

Rühr, P. T., van de Kamp, T., Faragó, T., Hammel, J. U., Wilde, F., Borisova, E., Edel, C., Frenzel, M., Baumbach, T., & Blanke, A. (2021). Juvenile ecology drives adult morphology in two insect orders. *Proceedings of the Royal Society B: Biological Sciences*, *288*, 20210616.

dos Santos Rolo, T., Ershov, A., van de Kamp, T., & Baumbach, T. (2014). In vivo X-ray cine-tomography for tracking morphological dynamics. *Proceedings of the National Academy of Sciences of the United States of America*, *111*(11), 3921–3926.

Schönitzer, B. K. (1986). Comparative morphology of the antenna cleaner in bees (Apoidea). *Journal of Zoological Systematics and Evolutionary Research*, *24*, 35–51. https://doi.org/10.1111/j.1439-0469.1986.tb00614.x

Schulman, V. K., Dobi, K. C., & Baylies, M. K. (2015). Morphogenesis of the somatic musculature in *Drosophila melanogaster*. *WIREs Developmental Biology*, *4*, 313–334.

Sharkey, M. J., & Wharton, R. A. (1997). Morphology and terminology. In R. A. Wharton, P. M. Marsh, & M. J. Sharkey (Eds.), *Manual of the new world genera of Braconidae (Hymenoptera)* (pp. 19–38). Special Publication of the International Society of Hymenopterists.

Sink, H. (2006). *Muscle development in* Drosophila. Springer.

Sless, T. J. L., Branstetter, M. G., Gillung, J. P., Krichilsky, E. A., Tobin, K. B., Straka, J., Rozen, Jr. J. G., Freitas, F. V., Martins, A. C., Bossert, S., Searle, J. B., & Danforth, B. N. (2022). Phylogenetic relationships and the evolution of host preferences in the largest clade of brood parasitic bees (Apidae: Nomadinae). *Molecular Phylogenetics and Evolution*, *166*, 107326. https://doi.org/10.1016/j.ympev.2021.107326

Snodgrass, R. E. (1925). *Anatomy and physiology of the honey bee*. McGraw-Hill Book Company.

Snodgrass, R. E. (1935). *Principles of insect morphology*. McGraw-Hill Book Company.

Snodgrass, R. E. (1942). The skeleto-muscular mechanisms of the honey bee. *Smithsonian Miscellaneous Collections*, *103*(2), 1–120.

Snodgrass, R. E. (1956). *Anatomy of the honey bee*. Cornell University Press.

Tonapi, G. T. (1958). A comparative study of spiracular structure and mechanisms in some hymenoptera. *Transactions of the Royal Entomological Society of London*, *110*, 489–519. https://doi.org/10.1111/j.1365-2311.1958.tb00381.x

Urban, D. (1963). Estudo comparativo da origem de alguns músculos cefálicos das abelhas (Hymenoptera-Apoidea). *Boletim Da Universidade Federal Do Paraná, Zoologia*, *2*(2), 21–33.

Vilhelmsen, L. (1996). The preoral cavity of lower Hymenoptera (Insecta): Comparative morphology and phylogenetic significance. *Zoologica Scripta*, *25*, 143–170. https://doi.org/10.1111/j.1463-6409.1996.tb00156.x

Vilhelmsen, L. (1997). The phylogeny of lower Hymenoptera (Insecta), with a summary of the early evolutionary history of the order. *Journal of Zoological Systematics and Evolutionary Research*, *35*, 49–70. https://doi.org/10.1111/j.1439-0469.1997.tb00404.x

Vilhelmsen, L. (2000). The ovipositor apparatus of basal Hymenoptera (Insecta): Phylogenetic implications and functional morphology. *Zoologica Scripta*, *29*, 319–345. https://doi.org/10.1046/j.1463-6409.2000.00046.x

Vilhelmsen, L. (2001). Phylogeny and classification of the extant basal lineages of the Hymenoptera (Insecta). *Zoological Journal of the Linnean Society*, *131*(4), 393–442. https://doi.org/10.1111/j.1096-3642.2001.tb01320.x

Vilhelmsen, L., Mikó, I., & Krogmann, L. (2010). Beyond the wasp-waist: Structural diversity and phylogenetic significance of the mesosoma in apocritan wasps (Insecta: Hymenoptera): Phylogeny of Hymenoptera. *Zoological Journal of the Linnean Society*, *159*(1), 22–194. https://doi.org/10.1111/j.1096-3642.2009.00576.x

Vogelgesang, M., Farago, T., Morgeneyer, T. F., Helfen, L., dos Santos Rolo, T., Myagotin, A., & Baumbach, T. (2016). Real-time image-content-based beamline control for smart 4D X-ray imaging. *Journal of Synchrotron Radiation*, *23*, 1254–1263.

Whitfield, J. B., Johnson, N. F., & Hamerski, M. R. (1989). Identity and phylogenetic significance of the metapostnotum in nonaculeate Hymenoptera. *Annals of the Entomological Society of America*, *82*(6), 663–673. https://doi.org/10.1093/aesa/82.6.663

Wille, A. (1956). Comparative studies of the thoracic musculature of bees. *The University of Kansas Science Bulletin*, *38*(6), 439–471. https://doi.org/10.1017/CBO9781107415324.004

Willsch, M., Friedrich, F., Baum, D., Jurisch, I., & Ohl, M. (2020). A comparative description of the mesosomal musculature in Sphecidae and Ampulicidae (Hymenoptera, Apoidea) using 3D techniques. *Deutsche Entomologische Zeitschrift*, *67*, 51–67. https://doi.org/10.3897/dez.67.49493

Wipfler, B., Machida, R., Müller, B., & Beutel, R. G. (2011). On the head morphology of Grylloblattodea (Insecta) and the systematic position of the order, with a new nomenclature for the head muscles of Dicondylia. *Systematic Entomology*, *36*, 241–266. https://doi.org/10.1111/j.1365-3113.2010.00556.x

Youssef, N. N. (1971). Topography of the cephalic musculature and nervous system of the honey bee *Apis mellifera* Linnaeus. *Smithsonian Contributions to Zoology*, *99*, 1–54. https://doi.org/10.5479/si.00810282.99

Zimmermann, D., & Vilhelmsen, L. (2016). The sister group of Aculeata (Hymenoptera)—Evidence from internal head anatomy, with emphasis on the tentorium. *Arthropod Systematics & Phylogeny*, *74*(2), 195–218.

SUPPORTING INFORMATION

Additional supporting information can be found online in the Supporting Information section at the end of this article.

How to cite this article: Meira, O. M., Beutel, R. G., Pohl, H., van de Kamp, T., Almeida, E. A. B., & Boudinot, B. E. (2024). Bee morphology: A skeletomuscular anatomy of *Thyreus* (Hymenoptera: Apidae). *Journal of Morphology*, 285, e21751. https://doi.org/10.1002/jmor.21751